


## AN ABSTRACT OF THE THESIS OF

Gregory G. Davidson for the degree of Master of Science in Nuclear Engineering  
presented on June 18, 2004.

Title: Finite Element Transport using Wachspress Rational Basis Functions on  
Quadrilaterals in Diffusive Regions. **Redacted for Privacy**

Abstract approved:

  
Todd S. Palmer

Wachspress rational functions are ratios of polynomials having certain properties which make them good candidates for basis functions in finite element methods. In addition, it had been theorized that Wachspress rational weight functions should provide a full-resolution discretization of the neutral particle transport equation in thick diffusive regions, but this had not been confirmed numerically.

In this study, we derive a discontinuous finite element discretization on quadrilaterals. We discuss different methods for constructing and integrating Wachspress rational functions. We perform an asymptotic analysis of the transport discretization in the interior of thick diffusive regions, and derive an asymptotic-P1 diffusion synthetic acceleration preconditioner. We then provide numerical results demonstrating Wachspress rational functions in the thick diffusive limit, and we provide comparisons with isoparametric bilinear basis functions, which are commonly used on quadrilaterals.

Analytic and computational results indicate that Wachspress rational functions provide a full-resolution spatial discretization in the thick diffusive limit.

©Copyright by Gregory G. Davidson

June 18, 2004

All Rights Reserved

Finite Element Transport using Wachspress Rational Basis Functions on  
Quadrilaterals in Diffusive Regions

by

Gregory G. Davidson

A THESIS

submitted to

Oregon State University

in partial fulfillment of  
the requirements for the  
degree of

Master of Science

Presented June 18, 2004

Commencement June 2005

Master of Science thesis of Gregory G. Davidson presented on June 18, 2004.

APPROVED:

Redacted for Privacy

---

Major Professor, representing Nuclear Engineering

Redacted for Privacy

---

Head of the Department of Nuclear Engineering and Radiation Health Physics

Redacted for Privacy

---

Dean of Graduate School

I understand that my thesis will become part of the permanent collection of Oregon State University libraries. My signature below authorizes release of my thesis to any reader upon request.

Redacted for Privacy

---

Gregory G. Davidson, Author

## ACKNOWLEDGEMENTS

I begin my acknowledgements with my thesis advisor, Dr. Todd Palmer. I have had the opportunity to work with Dr. Palmer for the last six years at Oregon State University, first as an undergraduate student, and now for the last two years as a Master's student. It was Dr. Palmer who first interested me in numerical transport, and he has guided me these last several years in my intellectual development. This thesis could not have been written without his guidance.

In addition to Dr. Palmer, I would also like to thank the other members of my committee: Dr. Jonathon Istok in the Civil, Construction and Environmental Engineering Department, Dr. Adel Faridani, in the Department of Mathematics, and Dr. Brian Woods, in the Department of Nuclear Engineering and Radiation Health Physics, all of Oregon State University.

Besides the aforementioned individuals, many other people (too numerous to name) provided me with the training and education needed to complete this work. I would like to thank the various scientists that I worked with at Lawrence Livermore National Laboratory, A Division, in particular Dr. Nick Gentile, Dr. Mike Zika, and Jeff Johnson. Jeff was always available for assistance with questions concerning C++ design and implementation, and Drs. Gentile and Zika taught me a great deal about transport methods, as did Dr. Carl Yehnert at Bechtel Bettis Atomic Power Laboratory. I would especially like to thank Dr. Jim Warsa of Los Alamos National Laboratory for performing the fine-mesh solution for test problem 3.

I can not underestimate the contributions of my fellow graduate students. In particular, my collaboration with Ian Davis was especially valuable. I enjoyed working with Ian very much, and I respect his advice and counsel.

My transport implementation depended in part on code written by others.

Dr. Rubin Landau implemented the Gauss-Legendre quadrature used to perform numerical integrals. John Gulick implemented the level-symmetric angular quadrature set.

I would like to thank my parents, Steve and Judy Davidson, and Michelle Hackett. Without their love and support I could never have completed this work,

Finally, I would like to thank the Krell Institute. They awarded me the Computational Science Graduate Fellowship, which funded this work.

## TABLE OF CONTENTS

	<u>Page</u>
1 INTRODUCTION . . . . .	1
2 DERIVATION OF THE DISCONTINUOUS FINITE ELEMENT TRANS- PORT DISCRETIZATION . . . . .	5
2.1 Finite Element Discretization on a General Zone . . . . .	5
2.2 Finite Element Discretization on a Quadrilateral . . . . .	9
2.3 Localization of the Finite Element Equations . . . . .	13
2.3.1 Mass-Matrix Lumping . . . . .	13
2.3.2 Surface-Matrix Lumping . . . . .	14
2.3.3 Full Lumping . . . . .	14
3 CONSTRUCTING THE BASIS FUNCTIONS . . . . .	16
3.1 Bilinear Functions in Isoparametric Space . . . . .	16
3.2 Wachspress Rational Functions via the Direct Method . . . . .	17
3.3 Wachspress Rational Functions via Dasgupta's Method . . . . .	25
3.4 Comparing the Direct Method and Dasgupta's Method . . . . .	30
4 INTEGRATING THE BASIS . . . . .	31
4.1 Integrals Over the Zone Area . . . . .	31
4.1.1 Integrals of Isoparametric Bilinear Functions . . . . .	31
4.1.2 Isoparametric Mapping of Wachspress Rational Basis Functions	34
4.1.3 Dasgupta's Integration Method . . . . .	35

## TABLE OF CONTENTS (Continued)

	<u>Page</u>
4.2 Edge Integrals . . . . .	39
5 ASYMPTOTIC ANALYSIS . . . . .	42
6 DIFFUSION SYNTHETIC ACCELERATION . . . . .	54
6.1 Asymptotic Diffusion Synthetic Acceleration . . . . .	56
6.2 Asymptotic-P1 Diffusion Synthetic Acceleration . . . . .	59
7 NUMERICAL RESULTS . . . . .	64
7.1 Test Problem 1 . . . . .	64
7.2 Test Problem 2 . . . . .	70
7.3 Test Problem 3 . . . . .	75
8 CONCLUSION . . . . .	80
BIBLIOGRAPHY . . . . .	85



## LIST OF FIGURES

<u>Figure</u>	<u>Page</u>
1 Typical Quadrilateral Zone . . . . .	9
2 A Quadrilateral Zone Mapped to Isoparametric Space . . . . .	17
3 Finding the External Diameter . . . . .	19
4 Finding the External Intersection Point . . . . .	19
5 Wachspress Rational Function Construction Example . . . . .	21
6 A Wachspress Rational Function . . . . .	23
7 A Trapezoidal Zone and its External Diameter . . . . .	23
8 Pathological Zones . . . . .	24
9 A Pentagonal Zone and its External Diameter . . . . .	25
10 Cyclical Ordering of Nodes . . . . .	25
11 Path Element in Surface Integral . . . . .	36
12 Closeup of Figure 11, $\lambda^+$ Surface Between Dashed Lines . . . . .	37
13 Basis Functions as Seen from Zone Edge . . . . .	40
14 Node with Logically Rectangular Connectivity . . . . .	46
15 Problem 1 — Orthogonal Mesh Configuration . . . . .	64
16 Problem 1 — Skewed Mesh Configuration . . . . .	65
17 Problem 1 — Orthogonal Unlumped Solution . . . . .	67
18 Problem 1 — Orthogonal Fully Lumped Solution . . . . .	67
19 Problem 1 — Orthogonal Log(Flux) Solution . . . . .	68
20 Problem 1 — Skewed Unlumped Solution . . . . .	68

# LIST OF FIGURES (Continued)

<u>Figure</u>		<u>Page</u>
21	Problem 1 — Skewed Fully Lumped Solution . . . . .	69
22	Problem 1 — Skewed Log(Flux) Solution . . . . .	69
23	Problem 2 — Diffusion Solution on an Orthogonal Grid . . . . .	71
24	Problem 2 — Diffusion Solution on a Skewed Grid . . . . .	71
25	Problem 2 — Error Function for Orthogonal Grid, $\epsilon = 10^{-1}$ . . . . .	72
26	Problem 2 — Error Function for Skewed Grid, $\epsilon = 10^{-1}$ . . . . .	72
27	Problem 2 — Error Function for Orthogonal Grid, $\epsilon = 10^{-3}$ . . . . .	73
28	Problem 2 — Error Function for Skewed Grid, $\epsilon = 10^{-3}$ . . . . .	73
29	Problem 2 — Error Function for Orthogonal Grid, $\epsilon = 10^{-5}$ . . . . .	74
30	Problem 2 — Error Function for Skewed Grid, $\epsilon = 10^{-5}$ . . . . .	74
31	Problem 2 — Convergence of Transport to Diffusion . . . . .	75
32	Problem 3 — Fine Mesh Solution . . . . .	76
33	Problem 3 — Error of BLD Coarse Solution . . . . .	77
34	Problem 3 — Logarithm of Error of BLD Coarse Solution . . . . .	78
35	Problem 3 — Error of Wachspress Coarse Solution . . . . .	78
36	Problem 3 — Logarithm of Error of Wachspress Coarse Solution . . . . .	79

## LIST OF TABLES

<u>Table</u>		<u>Page</u>
1	Properties of a Good Basis Function . . . . .	2
2	Comparison Between the Direct Method and Dasgupta's Method .	30
3	Problem 1 — Material Cross Sections . . . . .	65
4	Problem 3 — Maximum Error for Each Discretization . . . . .	77

# FINITE ELEMENT TRANSPORT USING WACHSPRESS RATIONAL BASIS FUNCTIONS ON QUADRILATERALS IN DIFFUSIVE REGIONS

## 1 INTRODUCTION

Particle transport deals with the study of rarefied fields of particles as they move through, and interact with, a background media. This topic has many applications and has been an interest of engineers and physicists for decades. Applications include nuclear reactor design and analysis, thermal radiation transport, astrophysics, radiation shielding, and radiodosimetric cancer therapies, among others.

As computer technology has become more advanced, physicists and engineers have increasingly applied numerical methods to the transport equation in order to find solutions to problems that were previously insoluble without great simplification and approximation. However, the transport equation has proven challenging to solve with digital computers in comparison to many other equations in science and engineering. This is due to several characteristics of the transport equation. The first-order form of the transport equation (which is the most common) is an integro-differential equation with a seven-dimensional phase space in its full, three-dimensional form (three space dimensions, two angular dimensions, one energy dimension, and one time dimension). In addition, this equation may behave as a hyperbolic, parabolic, or elliptic partial differential equation depending upon the particular problem.

Typically, solution methods for the transport equation fall into three broad categories: stochastic methods, deterministic methods, and hybrid methods. Stochastic methods solve the transport equation by statistical means (typically Monte

Carlo) whereas deterministic methods solve the transport equation by discretizing into a system of linear algebraic equations. Hybrid methods are some combination of deterministic and stochastic methods. We shall concern ourselves only with a specific deterministic method—finite element applied to the  $S_N$  equation. The  $S_N$  equation is derived by approximating integrals over angle with numerical quadrature. This will be dealt with more fully in Section 2. A derivation of the  $S_N$  equation is given in [Lew 93].

To employ the finite element method, the problem domain is broken into a collection of non-overlapping zones which are tessalated over the domain volume (or area, in the case of a two-dimensional problem). The spatial shape of the solution is then represented as a superposition of known spatial functions, termed *basis functions*. These functions must form a complete basis and span the volume of the zone continuously. Wachspress [Wac 75] lists the properties of a “good” basis function on a polygonal zone as given in Table 1.

- |  |
|--|
| <ol style="list-style-type: none"> <li>1. Continuous over the polygon</li> <li>2. Normalized to unity at vertex <math>i</math></li> <li>3. Linear on the two sides adjacent to <math>i</math></li> <li>4. Equal to zero on the sides opposite to <math>i</math></li> </ol> |
|--|

Table 1: Properties of a Good Basis Function

Linear polynomials fulfill these requirements on simple shapes such as squares or triangles in two dimensions, or hexahedra and tetrahedra in three dimensions. However, the set of all zone shapes for which “good” basis functions were known was limited, and was referred to as the finite element zoo. Wachspress discovered that certain rational functions can fulfill the above requirements for arbitrary convex polygons and polyhedra, as well as certain polycons (two-dimensional shapes with curved sides) and polypols (three-dimensional shapes with curved faces). This significantly expands the flexibility and power of the finite element method. An

exhaustive overview of the finite element method, and basis functions in particular, is given in [Zie 00].

Wachspress rational functions have not received much attention in the transport community. It has been suggested that Wachspress rational functions may be useful as interpolating functions in computer graphics [Das 01]. It has also been suggested that they might be useful in biomedical applications [Das 03a]. Recently, due to the work of Adams [Ada 01], there are new reasons to examine Wachspress rational functions in a finite element discretization of the transport equation. Adams found that weight functions with the properties exhibited by Wachspress rational functions should result in a full-resolution discretization. A finite element discretization that does not possess full-resolution will not give physically meaningful solutions in thick, diffusive regions. The reason that Wachspress rational functions provide a full-resolution discretization is because they meet Adams' litmus-test for weight functions: they possess *locality* and *surface-matching*. Locality refers to item 4 in Table 1: a weight function must be zero on the opposite edges of a zone to have locality. Surface matching refers to items 2 and 3 in Table 1. Surface matching means that the weight functions are mirror-images along a zone edge. The fact that Wachspress rational functions have the properties in Table 1 on such general zone shapes is what makes them so unique.

Particle transport in thick diffusive regions has several applications. Radiation hydrodynamics problems, such as in inertial-confinement fusion and astrophysics, typically contain some very diffusive regions [Rat 00]. Radiative heat transfer in glass is another area where thick and diffusive regions are encountered [Lar 02].

This thesis will investigate the use of Wachspress rational functions in a finite element discretization of the one-group, time-independent  $S_N$  transport equation on quadrilaterals, concentrating on the thick diffusive limit. We have chosen

quadrilaterals because they are the simplest shape on which Wachspress rational functions can be built such that they do not (always) degenerate to linear or bilinear functions. As such, quadrilaterals are a good starting point for investigating the properties of this basis. Section 2 presents a derivation of the finite element discretization of the  $S_N$  transport equation. Section 3 discusses two algorithms for constructing Wachspress rational basis functions. In addition, we present the basis functions currently used by the community for finite-element discretizations on quadrilaterals—*isoparametric bilinear basis functions*. Section 4 discusses methods for calculating spatial integrals of these basis functions. Section 5 presents an asymptotic analysis of a family of finite element discretizations. In Section 6 we derive an asymptotic and an asymptotic-P1 diffusion synthetic acceleration preconditioner which is necessary for rapid convergence of transport iterations in optically thick and diffusive regions. Section 7 contains results and Section 8 contains our conclusions.

## 2 DERIVATION OF THE DISCONTINUOUS FINITE ELEMENT TRANSPORT DISCRETIZATION

The finite element method involves the assumption of a functional form for the spatial distribution of the solution. The solution is written in terms of known spatial basis functions multiplied by unknown constants. To generate equations for these expansion coefficients, we apply the method of weighted residuals, and then substitute in the assumed basis expansion for the spatially-dependent functions. The method of weighted residuals operates by setting weighted integrals of the transport equation equal to zero, thereby setting weighted averages of the error equal to zero. The result is a set of linear equations that may be solved for the expansion coefficients.

In this section we will derive a finite-element discretization of the transport equation for a general two-dimensional zone shape. We will then simplify the resulting equation for the case of general convex quadrilaterals on a logically-rectangular grid.

### 2.1 Finite Element Discretization on a General Zone

We begin with the monoenergetic, time-independent transport equation in two dimensions, with isotropic scattering:

$$\hat{\Omega} \cdot \nabla \psi(x, y, \hat{\Omega}) + \sigma_t(x, y) \psi(x, y, \hat{\Omega}) = \frac{\sigma_s(x, y)}{2\pi} \phi(x, y) + q(x, y, \hat{\Omega}), \quad (1)$$

where



- $\hat{\Omega}$  = unit vector of particle travel,  
 $\psi(x, y, \hat{\Omega})$  = flux of particle at position  $(x, y)$  travelling in direction  $\hat{\Omega}$ ,  
 $\sigma_t(x, y)$  = total cross-section,  
 $\sigma_s(x, y)$  = scattering cross-section,  
 $\phi(x, y)$  = scalar flux, the zeroth angular moment of  $\psi(x, y, \hat{\Omega})$ ,  
 $q(x, y, \hat{\Omega})$  = particle source at position  $(x, y)$  in direction  $\hat{\Omega}$ .

We will discretize the angular variable with a level-symmetric quadrature set [Lew 93]. The transport equation may then be solved as a set of equations in discrete angles. At angular ordinate  $m$ , the transport equation is written

$$\hat{\Omega}_m \cdot \nabla \psi_m(x, y) + \sigma_t(x, y) \psi_m(x, y) = \frac{\sigma_s(x, y)}{W} \phi(x, y) + q_m(x, y), \quad (2)$$

where  $W$  is the sum of the angular quadrature weights,

$$\sum_{m=1}^M w_m = W. \quad (3)$$

This is called the  $S_N$  equation. The scalar flux may be calculated using

$$\phi(x, y) \equiv \int_{2\pi} d\hat{\Omega} \psi(x, y, \hat{\Omega}) \approx \sum_{m=1}^M w_m \psi_m(x, y). \quad (4)$$

Multiplying by the weight function  $\gamma_i(x, y)$  and integrating over a zone  $(p, q)$  gives us

$$\iint_{\Lambda} d\Lambda \left[ \gamma_i(x, y) \left( \hat{\Omega}_m \cdot \nabla \psi_m(x, y) + \sigma_t \psi_m(x, y) \right) \right] = \iint_{\Lambda} d\Lambda \left[ \gamma_i(x, y) \left( \frac{\sigma_s}{W} \phi(x, y) + q_m(x, y) \right) \right], \quad i = 1 \dots \Gamma_{p,q}, \quad (5)$$

where  $(x, y) \in \Lambda$ , the zone area, and where  $\Gamma_{p,q}$  refers to the number of weight functions in our basis in zone  $(p, q)$ . Here we have assumed that the cross sections  $\sigma_s$  and  $\sigma_t$  are constant within the zone. We now use Green's theorem on the first term:

$$\begin{aligned}
& \int_{\lambda} \hat{\mathbf{n}} \cdot \hat{\Omega}_m \gamma_i(x, y) \psi_m^\lambda(x, y) d\lambda - \iint_{\Lambda} \psi_m(x, y) \hat{\Omega}_m \cdot \nabla \gamma_i(x, y) d\Lambda \\
& + \iint_{\Lambda} d\Lambda \gamma_i(x, y) \left[ \sigma_t \psi_m(x, y) - \frac{\sigma_s}{W} \phi(x, y) - q_m(x, y) \right] = 0, \quad i = 1 \dots \Gamma_{p,q}. \quad (6)
\end{aligned}$$

Here  $\hat{\mathbf{n}}$  is defined to be the unit normal outward from the zone surface  $\lambda$ , and  $\psi_m^\lambda(x, y)$  is the angular flux on the zone surface. We now expand all of the spatial functions in terms of the basis functions. Note that there must be an equal number of basis functions as there are weight functions:

$$\psi_m(x, y) = \sum_{j=1}^{\Gamma_{p,q}} \psi_{m,j} b_j(x, y), \quad (7a)$$

$$\phi(x, y) = \sum_{j=1}^{\Gamma_{p,q}} \phi_j b_j(x, y), \quad (7b)$$

$$q_m(x, y) = \sum_{j=1}^{\Gamma_{p,q}} q_{m,j} b_j(x, y), \quad (7c)$$

$$\psi_m^\lambda(x, y) = \sum_{j=1}^{\Gamma_{p,q}} \psi_{m,j}^\lambda b_j(x, y). \quad (7d)$$

Inserting Eq. (7) into Eq. (6) we obtain

$$\begin{aligned}
& \int_{\lambda} \hat{\mathbf{n}} \cdot \hat{\Omega}_m \gamma_i(x, y) \sum_{j=1}^{\Gamma_{p,q}} \psi_{m,j}^\lambda b_j(x, y) d\lambda \\
& - \iint_{\Lambda} \sum_{j=1}^{\Gamma_{p,q}} \psi_{m,j} b_j(x, y) \hat{\Omega}_m \cdot \nabla \gamma_i(x, y) d\Lambda \\
& + \sum_{j=1}^{\Gamma_{p,q}} \left( \iint_{\Lambda} \gamma_i(x, y) b_j(x, y) d\Lambda \right) \left( \sigma_t \psi_{m,j} - \frac{\sigma_s}{W} \phi_j - q_{m,j} \right) = 0, \\
& i = 1 \dots \Gamma_{p,q}. \quad (8)
\end{aligned}$$

We will now define several matrices:

$$M_{i,j} = \iint_{\Lambda} \gamma_i(x, y) b_j(x, y) d\Lambda, \quad (9a)$$

$$L_{i,j} = \iint_{\Lambda} b_j(x,y) \frac{\partial}{\partial x} \gamma_i(x,y) d\Lambda, \quad (9b)$$

$$K_{i,j} = \iint_{\Lambda} b_j(x,y) \frac{\partial}{\partial y} \gamma_i(x,y) d\Lambda. \quad (9c)$$

All of these matrices are local to the zone. In the finite element literature,  $\underline{\underline{M}}$  is called the mass matrix. Using these definitions, Eq. (8) can be rewritten as

$$\begin{aligned} \int_{\lambda} \hat{\mathbf{n}} \cdot \hat{\boldsymbol{\Omega}}_m \gamma_i(x,y) \sum_{j=1}^{\Gamma_{p,q}} \psi_{m,j}^{\lambda} b_j(x,y) d\lambda - \mu_m \sum_{j=1}^{\Gamma_{p,q}} L_{i,j} \psi_{m,j} - \eta_m \sum_{j=1}^{\Gamma_{p,q}} K_{i,j} \psi_{m,j} \\ + \sigma_t \sum_{j=1}^{\Gamma_{p,q}} M_{i,j} \psi_{m,j} = \sum_{j=1}^{\Gamma_{p,q}} M_{i,j} \left( \frac{\sigma_s}{W} \phi_j + q_{m,j} \right), \quad i = 1 \dots \Gamma_{p,q}, \end{aligned} \quad (10)$$

where  $\mu_m$  and  $\eta_m$  are the  $x$ - and  $y$ -direction cosines:

$$\mu_m = \hat{\boldsymbol{\Omega}}_m \cdot \hat{\mathbf{e}}_x, \quad (11a)$$

$$\eta_m = \hat{\boldsymbol{\Omega}}_m \cdot \hat{\mathbf{e}}_y. \quad (11b)$$

We must now analyze the surface integral term. If we sum this term around all of the edges of the zone, the first term in Eq. (10) becomes

$$\sum_{f=1}^{F_{p,q}} \left( \hat{\mathbf{n}}_f \cdot \hat{\boldsymbol{\Omega}}_m \sum_{j=1}^{\Gamma_{p,q}} \left[ \int_{\lambda_f} \gamma_i(x,y) b_j(x,y) d\lambda_f \right] \psi_{m,j}^{\lambda_f} \right), \quad i = 1 \dots \Gamma_{p,q}, \quad (12)$$

where  $\lambda_f$  denotes the  $f$ -th edge of the zone,  $F_{p,q}$  denotes the total number of edges in the zone, and  $\psi_{m,j}^{\lambda_f}$  is the angular flux on edge  $\lambda_f$ . Substituting this back into Eq. (10) gives

$$\begin{aligned} \sum_{f=1}^{F_{p,q}} \left( \hat{\mathbf{n}}_f \cdot \hat{\boldsymbol{\Omega}}_m \sum_{j=1}^{\Gamma_{p,q}} \left[ \int_{\lambda_f} \gamma_i(x,y) b_j(x,y) d\lambda_f \right] \psi_{m,j}^{\lambda_f} \right) - \mu_m \sum_{j=1}^{\Gamma_{p,q}} L_{i,j} \psi_{m,j} \\ - \eta_m \sum_{j=1}^{\Gamma_{p,q}} K_{i,j} \psi_{m,j} + \sigma_t \sum_{j=1}^{\Gamma_{p,q}} M_{i,j} \psi_{m,j} = \sum_{j=1}^{\Gamma_{p,q}} M_{i,j} \left( \frac{\sigma_s}{W} \phi_j + q_{m,j} \right), \quad i = 1 \dots \Gamma_{p,q}. \end{aligned} \quad (13)$$

This is the discontinuous finite element discretization for a general zone with general weight and basis functions.

## 2.2 Finite Element Discretization on a Quadrilateral

We now derive the specific form of the finite element transport discretization for the case of a quadrilateral zone. We employ Galerkin weighting, such that our weight functions are equal to our basis functions, and we center our unknowns on the zone “corners,” (see Figure 1) so that there are four unknowns per zone. Corners occupy the same location as a grid node, but are considered interior to the zone.

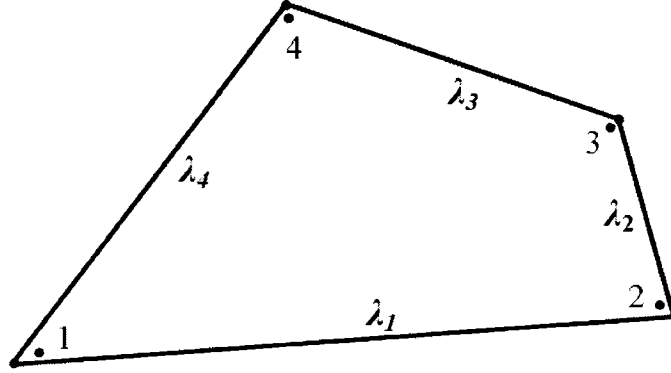


Figure 1: Typical Quadrilateral Zone

Our matrix definitions are similar to those in Section 2.1, except that the weight functions may be replaced with basis functions due to our Galerkin weighting:

$$M_{i,j} = \iint_{\Lambda} b_i(x,y)b_j(x,y) d\Lambda, \quad (14a)$$

$$L_{i,j} = \iint_{\Lambda} b_j(x,y) \frac{\partial}{\partial x} b_i(x,y) d\Lambda, \quad (14b)$$

$$K_{i,j} = \iint_{\Lambda} b_j(x,y) \frac{\partial}{\partial y} b_i(x,y) d\Lambda. \quad (14c)$$

Additionally, the surface term in Eq. (13) may be simplified considerably. Writing that term explicitly for quadrilaterals yields

$$\begin{aligned}
& \hat{\mathbf{n}}_1 \cdot \hat{\boldsymbol{\Omega}}_m \sum_{j=1}^4 \left( \int_{\lambda_1} b_i(x, y) b_j(x, y) d\lambda_1 \right) \psi_{m,j}^{\lambda_1} \\
& + \hat{\mathbf{n}}_2 \cdot \hat{\boldsymbol{\Omega}}_m \sum_{j=1}^4 \left( \int_{\lambda_2} b_i(x, y) b_j(x, y) d\lambda_2 \right) \psi_{m,j}^{\lambda_2} \\
& + \hat{\mathbf{n}}_3 \cdot \hat{\boldsymbol{\Omega}}_m \sum_{j=1}^4 \left( \int_{\lambda_3} b_i(x, y) b_j(x, y) d\lambda_3 \right) \psi_{m,j}^{\lambda_3} \\
& + \hat{\mathbf{n}}_4 \cdot \hat{\boldsymbol{\Omega}}_m \sum_{j=1}^4 \left( \int_{\lambda_4} b_i(x, y) b_j(x, y) d\lambda_4 \right) \psi_{m,j}^{\lambda_4}, \quad i = 1 \dots 4. \quad (15)
\end{aligned}$$

According to Table 1, a proper basis function is zero around all edges except the two edges adjacent to its “anchor” corner. Each basis is anchored at a single corner, and each corner is anchor to a single basis. Therefore,

$$b_1(x, y) = 0 \text{ on } \lambda_2 \text{ and } \lambda_3, \quad (16a)$$

$$b_2(x, y) = 0 \text{ on } \lambda_3 \text{ and } \lambda_4, \quad (16b)$$

$$b_3(x, y) = 0 \text{ on } \lambda_4 \text{ and } \lambda_1, \quad (16c)$$

$$b_4(x, y) = 0 \text{ on } \lambda_1 \text{ and } \lambda_2. \quad (16d)$$

Substituting Eqs. (16) into Eqs. (15) yields:

$$\begin{aligned}
& \sum_{f=1}^4 \hat{\mathbf{n}}_f \cdot \hat{\boldsymbol{\Omega}}_m \left[ \sum_{j=1}^4 \left( \int_{\lambda_f} b_1(x, y) b_j(x, y) d\lambda_f \right) \psi_{m,j}^{\lambda_f} \right] = \\
& \hat{\mathbf{n}}_1 \cdot \hat{\boldsymbol{\Omega}}_m \left[ \int_{\lambda_1} b_1(x, y) (b_1(x, y) \psi_{m,1}^{\lambda_1} + b_2(x, y) \psi_{m,2}^{\lambda_1}) d\lambda_1 \right] \\
& + \hat{\mathbf{n}}_4 \cdot \hat{\boldsymbol{\Omega}}_m \left[ \int_{\lambda_4} b_1(x, y) (b_1(x, y) \psi_{m,1}^{\lambda_4} + b_4(x, y) \psi_{m,4}^{\lambda_4}) d\lambda_4 \right], \quad (17a)
\end{aligned}$$

$$\begin{aligned}
\sum_{f=1}^4 \hat{\mathbf{n}}_f \cdot \hat{\boldsymbol{\Omega}}_m \left[ \sum_{j=1}^4 \left( \int_{\lambda_f} b_2(x, y) b_j(x, y) d\lambda_f \right) \psi_{m,j}^{\lambda_f} \right] = \\
\hat{\mathbf{n}}_1 \cdot \hat{\boldsymbol{\Omega}}_m \left[ \int_{\lambda_1} b_2(x, y) (b_1(x, y) \psi_{m,1}^{\lambda_1} + b_2(x, y) \psi_{m,2}^{\lambda_1}) d\lambda_1 \right] \\
+ \hat{\mathbf{n}}_2 \cdot \hat{\boldsymbol{\Omega}}_m \left[ \int_{\lambda_2} b_2(x, y) (b_2(x, y) \psi_{m,1}^{\lambda_2} + b_3(x, y) \psi_{m,4}^{\lambda_2}) d\lambda_2 \right], \quad (17b)
\end{aligned}$$

$$\begin{aligned}
\sum_{f=1}^4 \hat{\mathbf{n}}_f \cdot \hat{\boldsymbol{\Omega}}_m \left[ \sum_{j=1}^4 \left( \int_{\lambda_f} b_3(x, y) b_j(x, y) d\lambda_f \right) \psi_{m,j}^{\lambda_f} \right] = \\
\hat{\mathbf{n}}_2 \cdot \hat{\boldsymbol{\Omega}}_m \left[ \int_{\lambda_2} b_3(x, y) (b_2(x, y) \psi_{m,2}^{\lambda_2} + b_3(x, y) \psi_{m,3}^{\lambda_2}) d\lambda_2 \right] \\
+ \hat{\mathbf{n}}_3 \cdot \hat{\boldsymbol{\Omega}}_m \left[ \int_{\lambda_3} b_3(x, y) (b_3(x, y) \psi_{m,3}^{\lambda_3} + b_4(x, y) \psi_{m,4}^{\lambda_3}) d\lambda_3 \right], \quad (17c)
\end{aligned}$$

$$\begin{aligned}
\sum_{f=1}^4 \hat{\mathbf{n}}_f \cdot \hat{\boldsymbol{\Omega}}_m \left[ \sum_{j=1}^4 \left( \int_{\lambda_f} b_4(x, y) b_j(x, y) ds \right) \psi_{m,j}^{\lambda_f} \right] = \\
\hat{\mathbf{n}}_3 \cdot \hat{\boldsymbol{\Omega}}_m \left[ \int_{\lambda_3} b_4(x, y) (b_3(x, y) \psi_{m,3}^{\lambda_3} + b_4(x, y) \psi_{m,4}^{\lambda_3}) d\lambda_3 \right] \\
+ \hat{\mathbf{n}}_4 \cdot \hat{\boldsymbol{\Omega}}_m \left[ \int_{\lambda_4} b_4(x, y) (b_1(x, y) \psi_{m,1}^{\lambda_4} + b_4(x, y) \psi_{m,4}^{\lambda_4}) d\lambda_4 \right]. \quad (17d)
\end{aligned}$$

These expressions can be written in matrix form as

$$\hat{\boldsymbol{\Omega}}_m \cdot \underline{\underline{\mathbf{S}}}^h \underline{\underline{N}} \underline{\underline{\psi}}_m^h + \hat{\boldsymbol{\Omega}}_m \cdot \underline{\underline{\mathbf{S}}}^v \underline{\underline{U}} \underline{\underline{\psi}}_m^v, \quad (18)$$

where

$$\underline{\underline{\mathbf{S}}}^h = \begin{bmatrix} \hat{\mathbf{n}}_1 & 0 & 0 & 0 \\ 0 & \hat{\mathbf{n}}_1 & 0 & 0 \\ 0 & 0 & \hat{\mathbf{n}}_3 & 0 \\ 0 & 0 & 0 & \hat{\mathbf{n}}_3 \end{bmatrix}, \quad (19a)$$

$$\underline{\underline{\mathbf{S}}}^v = \begin{bmatrix} \hat{\mathbf{n}}_4 & 0 & 0 & 0 \\ 0 & \hat{\mathbf{n}}_2 & 0 & 0 \\ 0 & 0 & \hat{\mathbf{n}}_2 & 0 \\ 0 & 0 & 0 & \hat{\mathbf{n}}_4 \end{bmatrix}, \quad (19b)$$

$$\underline{\underline{N}} = \begin{bmatrix} \int_{\lambda_1} b_1^2 d\lambda_1 & \int_{\lambda_1} b_1 b_2 d\lambda_1 & 0 & 0 \\ \int_{\lambda_1} b_2 b_1 d\lambda_1 & \int_{\lambda_1} b_2^2 d\lambda_1 & 0 & 0 \\ 0 & 0 & \int_{\lambda_3} b_3^2 d\lambda_3 & \int_{\lambda_3} b_3 b_4 d\lambda_3 \\ 0 & 0 & \int_{\lambda_3} b_4 b_3 d\lambda_3 & \int_{\lambda_3} b_4^2 d\lambda_3 \end{bmatrix}, \quad (19c)$$

$$\underline{\underline{U}} = \begin{bmatrix} \int_{\lambda_4} b_1^2 d\lambda_4 & 0 & 0 & \int_{\lambda_4} b_1 b_4 d\lambda_4 \\ 0 & \int_{\lambda_2} b_2^2 d\lambda_2 & \int_{\lambda_2} b_2 b_3 d\lambda_2 & 0 \\ 0 & \int_{\lambda_2} b_3 b_2 d\lambda_2 & \int_{\lambda_2} b_3^2 d\lambda_2 & 0 \\ \int_{\lambda_4} b_4 b_1 d\lambda_4 & 0 & 0 & \int_{\lambda_4} b_4^2 d\lambda_4 \end{bmatrix}, \quad (19d)$$

$$\underline{\psi}_m^h = \begin{bmatrix} \psi_{m,1}^{\lambda_1} \\ \psi_{m,2}^{\lambda_1} \\ \psi_{m,3}^{\lambda_3} \\ \psi_{m,4}^{\lambda_3} \end{bmatrix}, \quad (19e)$$

$$\underline{\psi}_m^v = \begin{bmatrix} \psi_{m,1}^{\lambda_4} \\ \psi_{m,2}^{\lambda_2} \\ \psi_{m,3}^{\lambda_2} \\ \psi_{m,4}^{\lambda_4} \end{bmatrix}. \quad (19f)$$

Finally, we write the transport equation in matrix form for a zone  $(p, q)$  as follows:

$$\begin{aligned} \hat{\Omega}_m \cdot \underline{\underline{S}}_{p,q}^h \underline{\underline{N}}_{p,q} \psi_{m,p,q}^h + \hat{\Omega}_m \cdot \underline{\underline{S}}_{p,q}^v \underline{\underline{U}}_{p,q} \psi_{m,p,q}^v \\ + (\sigma_{t,p,q} \underline{\underline{M}}_{p,q} - \mu_{t,m} \underline{\underline{L}}_{p,q} - \eta_m \underline{\underline{K}}_{p,q}) \psi_{m,p,q} = \frac{\sigma_{s,p,q}}{W} \underline{\underline{M}}_{p,q} \phi_{p,q} + \underline{\underline{M}}_{p,q} \underline{\underline{q}}_{m,p,q}. \end{aligned} \quad (20)$$

To complete the system, we use the following upstream closures:

$$\psi_{m,p,q,1}^{\lambda_1} = \begin{cases} \text{upstream zone } \psi_{m,4} & \hat{\mathbf{n}}_1 \cdot \hat{\Omega}_m < 0 \\ \psi_{m,p,q,1} & \hat{\mathbf{n}}_1 \cdot \hat{\Omega}_m > 0 \end{cases}, \quad (21a)$$

$$\psi_{m,p,q,2}^{\lambda_1} = \begin{cases} \text{upstream zone } \psi_{m,3} & \hat{\mathbf{n}}_1 \cdot \hat{\Omega}_m < 0 \\ \psi_{m,p,q,2} & \hat{\mathbf{n}}_1 \cdot \hat{\Omega}_m > 0 \end{cases}, \quad (21b)$$

$$\psi_{m,p,q,3}^{\lambda_3} = \begin{cases} \text{upstream zone } \psi_{m,2} & \hat{\mathbf{n}}_3 \cdot \hat{\Omega}_m < 0 \\ \psi_{m,p,q,3} & \hat{\mathbf{n}}_3 \cdot \hat{\Omega}_m > 0 \end{cases}, \quad (21c)$$

$$\psi_{m,p,q,4}^{\lambda_3} = \begin{cases} \text{upstream zone } \psi_{m,1} & \hat{\mathbf{n}}_3 \cdot \hat{\Omega}_m < 0 \\ \psi_{m,p,q,4} & \hat{\mathbf{n}}_3 \cdot \hat{\Omega}_m > 0 \end{cases}, \quad (21d)$$

$$\psi_{m,p,q,1}^{\lambda_4} = \begin{cases} \text{upstream zone } \psi_{m,2} & \hat{\mathbf{n}}_4 \cdot \hat{\Omega}_m < 0 \\ \psi_{m,p,q,1} & \hat{\mathbf{n}}_4 \cdot \hat{\Omega}_m > 0 \end{cases}, \quad (21e)$$

$$\psi_{m,p,q,2}^{\lambda_2} = \begin{cases} \text{upsteam zone } \psi_{m,1} & \hat{\mathbf{n}}_2 \cdot \hat{\mathbf{\Omega}}_m < 0 \\ \psi_{m,p,q,2} & \hat{\mathbf{n}}_2 \cdot \hat{\mathbf{\Omega}}_m > 0 \end{cases}, \quad (21f)$$

$$\psi_{m,p,q,3}^{\lambda_2} = \begin{cases} \text{upsteam zone } \psi_{m,4} & \hat{\mathbf{n}}_2 \cdot \hat{\mathbf{\Omega}}_m < 0 \\ \psi_{m,p,q,3} & \hat{\mathbf{n}}_2 \cdot \hat{\mathbf{\Omega}}_m > 0 \end{cases}, \quad (21g)$$

$$\psi_{m,p,q,4}^{\lambda_4} = \begin{cases} \text{upsteam zone } \psi_{m,3} & \hat{\mathbf{n}}_4 \cdot \hat{\mathbf{\Omega}}_m < 0 \\ \psi_{m,p,q,4} & \hat{\mathbf{n}}_4 \cdot \hat{\mathbf{\Omega}}_m > 0 \end{cases}. \quad (21h)$$

Once the angular flux has been found, the scalar flux can be calculated via

$$\phi_{p,q} = \sum_{m=1}^M w_m \psi_{m,p,q}. \quad (22)$$

This process repeats until the scalar flux is converged. This is covered in more detail in Section 6.

## 2.3 Localization of the Finite Element Equations

As we shall see in the asymptotic analysis (Section 5) and in the results (Section 7), discontinuous finite element discretizations often gain robustness if their matrices are lumped [Ada 01]. A robust solution is nonnegative and free of unphysical oscillations. Lumping refers to altering the matrices such that the various unknowns in the equation are dependent only upon their corners and directly adjacent corners. The three types of lumping we will investigate are mass-matrix lumping, surface-matrix lumping, and full lumping (lumping of all matrices).

### 2.3.1 Mass-Matrix Lumping

The mass matrix is defined in Eq. (14a). We wish to localize the coupling, which is achieved by diagonalizing the mass matrix. The result is [Ada 01]:

$$M_{p,q,i,j}^{lump} = \delta_{i,j} \sum_{j'=1}^4 M_{p,q,i,j'}, \quad (23)$$

where  $\delta_{i,j}$  is the Kronecker delta function.



### 2.3.2 Surface-Matrix Lumping

In addition to mass-matrix lumping, surface-matrix lumping is often employed, for similar reasons. The equation for the surface lumped matrices for a quadrilateral zone is [Ada 01]:

$$\underline{\underline{N}}_{p,q}^{lump} = \begin{bmatrix} \int_{\lambda_1} b_1(x, y) d\lambda_1 & 0 & 0 & 0 \\ 0 & \int_{\lambda_1} b_2(x, y) d\lambda_1 & 0 & 0 \\ 0 & 0 & \int_{\lambda_3} b_3(x, y) d\lambda_3 & 0 \\ 0 & 0 & 0 & \int_{\lambda_3} b_4(x, y) d\lambda_3 \end{bmatrix}, \quad (24a)$$

and

$$\underline{\underline{U}}_{p,q}^{lump} = \begin{bmatrix} \int_{\lambda_4} b_1(x, y) d\lambda_4 & 0 & 0 & 0 \\ 0 & \int_{\lambda_2} b_2(x, y) d\lambda_2 & 0 & 0 \\ 0 & 0 & \int_{\lambda_2} b_3(x, y) d\lambda_2 & 0 \\ 0 & 0 & 0 & \int_{\lambda_4} b_4(x, y) d\lambda_4 \end{bmatrix}. \quad (24b)$$

### 2.3.3 Full Lumping

Finally, with full lumping we lump the leakage matrices in addition to the mass and surface matrices. The equation for matrix  $\underline{\underline{L}}_{p,q}^{lump}$  is

$$\underline{\underline{L}}_{p,q}^{lump} = \begin{bmatrix} L_{11} & L_{12} & 0 & 0 \\ L_{21} & L_{22} & 0 & 0 \\ 0 & 0 & L_{33} & L_{34} \\ 0 & 0 & L_{43} & L_{44} \end{bmatrix}, \quad (25)$$

where

$$L_{11} = \iint_{\Lambda} b_1(x, y) \frac{\partial b_1(x, y)}{\partial x} d\Lambda + \iint_{\Lambda} b_4(x, y) \frac{\partial b_1(x, y)}{\partial x} d\Lambda, \quad (26a)$$

$$L_{12} = \iint_{\Lambda} b_2(x, y) \frac{\partial b_1(x, y)}{\partial x} d\Lambda + \iint_{\Lambda} b_3(x, y) \frac{\partial b_1(x, y)}{\partial x} d\Lambda, \quad (26b)$$

$$L_{21} = \iint_{\Lambda} b_1(x, y) \frac{\partial b_2(x, y)}{\partial x} d\Lambda + \iint_{\Lambda} b_4(x, y) \frac{\partial b_2(x, y)}{\partial x} d\Lambda, \quad (26c)$$

$$L_{22} = \iint_{\Lambda} b_2(x, y) \frac{\partial b_2(x, y)}{\partial x} d\Lambda + \iint_{\Lambda} b_3(x, y) \frac{\partial b_2(x, y)}{\partial x} d\Lambda, \quad (26d)$$

$$L_{33} = \iint_{\Lambda} b_3(x, y) \frac{\partial b_3(x, y)}{\partial x} d\Lambda + \iint_{\Lambda} b_2(x, y) \frac{\partial b_3(x, y)}{\partial x} d\Lambda, \quad (26e)$$

$$L_{34} = \iint_{\Lambda} b_4(x, y) \frac{\partial b_3(x, y)}{\partial x} d\Lambda + \iint_{\Lambda} b_1(x, y) \frac{\partial b_3(x, y)}{\partial x} d\Lambda, \quad (26f)$$

$$L_{43} = \iint_{\Lambda} b_3(x, y) \frac{\partial b_4(x, y)}{\partial x} d\Lambda + \iint_{\Lambda} b_2(x, y) \frac{\partial b_4(x, y)}{\partial x} d\Lambda, \quad (26g)$$

$$L_{44} = \iint_{\Lambda} b_4(x, y) \frac{\partial b_4(x, y)}{\partial x} d\Lambda + \iint_{\Lambda} b_1(x, y) \frac{\partial b_4(x, y)}{\partial x} d\Lambda. \quad (26h)$$

The equation for matrix  $\underline{\underline{K}}_{p,q}^{lump}$  is

$$\underline{\underline{K}}_{p,q}^{lump} = \begin{bmatrix} K_{11} & 0 & 0 & K_{14} \\ 0 & K_{22} & K_{23} & 0 \\ 0 & K_{32} & K_{33} & 0 \\ K_{41} & 0 & 0 & K_{44} \end{bmatrix}, \quad (27)$$

where

$$K_{11} = \iint_{\Lambda} b_1(x, y) \frac{\partial b_1(x, y)}{\partial x} d\Lambda + \iint_{\Lambda} b_2(x, y) \frac{\partial b_1(x, y)}{\partial x} d\Lambda, \quad (28a)$$

$$K_{14} = \iint_{\Lambda} b_3(x, y) \frac{\partial b_1(x, y)}{\partial x} d\Lambda + \iint_{\Lambda} b_4(x, y) \frac{\partial b_1(x, y)}{\partial x} d\Lambda, \quad (28b)$$

$$K_{22} = \iint_{\Lambda} b_1(x, y) \frac{\partial b_2(x, y)}{\partial x} d\Lambda + \iint_{\Lambda} b_2(x, y) \frac{\partial b_2(x, y)}{\partial x} d\Lambda, \quad (28c)$$

$$K_{23} = \iint_{\Lambda} b_3(x, y) \frac{\partial b_2(x, y)}{\partial x} d\Lambda + \iint_{\Lambda} b_4(x, y) \frac{\partial b_2(x, y)}{\partial x} d\Lambda, \quad (28d)$$

$$K_{32} = \iint_{\Lambda} b_1(x, y) \frac{\partial b_3(x, y)}{\partial x} d\Lambda + \iint_{\Lambda} b_2(x, y) \frac{\partial b_3(x, y)}{\partial x} d\Lambda, \quad (28e)$$

$$K_{33} = \iint_{\Lambda} b_3(x, y) \frac{\partial b_3(x, y)}{\partial x} d\Lambda + \iint_{\Lambda} b_4(x, y) \frac{\partial b_3(x, y)}{\partial x} d\Lambda, \quad (28f)$$

$$K_{41} = \iint_{\Lambda} b_1(x, y) \frac{\partial b_4(x, y)}{\partial x} d\Lambda + \iint_{\Lambda} b_2(x, y) \frac{\partial b_4(x, y)}{\partial x} d\Lambda, \quad (28g)$$

$$K_{44} = \iint_{\Lambda} b_3(x, y) \frac{\partial b_4(x, y)}{\partial x} d\Lambda + \iint_{\Lambda} b_4(x, y) \frac{\partial b_4(x, y)}{\partial x} d\Lambda. \quad (28h)$$

### 3 CONSTRUCTING THE BASIS FUNCTIONS

The requirements for proper basis functions were given in Table 1. Wachspress rational basis functions fulfill all of these requirements, and may be applied to any convex polygon or polyhedron of unlimited order, as well as to certain polycons (two-dimensional shapes with curved sides) and certain polypols (three-dimensional shapes with curved faces). Bilinear basis functions fulfill these requirements on orthogonal (rectangular) zones. For quadrilaterals, bilinear basis functions are often built and integrated on an orthogonal zone in an isoparametric space, and then mapped onto a quadrilateral in Cartesian space using a coordinate transformation matrix.

We will present the bilinear basis functions in isoparametric space, and two methods for constructing Wachspress rational functions in Cartesian space. The first method we call the direct method. This method is an implementation of the algorithm suggested by Wachspress [Wac 75], and results in equations of the same form as those in Wachspress's book. However, the applicability of the algorithm presented here is limited to quadrilaterals. Constructing the denominator of the Wachspress rational function via the direct method becomes difficult for higher order shapes due to the non-linearity of the external diameter (explained in Section 3.2). The second method we present is Dasgupta's construction method [Das 03a], which outlines a new methodology for constructing Wachspress rational basis functions on arbitrary polygonal zones.

#### 3.1 Bilinear Functions in Isoparametric Space

Regardless of the shape of the quadrilateral zone in Cartesian space, the zone is mapped such that in isoparametric space it looks identical to Figure 2. The

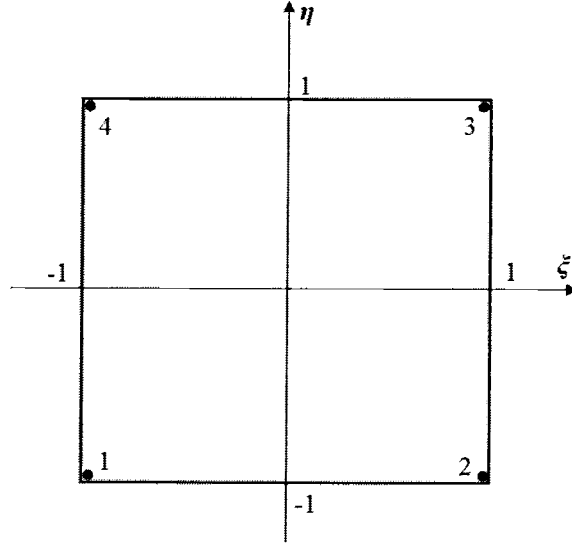


Figure 2: A Quadrilateral Zone Mapped to Isoparametric Space

bilinear basis functions defined in the isoparametric space are [Ada 01]:

$$b_1(\xi, \eta) = \frac{(1 - \xi)(1 - \eta)}{4}, \quad (29a)$$

$$b_2(\xi, \eta) = \frac{(1 + \xi)(1 - \eta)}{4}, \quad (29b)$$

$$b_3(\xi, \eta) = \frac{(1 + \xi)(1 + \eta)}{4}, \quad (29c)$$

$$b_4(\xi, \eta) = \frac{(1 - \xi)(1 + \eta)}{4}. \quad (29d)$$

In Section 4 we will demonstrate how to integrate these basis functions in isoparametric space and then map the integral back to Cartesian space.

### 3.2 Wachspress Rational Functions via the Direct Method

Wachspress rational basis functions are ratios of polynomials. For a polygonal zone with  $F$  sides, the Wachspress rational basis function is of the form [Das 03a]:

$$b_i(x, y) = \frac{P^{(F-2)}(x, y)}{P^{(F-3)}(x, y)}, \quad (30)$$

where  $P^{(m)}$  is a polynomial of degree  $m$  in  $(x, y)$ .

It is the denominator of the rational function that makes Wachspress functions unique, and gives them the ability to fulfill the requirements listed in Table 1 on arbitrary convex polygonal and polyhedral zones. These basis functions can also be constructed on certain polycons and polypols [Wac 75]. Here we present the direct method for building the basis function on a quadrilateral.

We begin by finding a linear equation for each of the four edges of the quadrilateral. The equation for edge  $\lambda_i$  is of the form

$$l_i(x, y) = c_i x + d_i y + e_i. \quad (31)$$

On edge  $\lambda_i$ ,  $l_i(x, y) = 0$ . These equations are not unique; they have three degrees of freedom, but only two are required to determine the line. For the direct method we choose (arbitrarily):

$$d_i = \begin{cases} 0 & : \text{ vertical line segment,} \\ -1 & : \text{ otherwise.} \end{cases} \quad (32)$$

The other constants may then be determined using the positions of the two nodes that the edge connects.

The next step in building a Wachspress rational function is locating the external nodes that determine the external diameter of the zone. By extending the edges of a zone, intersections may be found, as in Figure 3. These intersections are termed external intersection points (EIPs). The external diameter is the segment that connects these points. A quadrilateral will have at most two EIPs, and therefore a linear external diameter.

To find an intersection point for two edges, we describe the two edges using parametric equations. Consider the two line segments in Figure 4. Edge 1 can be described by:

$$x = (x_2 - x_1)s + x_1, \quad (33a)$$

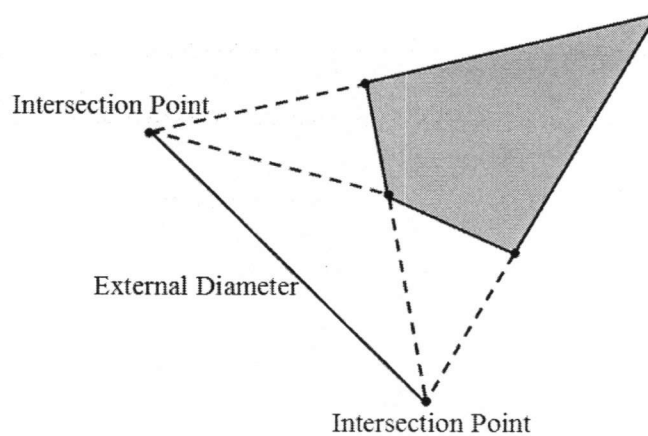


Figure 3: Finding the External Diameter

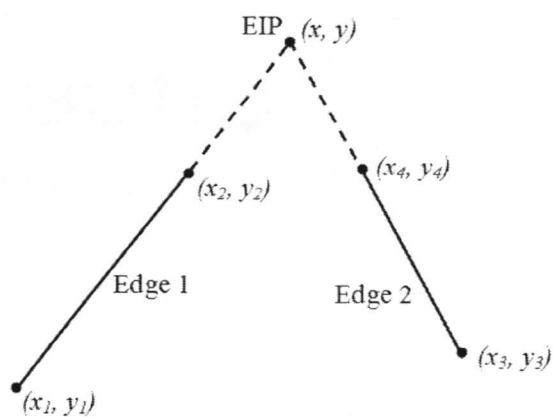


Figure 4: Finding the External Intersection Point

$$y = (y_2 - y_1)s + y_1, \quad (33b)$$

while edge 2 can be described by:

$$x = (x_4 - x_3)t + x_3, \quad (34a)$$

$$y = (y_4 - y_3)t + y_3. \quad (34b)$$

Setting the two  $x$  equations equal to each other, we find

$$s = \frac{(x_4 - x_3)t + (x_3 - x_1)}{(x_2 - x_1)}. \quad (35)$$

Setting the two  $y$  equations equal to each other, and substituting in Eq. (35) gives us

$$t = \frac{(y_3 - y_1)(x_2 - x_1) + (y_1 - y_2)(x_3 - x_1)}{(y_2 - y_1)(x_4 - x_3) + (x_1 - x_2)(y_4 - y_3)}. \quad (36)$$

Substituting  $t$  into Eqs. (34) gives us the location of the intersection point. After we have found both external intersection points, the equation for the external diameter may be found just as the equation for each edge of the zone was found.

A proper basis will interpolate a uniform field exactly; therefore [Das 03a],

$$\sum_i b_i(x, y) = 1. \quad (37)$$

Wachspress rational basis functions are always anchored to a corner. By normalizing the function to unity at its anchor corner, we will enforce Eq. (37). Since each function is anchored to a single corner, and each corner is anchor to only one function, the number of basis functions in a zone is equal to the number of corners in the zone (in this case, four). Therefore, we must build four basis functions in each quadrilateral zone. The equation for the basis function located at node  $i$ , as given in [Wac 75], is

$$b_i = k_i \frac{l_{opp1}(x, y) l_{opp2}(x, y)}{l_{ext}(x, y)}, \quad (38)$$

where  $l_{opp1}(x, y)$  is the equation for one line segment opposite (not containing as an endpoint) node  $i$ , and  $l_{opp2}(x, y)$  is the equation for the other line segment opposite node  $i$ . The function  $l_{ext}(x, y)$  is the equation of the external diameter line segment, and  $k_i$  is a normalization constant, which normalizes the basis function to unity at its corner. After the equations for the edges and the external diameter have been determined,  $k_i$  may be calculated:

$$k_i = \frac{l_{ext}(x_i, y_i)}{l_{opp1}(x_i, y_i) l_{opp2}(x_i, y_i)}, \quad (39)$$

where  $(x_i, y_i)$  are the coordinates of node  $i$ .

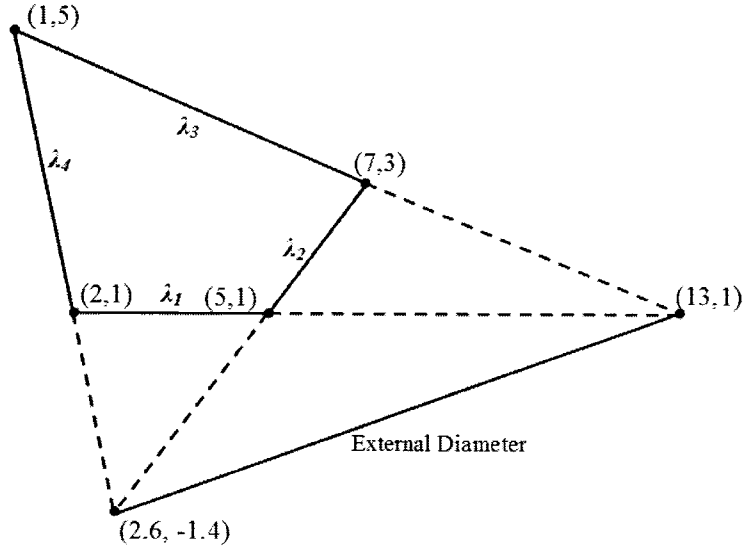


Figure 5: Wachspress Rational Function Construction Example

As an example, consider the zone pictured in Figure 5. The equations for the edges are:

$$l_1(x, y) = -y + 1, \quad (40a)$$

$$l_2(x, y) = x - y - 4, \quad (40b)$$

$$l_3(x, y) = -0.33333x - y + 5.33333, \quad (40c)$$

$$l_4(x, y) = -4x - y + 9. \quad (40d)$$



and the equation for the external diameter is

$$l_{ext}(x, y) = 0.23077x - y - 2. \quad (41)$$

To calculate the normalization coefficient, we set each basis function to unity at its anchor corner and solve for  $k$ :

$$k_1 = \frac{l_{ext}(2, 1)}{l_2(2, 1) l_3(2, 1)} = 0.230769, \quad (42a)$$

$$k_2 = \frac{l_{ext}(4, 1)}{l_3(4, 1) l_4(4, 1)} = 0.057692, \quad (42b)$$

$$k_3 = \frac{l_{ext}(6, 3)}{l_4(6, 3) l_1(6, 3)} = -0.076923, \quad (42c)$$

$$k_4 = \frac{l_{ext}(1, 6)}{l_1(1, 6) l_2(1, 6)} = -0.211538, \quad (42d)$$

The complete definitions of the basis functions are:

$$b_1(x, y) = 0.230769 \frac{(x - y - 4)(-0.33333x - y + 5.33333)}{0.23077x - y - 2}, \quad (43a)$$

$$b_2(x, y) = 0.057692 \frac{(-0.33333x - y + 5.33333)(-4x - y + 9)}{0.23077x - y - 2}, \quad (43b)$$

$$b_3(x, y) = -0.076923 \frac{(-4x - y + 9)(-y + 1)}{0.23077x - y - 2}, \quad (43c)$$

$$b_4(x, y) = -0.211538 \frac{(-y + 1)(x - y - 4)}{0.23077x - y - 2}. \quad (43d)$$

Basis function  $b_1(x, y)$  is shown in Figure 6.

There are four special cases that must be considered. The first case is that of the trapezoid (see Figure 7), where only one external intersection point exists. In this case, the external diameter is parallel to the two parallel edges composing the trapezoid.

The second case is that of the parallelogram, in which all edges are parallel, and hence there are no external nodes or diameters. In this case, the equation for

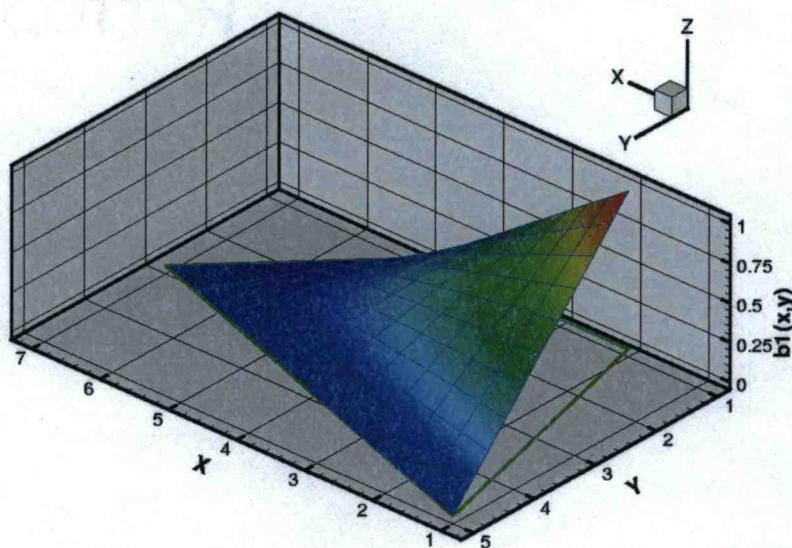


Figure 6: A Wachspress Rational Function

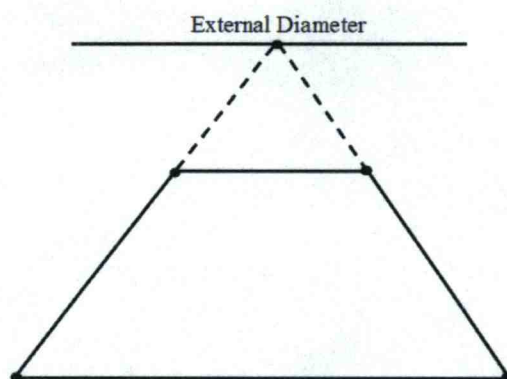


Figure 7: A Trapezoidal Zone and its External Diameter

the external diameter is set equal to unity, and the Wachspress rational functions simplify to the bilinear basis functions in Cartesian geometry.

The third and fourth special cases occur when the quadrilateral collapses into a triangle, as in Figure 8. This can occur when three nodes are co-linear, or when two nodes are on top of each other.

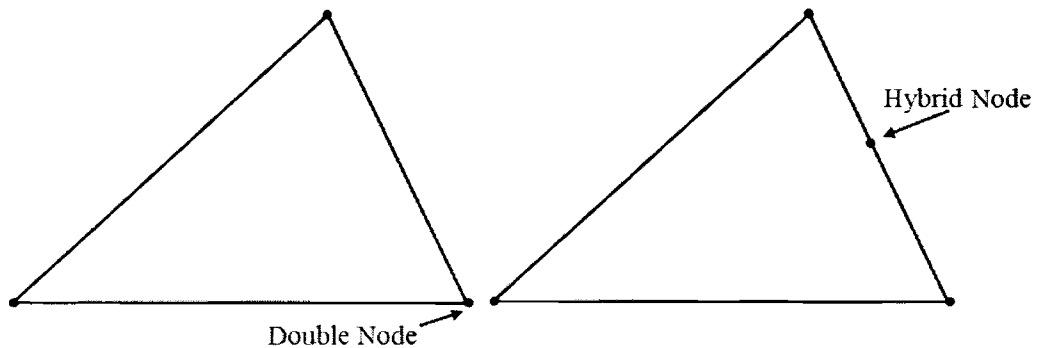


Figure 8: Pathological Zones

The zone on the left in Figure 8 has a double node, is not compatible with quadrilateral finite elements, and may have to be recognized by the code in a preprocessing step. The zone on the right contains a hybrid node. Rational basis functions may be built at these hybrid nodes, but the method to do so is beyond the scope of this study.

We should note that the direct method, as given above, is much more complicated to implement for zones with more than four edges. Consider the pentagonal zone in Figure 9. Here we can see that a general pentagonal zone has five external intersection points. The external diameter is no longer linear (and is no longer simple to calculate), but is instead a second-order conic. Although it is possible to calculate this curve, Dasgupta [Das 03a] has discovered an alternative formulation for the denominator of a Wachspress rational function that does not require finding the external diameter.

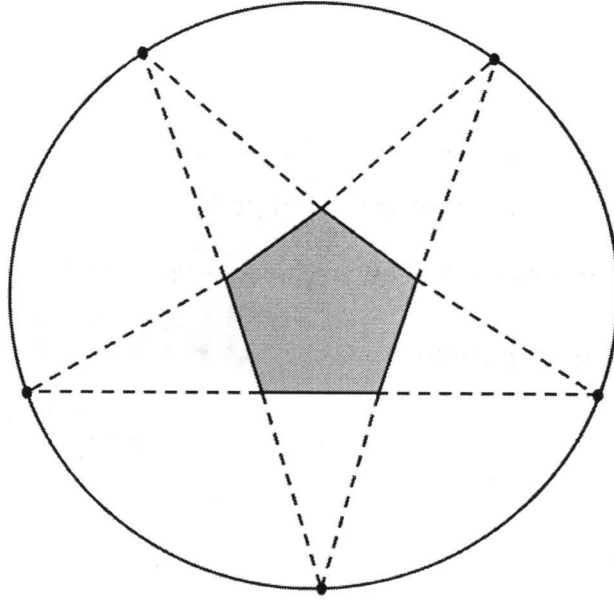


Figure 9: A Pentagonal Zone and its External Diameter

### 3.3 Wachspress Rational Functions via Dasgupta's Method

We will now summarize Dasgupta's method for constructing Wachspress rational basis functions. This algorithm is presented in [Das 03a]. Suppose we have a convex polygon with  $F$  cyclically ordered nodes. A line segment  $\lambda_i$  con-

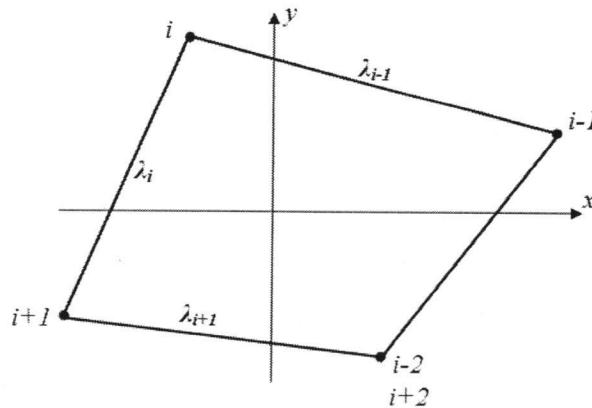


Figure 10: Cyclical Ordering of Nodes

nects nodes  $i$  and  $i+1$ . Therefore,  $\lambda_F$  connects nodes  $F$  and 1. As before, we wish to find a linear equation to describe each edge of the zone. As for the di-

rect method, we know that a given line segment can be described by the equation  $l_i(x, y) = c_i x + d_i y + e_i$ . If we translate the coordinates of the zone such that the origin falls interior to the zone, then we know that the equation for segment  $\lambda_i$  can be written uniquely as

$$l_i(x, y) = 1 - c_i x - d_i y = 0, \quad (44)$$

where  $l_i(x, y) > 0$  everywhere within the zone, and where the coefficients  $c_i$  and  $d_i$  are determined by

$$c_i = \frac{y_{i+1} - y_i}{x_i y_{i+1} - x_{i+1} y_i}, \quad (45a)$$

and

$$d_i = \frac{x_i - x_{i+1}}{x_i y_{i+1} - x_{i+1} y_i}. \quad (45b)$$

As with the direct method, each basis function is anchored to a single corner. Forming the numerator is identical; it is proportional to the product of the equations for all of the line segments opposite (not containing as an endpoint) the corner upon which the function is anchored:

$$Num_i(x, y) \propto \prod_{\substack{j=F \\ j \neq i-1 \\ j \neq i}}^{j=F} l_j(x, y). \quad (46)$$

This forces the function to be zero on all of the opposite edges. Now recall that a proper basis function will interpolate a uniform field exactly. This means we must weight our basis functions,

$$b_i(x, y) = \frac{1}{\varphi_i(x, y)} \prod_{\substack{j=F \\ j \neq i-1 \\ j \neq i}}^{j=F} l_j(x, y). \quad (47)$$

We will then relate our weight functions through scalar weights  $\kappa_i$ :

$$\varphi_i(x, y) = \frac{\varphi_0(x, y)}{\kappa_i}. \quad (48)$$

Now we have

$$\frac{1}{\varphi_0(x, y)} \sum_{i=1}^F \left( \kappa_i \prod_{\substack{j=1 \\ j \neq i-1 \\ j \neq i}}^F l_j(x, y) \right) = 1. \quad (49)$$

The weights  $\kappa_i$  are relative weights, and we therefore choose (arbitrarily)  $\kappa_1 = 1$ .

The weight function  $\varphi_0(x, y)$  can now be written

$$\varphi_0(x, y) = \sum_{i=1}^F \left( \kappa_i \prod_{\substack{j=1 \\ j \neq i-1 \\ j \neq i}}^F l_j(x, y) \right) = \sum_{i=1}^F Num_i(x, y). \quad (50)$$

We must now select our  $\kappa_i$  so that  $\varphi_0(x, y)$  is the algebraic curve through the external intersection points, i.e., the external diameter. The direct method calculates the equation for this curve (or line, in the case of a quadrilateral) directly. However, the number of external intersection points in a polygon with  $F$  sides is  $(F^2 - 3F)/2$  [Das 03a], and the external diameter for such a polygon is an order  $F-3$  polynomial in  $(x, y)$ . Finding this curve can be complex for any polygon with more than four sides. Dasgupta found an alternative method for calculating the coefficients  $\kappa_i$ .

Consider a particular basis function  $b_i(x, y)$ . Its form is

$$b_i(x, y) = \frac{\kappa_i \prod_{\substack{j=1 \\ j \neq i-1 \\ j \neq i}}^F l_j(x, y)}{\varphi_0(x, y)}. \quad (51)$$

If we examine  $b_i(x, y)$  along edge  $\lambda_i$ , where it is linear, then all terms in  $\varphi_0(x, y)$  containing  $l_i(x, y)$  will vanish because this function is zero along this edge. In addition, after canceling out shared linear terms in the numerator and denominator, basis  $b_i(x, y)$  along edge  $\lambda_i$  will simplify to

$$b_i(x, y)|_{l_i=0} = \frac{\kappa_i l_{i+1}(x, y)}{\kappa_i l_{i+1}(x, y) + \kappa_{i+1} l_{i-1}(x, y)}. \quad (52)$$

If we insert Eq. (44) into Eq. (52) we have

$$b_i(x, y)|_{l_i=0} = \frac{\kappa_i (1 - c_{i+1}x - d_{i+1}y)}{\kappa_i (1 - c_{i+1}x - d_{i+1}y) + \kappa_{i+1} (1 - c_{i-1}x - d_{i-1}y)}. \quad (53)$$

Recall in Table 1 that we require the basis functions to be linear on the boundary.

In general, Eq. (53) will not be linear because of the terms in the denominator.

However, if we can find values of  $\kappa_i$  and  $\kappa_{i+1}$  such that

$$\kappa_i (1 - c_{i+1}x - d_{i+1}y) + \kappa_{i+1} (1 - c_{i-1}x - d_{i-1}y) = \text{constant}, \quad (54)$$

then the basis function will possess the proper behavior.

Along  $\lambda_i$ , a given point can be determined by the parametric equations

$$x = x_i + (x_{i+1} - x_i)t, \quad (55a)$$

and

$$y = y_i + (y_{i+1} - y_i)t. \quad (55b)$$

Substituting this into Eq. (54) gives

$$\begin{aligned} & (\kappa_i + \kappa_{i+1} - \kappa_i c_{i+1}x_i - \kappa_i d_{i+1}y_i - \kappa_{i+1}c_{i-1}x_i - \kappa_{i+1}d_{i-1}y_i) \\ & + t (-\kappa_i c_{i+1}x_{i+1} + \kappa_i c_{i+1}x_i - \kappa_i d_{i+1}y_{i+1} + \kappa_i d_{i+1}y_i) \\ & + t (-\kappa_{i+1}c_{i-1}x_{i+1} + \kappa_{i+1}c_{i-1}x_i - \kappa_{i+1}d_{i-1}y_{i+1} + \kappa_{i+1}d_{i-1}y_i) = \text{constant}. \end{aligned} \quad (56)$$

This term is constant only when the coefficient of  $t$  equals zero, which is when

$$\kappa_{i+1} = \kappa_i \left( \frac{c_{i+1}(x_i - x_{i+1}) + d_{i+1}(y_i - y_{i+1})}{c_{i-1}(x_{i+1} - x_i) + d_{i-1}(y_{i+1} - y_i)} \right). \quad (57)$$

We will now summarize the algorithm for constructing Wachspress rational functions on a convex polygon with  $F$  sides using Dasgupta's method. First, select the origin to be an interior point within the polygon. The nodes are numbered

cyclically and clockwise from 1 to  $F$ . An edge  $\lambda_i$  is defined to connect nodes  $i$  and  $i+1$ . The equation for this edge is

$$l_i(x, y) = 1 - c_i x - d_i y, \quad (58)$$

where

$$c_i = \frac{y_{i+1} - y_i}{x_i y_{i+1} - x_{i+1} y_i}, \quad (59a)$$

and

$$d_i = \frac{x_i - x_{i+1}}{x_i y_{i+1} - x_{i+1} y_i}. \quad (59b)$$

The basis function is defined by

$$b_i(x, y) = \frac{Num_i(x, y)}{\varphi_0(x, y)}, \quad (60)$$

where

$$\varphi_0(x, y) = \sum_i Num_i(x, y), \quad (61)$$

and the numerator terms are defined by

$$Num_i(x, y) = \kappa_i \prod_{\substack{j=F \\ j \neq i-1 \\ j \neq i}}^{j=F} l_j(x, y). \quad (62)$$

The equations for the weights are

$$\kappa_1 = 1, \quad (63a)$$

and

$$\kappa_i = \kappa_{i-1} \left( \frac{c_i (x_{i-1} - x_i) + d_i (y_{i-1} - y_i)}{c_{i-2} (x_i - x_{i-1}) + d_{i-2} (y_i - y_{i-1})} \right). \quad (63b)$$

These equations are valid for all convex polygons with  $n \geq 3$ .



### 3.4 Comparing the Direct Method and Dasgupta's Method

The preceeding subsections detailing the direct method and Dasgupta's method present an obvious question: which method is superior? Table 2 gives wall-clock times for the direct method and Dasgupta's method for a varying number of quadrilateral zones. These tests were run on a 750 MHz Sun UltraSPARC III CPU.

Number of Zones	Direct Method [s]	Dasgupta's Method [s]
10,000	0.50	0.72
100,000	5.13	7.45
1,000,000	51.17	74.63

Table 2: Comparison Between the Direct Method and Dasgupta's Method

Here we can see that the direct method is roughly forty-five percent faster than Dasgupta's method. For this reason, we have used the direct method when constructing the basis functions for our results. However, the complexity of the direct method grows enormously when quadrilaterals are not used. For this reason, we recommend using Dasgupta's construction method for finite-element codes when zones other than quadrilaterals are used. Finally, we point out that both the direct method and Dasgupta's method are inherently parallel.

## 4 INTEGRATING THE BASIS

Recall from Section 2 that there are two types of integrals that must be calculated. The first type involve basis functions integrated over the area of the zone. These integrals are

$$\iint_{\Lambda} b_i(x, y) b_j(x, y) d\Lambda, \quad (64a)$$

$$\iint_{\Lambda} b_j(x, y) \frac{\partial}{\partial x} b_i(x, y) d\Lambda, \quad (64b)$$

and

$$\iint_{\Lambda} b_j(x, y) \frac{\partial}{\partial y} b_i(x, y) d\Lambda. \quad (64c)$$

The second type is integrals over the edges of a zone,

$$\int_{\lambda} b_i(x, y) b_j(x, y) d\lambda, \quad (65a)$$

and

$$\int_{\lambda} b_i(x, y) d\lambda. \quad (65b)$$

In this section, we will investigate methods to perform both types of integrals.

### 4.1 Integrals Over the Zone Area

In Section 3 we present two different basis functions: bilinear basis functions, which we built in an isoparametric space, and Wachspress rational basis functions, which we built in Cartesian space. We will look at performing areal integrals of these two bases separately.

#### 4.1.1 Integrals of Isoparametric Bilinear Functions

The purpose of an isoparametric mapping is to take any arbitrary quadrilateral zone, and map it onto a new coordinate system so that in the new mapping

it is a square (see Figure 2). Although bilinear basis functions cannot be built upon general quadrilaterals, they can be constructed on squares (and rectangles). However, this is not useful unless we have some way to map the integrals of these bilinear basis functions back into Cartesian space. We can use the rules of calculus to create a transformation matrix from one coordinate system to another. The derivatives of a basis function in the transformed  $(\xi, \eta)$  space can be written as [Zie 00]:

$$\frac{\partial b_i}{\partial \xi} = \frac{\partial b_i}{\partial x} \frac{\partial x}{\partial \xi} + \frac{\partial b_i}{\partial y} \frac{\partial y}{\partial \xi}, \quad (66a)$$

and

$$\frac{\partial b_i}{\partial \eta} = \frac{\partial b_i}{\partial x} \frac{\partial x}{\partial \eta} + \frac{\partial b_i}{\partial y} \frac{\partial y}{\partial \eta}. \quad (66b)$$

In matrix form, we write

$$\begin{bmatrix} \frac{\partial b_i}{\partial \xi} \\ \frac{\partial b_i}{\partial \eta} \end{bmatrix} = \begin{bmatrix} \frac{\partial x}{\partial \xi} & \frac{\partial y}{\partial \xi} \\ \frac{\partial x}{\partial \eta} & \frac{\partial y}{\partial \eta} \end{bmatrix} \begin{bmatrix} \frac{\partial b_i}{\partial x} \\ \frac{\partial b_i}{\partial y} \end{bmatrix} = \underline{\underline{J}} \begin{bmatrix} \frac{\partial b_i}{\partial x} \\ \frac{\partial b_i}{\partial y} \end{bmatrix}, \quad (67)$$

where matrix  $\underline{\underline{J}}$  is termed the Jacobian matrix. We can write this matrix in terms of the isoparametric spatial functions (which are identical to the bilinear basis functions in an isoparametric zone) and the node positions in the zone:

$$\underline{\underline{J}} = \begin{bmatrix} \frac{\partial N_1}{\partial \xi} & \frac{\partial N_2}{\partial \xi} & \frac{\partial N_3}{\partial \xi} & \frac{\partial N_4}{\partial \xi} \\ \frac{\partial N_1}{\partial \eta} & \frac{\partial N_2}{\partial \eta} & \frac{\partial N_3}{\partial \eta} & \frac{\partial N_4}{\partial \eta} \end{bmatrix} \begin{bmatrix} x_1 & y_1 \\ x_2 & y_2 \\ x_3 & y_3 \\ x_4 & y_4 \end{bmatrix}. \quad (68)$$

Using this, we can now write [Zie 00]:

$$dx dy = \det \underline{\underline{J}} d\xi d\eta. \quad (69)$$

The Jacobian matrix allows us to transform integrals from one coordinate space to another. This enables us to integrate basis functions in the isoparametric space, and then map the integral into Cartesian space. If the integral contains derivatives,

then these too must be mapped into the Cartesian space, via

$$\begin{bmatrix} \frac{\partial b_i}{\partial x} \\ \frac{\partial b_i}{\partial y} \end{bmatrix} = \underline{\underline{J}}^{-1} \begin{bmatrix} \frac{\partial b_i}{\partial \xi} \\ \frac{\partial b_i}{\partial \eta} \end{bmatrix}. \quad (70)$$

The Jacobian matrix is small enough that we can calculate its inverse directly,

$$\underline{\underline{J}}^{-1} = \begin{bmatrix} \frac{J_{2,2}}{\det \underline{\underline{J}}} & \frac{-J_{1,2}}{\det \underline{\underline{J}}} \\ \frac{-J_{2,1}}{\det \underline{\underline{J}}} & \frac{J_{1,1}}{\det \underline{\underline{J}}} \end{bmatrix}. \quad (71)$$

We now have everything we need to calculate the three areal integrals. The isoparametric bilinear integrals are

$$\iint_{\Lambda} b_i(x, y) b_j(x, y) \, dx dy = \int_{-1}^1 \int_{-1}^1 b_i(\xi, \eta) b_j(\xi, \eta) \det \underline{\underline{J}} \, d\xi d\eta, \quad (72a)$$

$$\iint_{\Lambda} b_j(x, y) \frac{\partial}{\partial x} b_i(x, y) \, dx dy =$$

$$\int_{-1}^1 \int_{-1}^1 b_j(\xi, \eta) \left( \frac{J_{2,2}}{\det \underline{\underline{J}}} \frac{\partial}{\partial \xi} - \frac{J_{1,2}}{\det \underline{\underline{J}}} \frac{\partial}{\partial \eta} \right) b_i(\xi, \eta) \, d\xi d\eta, \quad (72b)$$

and

$$\iint_{\Lambda} b_j(x, y) \frac{\partial}{\partial y} b_i(x, y) \, dx dy =$$

$$\int_{-1}^1 \int_{-1}^1 b_j(\xi, \eta) \left( \frac{-J_{2,1}}{\det \underline{\underline{J}}} \frac{\partial}{\partial \xi} + \frac{J_{1,1}}{\det \underline{\underline{J}}} \frac{\partial}{\partial \eta} \right) b_i(\xi, \eta) \, d\xi d\eta. \quad (72c)$$

These integrals may now be evaluated using a Gauss-Legendre quadrature set. Numerical integration approximates the integral by summing the products of the function and weighted values at the points given in the quadrature set:

$$\int_{-1}^1 \int_{-1}^1 F(\xi, \eta) \, d\xi d\eta = \sum_{i=1}^N \sum_{j=1}^N H_i H_j F(\xi_i, \eta_j). \quad (73)$$

Here,  $H$  refers to the weight for the particular quadrature point, and  $N$  is the number of quadrature points.  $F(\xi_i, \eta_j)$  is the integrand in Eqs. (72).

#### 4.1.2 *Isoparametric Mapping of Wachspress Rational Basis Functions*

The bilinear basis functions were built and integrated in isoparametric space, and the integral was then mapped into Cartesian space. In contrast, the Wachspress rational functions are constructed in Cartesian space, and we can integrate these functions by mapping them into an isoparametric space, integrating them in that space, and then mapping that integral back into Cartesian space.

The generality of quadrilateral zones requires that we perform numerical integrations. Because these functions are readily evaluated, they are ideal for Gauss-Legendre quadrature. However, it is not possible to create a quadrature set that will correctly integrate over an arbitrary quadrilateral. For this reason, we will map the function onto the isoparametric square (see Section 4.1.1). We can integrate the function using a quadrature set defined for the square, using Eq. (73), and then map back into the Cartesian space.

Again, as in Section 4.1.1 we define the Jacobian matrix using Eq. (68). Any  $(x, y)$  coordinates can be found from a given set of  $(\xi, \eta)$  coordinates using a superposition of the the isoparametric shape functions and the node positions [Zie 00]:

$$x = N_1(\xi, \eta)x_1 + N_2(\xi, \eta)x_2 + N_3(\xi, \eta)x_3 + N_4(\xi, \eta)x_4, \quad (74a)$$

$$y = N_1(\xi, \eta)y_1 + N_2(\xi, \eta)y_2 + N_3(\xi, \eta)y_3 + N_4(\xi, \eta)y_4. \quad (74b)$$

The final form of the integral becomes

$$\iint_{\Lambda} F(x, y) d\Lambda = \int_{-1}^1 \int_{-1}^1 F(x(\xi, \eta), y(\xi, \eta)) d\xi d\eta =$$

$$\sum_{i=1}^N \sum_{j=1}^N H_i H_j F(x(\xi_i, \eta_j), y(\xi_i, \eta_j)) \det \underline{\underline{J}}, \quad (75)$$

where

$$F(x, y) = \begin{cases} \iint_{\Lambda} b_i(x, y) b_j(x, y) d\Lambda, \\ \iint_{\Lambda} b_j(x, y) \frac{\partial}{\partial x} b_i(x, y) d\Lambda, \\ \iint_{\Lambda} b_j(x, y) \frac{\partial}{\partial y} b_i(x, y) d\Lambda, \end{cases} \quad (76)$$

depending on the areal integral desired.

#### 4.1.3 Dasgupta's Integration Method

Dasgupta [Das 03b] has proposed an alternative method for integrating functions over polygonal regions. The concept behind this method is to repeatedly apply the divergence theorem to convert integrals in  $\mathcal{R}^n$  space into a series of line integrals over the boundary of that space, provided the boundary of that space is linear (not curved). We shall summarize from this paper the method by which integrals over two-dimensional polygons can be evaluated as a series of line integrals over the boundary of the polygon. Note that this work is not limited to two-dimensions, however. Polyhedral and higher-order spaces may also be integrated by this method.

Consider the following integral:

$$\iint_{\Lambda} v(x, y) d\Lambda. \quad (77)$$

We define a vector function  $\hat{\theta}$  as

$$\iint_{\Lambda} v(x, y) d\Lambda = \int_{\lambda} \hat{\theta} \cdot \hat{\mathbf{n}} d\lambda, \quad (78)$$

where

$$\hat{\theta} = \theta_1 \hat{i} + \theta_2 \hat{j}, \quad (79)$$

and

$$\hat{\mathbf{n}} = n_1 \hat{i} + n_2 \hat{j}. \quad (80)$$

In addition,

$$\theta_1(x, y) = \int v(x, y) dx + c(y), \quad (81)$$

where  $c(y)$  is arbitrary, and

$$\theta_2(x, y) = 0. \quad (82)$$

We now wish to prove that

$$\int_{\lambda} c(y) \hat{i} \cdot \hat{\mathbf{n}} d\lambda = \int_{\lambda} c(y) n_1 d\lambda = 0. \quad (83)$$

To facilitate this, we reproduce a diagram in Figure 11 found in [Das 03b]. We

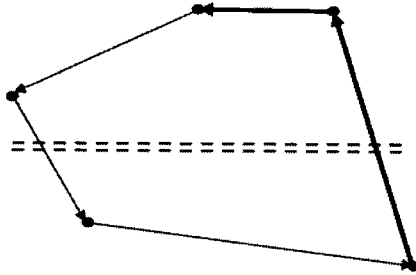


Figure 11: Path Element in Surface Integral

know that  $n_1$  is the cosine of the angle between the outward normal of  $\lambda$  and  $\hat{i}$ . We shall split the surface into two parts,  $\lambda^+$ , where  $n_1$  is positive, and  $\lambda^-$ , where  $n_1$  is negative. In Figure 11,  $\lambda^+$  is shown using thick line segments, while  $\lambda^-$  is shown using thin line segments.

In Figure 12, we see an enlarged view of  $\lambda^+$  between the dashed lines. Looking at this figure, we can see that  $n_1 = \cos(\gamma)$  and that  $\partial\lambda_0 = \partial\lambda \cos(\gamma)$ . Now, in Eq. (83) the value  $n_1 d\lambda$  will be  $\lambda_0$  where  $n_1$  is positive, and  $-\lambda_0$  where  $n_1$  is negative. The value of  $c(y)$  will be the same,  $c(y_0)$ , everywhere along the horizontal dashed lines. Therefore,

$$n_1 c(y) d\lambda = n_1 c(y) d\lambda^+ + n_1 c(y) d\lambda^- = c(y_0) d\lambda_0 - c(y_0) d\lambda_0 = 0. \quad (84)$$

Summed over the entire (closed) boundary  $\lambda$  the net contribution of  $n_1 c(y) d\lambda$  is zero. Therefore,

$$\theta_1(x, y) = \int v(x, y) dx. \quad (85)$$

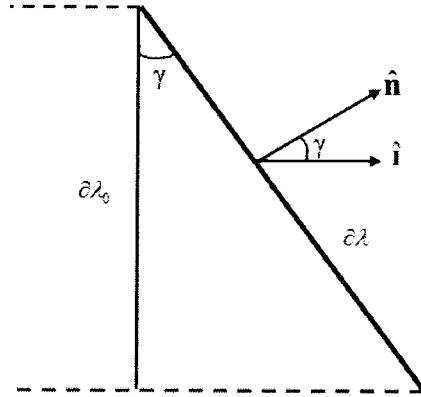


Figure 12: Closeup of Figure 11,  $\lambda^+$  Surface Between Dashed Lines

From the conclusions above, we now have

$$\iint_{\Lambda} v(x, y) d\Lambda = \int_{\lambda} \theta_1(x, y) n_1 d\lambda. \quad (86)$$

The boundary of a polygon is a set of line segments. Therefore,

$$\int_{\lambda} \theta_1(x, y) n_1 d\lambda = \sum_{f=1}^F \int_{\lambda_f} \theta_1(x, y) n_1^{(f)} d\lambda. \quad (87)$$

We have now successfully converted an areal integral of an arbitrary function into a sum of line integrals around the linear boundaries of the area. The line



integrals can be carried out using a Gauss-Legendre quadrature if the line integral is mapped into the correct range (for instance, zero to one). Consider an integral

$$\int_0^{|\lambda|} \theta(x, y) \cos(\gamma) d\lambda, \quad (88)$$

between nodal points  $(x_1, y_1)$  and  $(x_2, y_2)$  that are  $|\lambda|$  apart. Recall that  $n_1 = \cos(\gamma)$ . We can define this range using the parametric equations

$$x = x_1 + \tau(x_2 - x_1) \quad (89a)$$

and

$$y = y_1 + \tau(y_2 - y_1), \quad (89b)$$

where

$$\tau = \frac{x - x_1}{x_2 - x_1} = \frac{y - y_1}{y_2 - y_1}. \quad (90)$$

Also,

$$\cos(\gamma) = \frac{y_2 - y_1}{|\lambda|} \quad (91)$$

and

$$d\lambda = |\lambda| d\tau. \quad (92)$$

Plugging all of these into Eq. (88) gives

$$\int_0^{|\lambda|} \theta(x, y) \cos(\gamma) d\lambda = (y_2 - y_1) \int_0^1 \theta[x_1 + \tau(x_2 - x_1), y_1 + \tau(y_2 - y_1)] d\tau. \quad (93)$$

All of the preceding analysis is summarized and adapted from [Das 03b]. This procedure is simple to understand and performing the line integrals using a Gauss-Legendre quadrature is trivial. The principle difficulty lies in calculating the indefinite integral

$$\theta_1(x, y) = \int v(x, y) dx. \quad (94)$$

Products of Wachspress rational basis functions (and their derivatives) are so algebraically complex that calculating and implementing the above equation in a code

is extremely difficult, if not impossible, for general polygons. Dasgupta recommends using a dynamic computer algebra system such as Mathematica. However, it is unlikely that using Mathematica to calculate all of the integrals necessary for a typical transport problem (involving millions of zones or more) could be accomplished in an acceptable amount of time.

We have presented two methods for integrating Wachspress rational basis functions. The first method involves mapping the quadrilateral onto an isoparametric square and is limited in practicability because the isoparametric mapping is only available to quadrilaterals; it cannot be extended to other polygons. Dasgupta's method works for any polygon, and can also be extended to polyhedra, but the algebraic complexity of Wachspress rational functions probably preclude this method from being useful in an industrial transport code. More research is needed in this area.

## 4.2 Edge Integrals

One of the requirements set down for "proper" basis functions (which include both the bilinear and Wachspress rational basis functions) in Table 1 is that they are always equal to unity at their anchor node, and zero at all other nodes. They decrease linearly along the edge of the zone, as in Figure 13.

Given an edge  $\lambda_i$  connecting nodes  $N_i$  and  $N_{i+1}$ , the basis functions which are nonzero along this edge are  $b_i(x, y)$  and  $b_{i+1}(x, y)$ . The basis functions along the edge may be written as

$$b_i(s) = \frac{|\lambda_i| - s}{|\lambda_i|}, \quad (95a)$$

and

$$b_{i+1}(s) = \frac{s}{|\lambda_i|}, \quad (95b)$$

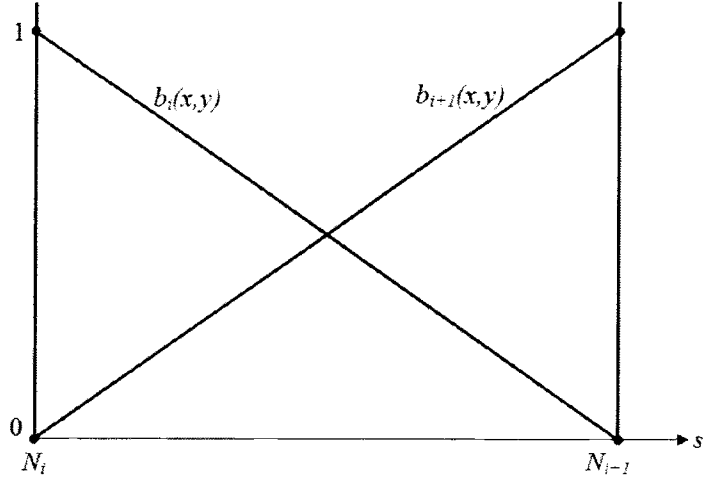


Figure 13: Basis Functions as Seen from Zone Edge

where coordinate  $s$  has its origin at node  $N_i$  and points towards node  $N_{i+1}$ . The length of edge  $\lambda_i$  is  $|\lambda_i|$ .

Recall from Section 2 that there are three surface integrals we wish to compute. The analytic solutions to these integrals are given below:

$$\int_0^{|\lambda_i|} b_i(s)b_i(s) ds = \int_0^{|\lambda_i|} \frac{(|\lambda_i| - s)^2}{|\lambda_i|^2} ds = \frac{|\lambda_i|}{3}, \quad (96a)$$

$$\int_0^{|\lambda_i|} b_i(s)b_{i+1}(s) ds = \int_0^{|\lambda_i|} \frac{s(|\lambda_i| - s)}{|\lambda_i|^2} ds = \frac{|\lambda_i|}{6}, \quad (96b)$$

and

$$\int_0^{|\lambda_i|} b_i(s) ds = \int_0^{|\lambda_i|} \frac{|\lambda_i| - s}{|\lambda_i|} ds = \frac{|\lambda_i|}{2}. \quad (96c)$$

Using these equations, we know that the unlumped surface matrices are

$$\underline{\underline{N}} = \begin{bmatrix} \frac{|\lambda_1|}{3} & \frac{|\lambda_1|}{6} & 0 & 0 \\ \frac{|\lambda_1|}{6} & \frac{|\lambda_1|}{3} & 0 & 0 \\ 0 & 0 & \frac{|\lambda_3|}{3} & \frac{|\lambda_3|}{6} \\ 0 & 0 & \frac{|\lambda_3|}{6} & \frac{|\lambda_3|}{3} \end{bmatrix} \quad (97a)$$

and

$$\underline{\underline{U}} = \begin{bmatrix} \frac{|\lambda_4|}{3} & 0 & 0 & \frac{|\lambda_4|}{6} \\ 0 & \frac{|\lambda_2|}{3} & \frac{|\lambda_2|}{6} & 0 \\ 0 & \frac{|\lambda_2|}{6} & \frac{|\lambda_2|}{3} & 0 \\ \frac{|\lambda_4|}{6} & 0 & 0 & \frac{|\lambda_4|}{3} \end{bmatrix}. \quad (97b)$$

The lumped surface matrices are

$$\underline{\underline{N}} = \begin{bmatrix} \frac{|\lambda_1|}{2} & 0 & 0 & 0 \\ 0 & \frac{|\lambda_1|}{2} & 0 & 0 \\ 0 & 0 & \frac{|\lambda_3|}{2} & 0 \\ 0 & 0 & 0 & \frac{|\lambda_3|}{2} \end{bmatrix} \quad (98a)$$

and

$$\underline{\underline{U}} = \begin{bmatrix} \frac{|\lambda_4|}{2} & 0 & 0 & 0 \\ 0 & \frac{|\lambda_2|}{2} & 0 & 0 \\ 0 & 0 & \frac{|\lambda_2|}{2} & 0 \\ 0 & 0 & 0 & \frac{|\lambda_4|}{2} \end{bmatrix}. \quad (98b)$$

## 5 ASYMPTOTIC ANALYSIS

Asymptotic analysis is a tool used to examine the transport equation in the thick, diffusive limit. Consider the exact transport equation,

$$\hat{\Omega} \cdot \nabla \psi + \sigma_t(\mathbf{r}) \psi(\mathbf{r}, \hat{\Omega}) = \frac{1}{4\pi} (\sigma_t(\mathbf{r}) - \sigma_a(\mathbf{r})) \phi(\mathbf{r}) + q(\mathbf{r}, \hat{\Omega}), \quad (99a)$$

$$\phi(\mathbf{r}) = \int_{4\pi} d\Omega \psi(\mathbf{r}, \hat{\Omega}). \quad (99b)$$

We can scale this transport equation with a small parameter  $\epsilon$  such that as  $\epsilon \rightarrow 0$ , the problem will become increasingly optically thick and diffusive. The scaled exact transport equation is

$$\hat{\Omega} \cdot \nabla \psi + \frac{\sigma_t(\mathbf{r})}{\epsilon} \psi(\mathbf{r}, \hat{\Omega}) = \frac{1}{4\pi} \left( \frac{\sigma_t(\mathbf{r})}{\epsilon} - \epsilon \sigma_a(\mathbf{r}) \right) \phi(\mathbf{r}) + \epsilon q(\mathbf{r}, \hat{\Omega}). \quad (100)$$

We will postulate that the solution is a power series in  $\epsilon$ :

$$\psi = \psi^{(0)} + \epsilon \psi^{(1)} + \epsilon^2 \psi^{(2)}, \quad (101a)$$

$$\phi = \phi^{(0)} + \epsilon \phi^{(2)} + \epsilon^2 \phi^{(2)}. \quad (101b)$$

If we substitute the power series expansion of the angular and scalar flux into the scaled transport equation and analyze each power of  $\epsilon$ , we find that the leading order angular flux is isotropic

$$\psi^{(0)}(\mathbf{r}, \hat{\Omega}) = \frac{1}{4\pi} \phi^{(0)}(\mathbf{r}), \quad (102)$$

and satisfies a diffusion equation

$$-\nabla \cdot \frac{1}{3\sigma(\mathbf{r})} \nabla \phi^{(0)} + \sigma_a(\mathbf{r}) \phi^{(0)}(\mathbf{r}) = Q(\mathbf{r}), \quad (103)$$

where

$$Q(\mathbf{r}) = \int_{4\pi} d\Omega q(\mathbf{r}, \hat{\Omega}). \quad (104)$$

The preceding analysis on the exact transport equation was taken from [Ada 01]. A boundary analysis in the thick diffusive limit may also be performed, but we will not show that here.

We wish to examine how our transport discretization (Eq. (20)) performs in the thick diffusive limit. An asymptotic analysis of the discretized transport equation will give us a discretized diffusion equation. Analyzing the structure of the diffusion discretization will tell us whether the transport discretization will perform robustly in the thick diffusive limit. In addition, the diffusion discretization can be used in a diffusion synthetic acceleration (DSA) scheme (see Section 6.1). The asymptotic DSA only requires us to perform an asymptotic analysis on the interior of our problem, so we will neglect the boundary analysis. We begin by scaling Eq. (20) as follows:

$$\sigma_{t,p,q} \rightarrow \frac{\sigma_{t,p,q}}{\epsilon}, \quad (105a)$$

$$\sigma_{s,p,q} \rightarrow \frac{\sigma_{t,p,q}}{\epsilon} - \epsilon \sigma_{a,p,q}, \quad (105b)$$

$$q_{m,p,q} \rightarrow \epsilon q_{m,p,q}. \quad (105c)$$

As  $\epsilon \rightarrow 0$ , the problem will become increasingly optically thick and diffusive. We substitute Eqs. (105) into Eq. (20) giving us

$$\begin{aligned} \hat{\Omega}_m \cdot \underline{\underline{S}}_{p,q}^h \underline{\underline{N}}_{p,q} \psi_{m,p,q}^h + \hat{\Omega}_m \cdot \underline{\underline{S}}_{p,q}^v \underline{\underline{U}}_{p,q} \psi_{m,p,q}^v + \left( \frac{\sigma_{t,p,q}}{\epsilon} \underline{\underline{M}}_{p,q} - \mu_m \underline{\underline{L}}_{p,q} - \eta_m \underline{\underline{K}}_{p,q} \right) \psi_{m,p,q} = \\ \frac{1}{W} \underline{\underline{M}}_{p,q} \left( \frac{\sigma_{t,p,q}}{\epsilon} - \epsilon \sigma_{a,p,q} \right) \phi_{p,q} + \epsilon \underline{\underline{M}}_{p,q} q_{m,p,q}. \end{aligned} \quad (106)$$

We now expand the angular and scalar fluxes as a power series in  $\epsilon$ :

$$\psi_{m,p,q} = \psi_{m,p,q}^{(0)} + \epsilon \psi_{m,p,q}^{(1)} + \epsilon^2 \psi_{m,p,q}^{(2)}, \quad (107a)$$

$$\psi_{m,p,q}^h = \psi_{m,p,q}^{h,(0)} + \epsilon \psi_{m,p,q}^{h,(1)} + \epsilon^2 \psi_{m,p,q}^{h,(2)}, \quad (107b)$$

$$\psi_{m,p,q}^v = \psi_{m,p,q}^{v,(0)} + \epsilon \psi_{m,p,q}^{v,(1)} + \epsilon^2 \psi_{m,p,q}^{v,(2)}, \quad (107c)$$

$$\phi_{p,q} = \underline{\phi}_{p,q}^{(0)} + \epsilon \underline{\phi}_{p,q}^{(1)} + \epsilon^2 \underline{\phi}_{p,q}^{(2)}. \quad (107d)$$

We substitute Eqs. (107) into Eq. (106) and rearrange by powers of  $\epsilon$  to find

$$\begin{aligned} & \frac{1}{\epsilon} \left[ \sigma_{t,p,q} \underline{\underline{M}}_{p,q} \underline{\psi}_{m,p,q}^{(0)} - \frac{1}{W} \sigma_{t,p,q} \underline{\underline{M}}_{p,q} \underline{\phi}_{p,q}^{(0)} \right] \\ & + \epsilon^{(0)} \left[ \hat{\Omega}_m \cdot \underline{\underline{S}}_{p,q}^h \underline{\underline{N}}_{p,q} \underline{\psi}_{m,p,q}^{h,(0)} + \hat{\Omega}_m \cdot \underline{\underline{S}}_{p,q}^v \underline{\underline{U}}_{p,q} \underline{\psi}_{m,p,q}^{v,(0)} \right] \\ & + \epsilon^{(0)} \left[ \sigma_{t,p,q} \underline{\underline{M}}_{p,q} \underline{\psi}_{m,p,q}^{(1)} - (\mu_m \underline{\underline{L}}_{p,q} + \eta_m \underline{\underline{K}}_{p,q}) \underline{\psi}_{m,p,q}^{(0)} - \frac{1}{W} \sigma_{t,p,q} \underline{\underline{M}}_{p,q} \underline{\phi}_{p,q}^{(1)} \right] \\ & + \epsilon^{(1)} \left[ \hat{\Omega}_m \cdot \underline{\underline{S}}_{p,q}^h \underline{\underline{N}}_{p,q} \underline{\psi}_{m,p,q}^{h,(1)} + \hat{\Omega}_m \cdot \underline{\underline{S}}_{p,q}^v \underline{\underline{U}}_{p,q} \underline{\psi}_{m,p,q}^{v,(1)} \right] \\ & + \epsilon^{(1)} \left[ \sigma_{t,p,q} \underline{\underline{M}}_{p,q} \underline{\psi}_{m,p,q}^{(2)} - (\mu_m \underline{\underline{L}}_{p,q} + \eta_m \underline{\underline{K}}_{p,q}) \underline{\psi}_{m,p,q}^{(1)} \right] \\ & + \epsilon^{(1)} \left[ -\frac{1}{W} \underline{\underline{M}}_{p,q} (\sigma_{t,p,q} \underline{\phi}_{p,q}^{(2)} - \sigma_{a,p,q} \underline{\phi}_{p,q}^{(0)}) - \underline{\underline{M}}_{p,q} \underline{q}_{m,p,q} \right] = 0, \quad (108) \end{aligned}$$

along with the upstream closures

$$\psi_{m,p,q,1}^{\lambda_1} = \begin{cases} \psi_{m,p,q-1,4}^{(0)} + \epsilon \psi_{m,p,q-1,4}^{(1)} + \epsilon^2 \psi_{m,p,q-1,4}^{(2)} & \hat{\mathbf{n}}_1 \cdot \hat{\Omega}_m < 0 \\ \psi_{m,p,q,1}^{(0)} + \epsilon \psi_{m,p,q,1}^{(1)} + \epsilon^2 \psi_{m,p,q,1}^{(2)} & \hat{\mathbf{n}}_1 \cdot \hat{\Omega}_m > 0 \end{cases}, \quad (109a)$$

$$\psi_{m,p,q,2}^{\lambda_1} = \begin{cases} \psi_{m,p,q-1,3}^{(0)} + \epsilon \psi_{m,p,q-1,3}^{(1)} + \epsilon^2 \psi_{m,p,q-1,3}^{(2)} & \hat{\mathbf{n}}_1 \cdot \hat{\Omega}_m < 0 \\ \psi_{m,p,q,2}^{(0)} + \epsilon \psi_{m,p,q,2}^{(1)} + \epsilon^2 \psi_{m,p,q,2}^{(2)} & \hat{\mathbf{n}}_1 \cdot \hat{\Omega}_m > 0 \end{cases}, \quad (109b)$$

$$\psi_{m,p,q,3}^{\lambda_{3,(0)}} = \begin{cases} \psi_{m,p,q+1,2}^{(0)} + \epsilon \psi_{m,p,q+1,2}^{(1)} + \epsilon^2 \psi_{m,p,q+1,2}^{(2)} & \hat{\mathbf{n}}_3 \cdot \hat{\Omega}_m < 0 \\ \psi_{m,p,q,3}^{(0)} + \epsilon \psi_{m,p,q,3}^{(1)} + \epsilon^2 \psi_{m,p,q,3}^{(2)} & \hat{\mathbf{n}}_3 \cdot \hat{\Omega}_m > 0 \end{cases}, \quad (109c)$$

$$\psi_{m,p,q,4}^{\lambda_{3,(0)}} = \begin{cases} \psi_{m,p,q+1,1}^{(0)} + \epsilon \psi_{m,p,q+1,1}^{(1)} + \epsilon^2 \psi_{m,p,q+1,1}^{(2)} & \hat{\mathbf{n}}_3 \cdot \hat{\Omega}_m < 0 \\ \psi_{m,p,q,4}^{(0)} + \epsilon \psi_{m,p,q,4}^{(1)} + \epsilon^2 \psi_{m,p,q,4}^{(2)} & \hat{\mathbf{n}}_3 \cdot \hat{\Omega}_m > 0 \end{cases}, \quad (109d)$$

$$\psi_{m,p,q,1}^{\lambda_{4,(0)}} = \begin{cases} \psi_{m,p-1,q,2}^{(0)} + \epsilon \psi_{m,p-1,q,2}^{(1)} + \epsilon^2 \psi_{m,p-1,q,2}^{(2)} & \hat{\mathbf{n}}_4 \cdot \hat{\Omega}_m < 0 \\ \psi_{m,p,q,1}^{(0)} + \epsilon \psi_{m,p,q,1}^{(1)} + \epsilon^2 \psi_{m,p,q,1}^{(2)} & \hat{\mathbf{n}}_4 \cdot \hat{\Omega}_m > 0 \end{cases}, \quad (109e)$$

$$\psi_{m,p,q,2}^{\lambda_{2,(0)}} = \begin{cases} \psi_{m,p+1,q,1}^{(0)} + \epsilon \psi_{m,p+1,q,1}^{(1)} + \epsilon^2 \psi_{m,p+1,q,1}^{(2)} & \hat{\mathbf{n}}_2 \cdot \hat{\Omega}_m < 0 \\ \psi_{m,p,q,2}^{(0)} + \epsilon \psi_{m,p,q,2}^{(1)} + \epsilon^2 \psi_{m,p,q,2}^{(2)} & \hat{\mathbf{n}}_2 \cdot \hat{\Omega}_m > 0 \end{cases}, \quad (109f)$$

$$\psi_{m,p,q,3}^{\lambda_{2,(0)}} = \begin{cases} \psi_{m,p+1,q,4}^{(0)} + \epsilon \psi_{m,p+1,q,4}^{(1)} + \epsilon^2 \psi_{m,p+1,q,4}^{(2)} & \hat{\mathbf{n}}_2 \cdot \hat{\Omega}_m < 0 \\ \psi_{m,p,q,3}^{(0)} + \epsilon \psi_{m,p,q,3}^{(1)} + \epsilon^2 \psi_{m,p,q,3}^{(2)} & \hat{\mathbf{n}}_2 \cdot \hat{\Omega}_m > 0 \end{cases}, \quad (109g)$$

$$\psi_{m,p,q,4}^{\lambda_4,(0)} = \begin{cases} \psi_{m,p-1,q,3}^{(0)} + \epsilon \psi_{m,p-1,q,3}^{(1)} + \epsilon^2 \psi_{m,p-1,q,3}^{(2)} & \hat{\mathbf{n}}_4 \cdot \hat{\boldsymbol{\Omega}}_m < 0 \\ \psi_{m,p,q,4}^{(0)} + \epsilon \psi_{m,p,q,4}^{(1)} + \epsilon^2 \psi_{m,p,q,4}^{(2)} & \hat{\mathbf{n}}_4 \cdot \hat{\boldsymbol{\Omega}}_m > 0 \end{cases}. \quad (109h)$$

We will now set the coefficients of each power of  $\epsilon$  equal to zero and analyze each term. The  $\epsilon^{(-1)}$  equation is

$$\sigma_{t,p,q} \underline{\underline{M}}_{p,q} \underline{\psi}_{m,p,q}^{(0)} - \frac{1}{W} \sigma_{t,p,q} \underline{\underline{M}}_{p,q} \underline{\phi}_{p,q}^{(0)} = 0. \quad (110)$$

If we assume that the mass matrix  $\underline{\underline{M}}_{p,q}$  is invertible (which is true for our discretization), then

$$\underline{\psi}_{m,p,q}^{(0)} = \frac{1}{W} \underline{\phi}_{p,q}^{(0)}. \quad (111)$$

Therefore, the leading order angular flux is isotropic.

We now examine the  $\epsilon^{(0)}$  equation:

$$\begin{aligned} \hat{\boldsymbol{\Omega}}_m \cdot \underline{\underline{S}}_{p,q}^h \underline{N}_{p,q} \underline{\psi}_{m,p,q}^{h,(0)} + \hat{\boldsymbol{\Omega}}_m \cdot \underline{\underline{S}}_{p,q}^v \underline{U}_{p,q} \underline{\psi}_{m,p,q}^{v,(0)} + \sigma_{t,p,q} \underline{\underline{M}}_{p,q} \underline{\psi}_{m,p,q}^{(1)} \\ - (\mu_m \underline{L}_{p,q} + \eta_m \underline{K}_{p,q}) \underline{\psi}_{m,p,q}^{(0)} - \frac{1}{W} \sigma_{t,p,q} \underline{\underline{M}}_{p,q} \underline{\phi}_{p,q}^{(1)} = 0, \end{aligned} \quad (112)$$

along with the  $\epsilon^{(0)}$  upstream closures

$$\psi_{m,p,q,1}^{\lambda_1,(0)} = \begin{cases} \psi_{m,p,q-1,4}^{(0)} & \hat{\mathbf{n}}_1 \cdot \hat{\boldsymbol{\Omega}}_m < 0 \\ \psi_{m,p,q,1}^{(0)} & \hat{\mathbf{n}}_1 \cdot \hat{\boldsymbol{\Omega}}_m > 0 \end{cases}, \quad (113a)$$

$$\psi_{m,p,q,2}^{\lambda_1,(0)} = \begin{cases} \psi_{m,p,q-1,3}^{(0)} & \hat{\mathbf{n}}_1 \cdot \hat{\boldsymbol{\Omega}}_m < 0 \\ \psi_{m,p,q,2}^{(0)} & \hat{\mathbf{n}}_1 \cdot \hat{\boldsymbol{\Omega}}_m > 0 \end{cases}, \quad (113b)$$

$$\psi_{m,p,q,3}^{\lambda_3,(0)} = \begin{cases} \psi_{m,p,q+1,2}^{(0)} & \hat{\mathbf{n}}_3 \cdot \hat{\boldsymbol{\Omega}}_m < 0 \\ \psi_{m,p,q,3}^{(0)} & \hat{\mathbf{n}}_3 \cdot \hat{\boldsymbol{\Omega}}_m > 0 \end{cases}, \quad (113c)$$

$$\psi_{m,p,q,4}^{\lambda_3,(0)} = \begin{cases} \psi_{m,p,q+1,1}^{(0)} & \hat{\mathbf{n}}_3 \cdot \hat{\boldsymbol{\Omega}}_m < 0 \\ \psi_{m,p,q,4}^{(0)} & \hat{\mathbf{n}}_3 \cdot \hat{\boldsymbol{\Omega}}_m > 0 \end{cases}, \quad (113d)$$

$$\psi_{m,p,q,1}^{\lambda_4,(0)} = \begin{cases} \psi_{m,p-1,q,2}^{(0)} & \hat{\mathbf{n}}_4 \cdot \hat{\boldsymbol{\Omega}}_m < 0 \\ \psi_{m,p,q,1}^{(0)} & \hat{\mathbf{n}}_4 \cdot \hat{\boldsymbol{\Omega}}_m > 0 \end{cases}, \quad (113e)$$

$$\psi_{m,p,q,2}^{\lambda_2,(0)} = \begin{cases} \psi_{m,p+1,q,1}^{(0)} & \hat{\mathbf{n}}_2 \cdot \hat{\boldsymbol{\Omega}}_m < 0 \\ \psi_{m,p,q,2}^{(0)} & \hat{\mathbf{n}}_2 \cdot \hat{\boldsymbol{\Omega}}_m > 0 \end{cases}, \quad (113f)$$



$$\psi_{m,p,q,3}^{\lambda_2,(0)} = \begin{cases} \psi_{m,p+1,q,4}^{(0)} & \hat{\mathbf{n}}_2 \cdot \hat{\boldsymbol{\Omega}}_m < 0 \\ \psi_{m,p,q,3}^{(0)} & \hat{\mathbf{n}}_2 \cdot \hat{\boldsymbol{\Omega}}_m > 0 \end{cases}, \quad (113g)$$

$$\psi_{m,p,q,4}^{\lambda_4,(0)} = \begin{cases} \psi_{m,p-1,q,3}^{(0)} & \hat{\mathbf{n}}_4 \cdot \hat{\boldsymbol{\Omega}}_m < 0 \\ \psi_{m,p,q,4}^{(0)} & \hat{\mathbf{n}}_4 \cdot \hat{\boldsymbol{\Omega}}_m > 0 \end{cases}. \quad (113h)$$

Summing Eq. (112) over the quadrature set yields

$$\sum_m w_m \left( \hat{\boldsymbol{\Omega}}_m \cdot \underline{\underline{\mathbf{S}}}_{p,q}^h \underline{\underline{N}}_{p,q} \psi_{m,p,q}^{h,(0)} + \hat{\boldsymbol{\Omega}}_m \cdot \underline{\underline{\mathbf{S}}}_{p,q}^v \underline{\underline{U}}_{p,q} \psi_{m,p,q}^{v,(0)} \right) = 0. \quad (114)$$

We can use Eq. (114) to prove that the leading order scalar flux is continuous around a node. In order to do so, we shall assume that the surface matrices  $\underline{\underline{N}}$  and  $\underline{\underline{U}}$  are lumped (see Section 2.3.2). This yields

$$\sum_m w_m \hat{\boldsymbol{\Omega}}_m \cdot \hat{\mathbf{n}}_1 \frac{|\lambda_1|}{2} \psi_{m,p,q,1}^{\lambda_1,(0)} + \sum_m w_m \hat{\boldsymbol{\Omega}}_m \cdot \hat{\mathbf{n}}_4 \frac{|\lambda_4|}{2} \psi_{m,p,q,1}^{\lambda_4,(0)} = 0, \quad (115a)$$

$$\sum_m w_m \hat{\boldsymbol{\Omega}}_m \cdot \hat{\mathbf{n}}_1 \frac{|\lambda_1|}{2} \psi_{m,p,q,2}^{\lambda_1,(0)} + \sum_m w_m \hat{\boldsymbol{\Omega}}_m \cdot \hat{\mathbf{n}}_2 \frac{|\lambda_2|}{2} \psi_{m,p,q,2}^{\lambda_2,(0)} = 0, \quad (115b)$$

$$\sum_m w_m \hat{\boldsymbol{\Omega}}_m \cdot \hat{\mathbf{n}}_3 \frac{|\lambda_3|}{2} \psi_{m,p,q,3}^{\lambda_3,(0)} + \sum_m w_m \hat{\boldsymbol{\Omega}}_m \cdot \hat{\mathbf{n}}_2 \frac{|\lambda_2|}{2} \psi_{m,p,q,3}^{\lambda_2,(0)} = 0, \quad (115c)$$

$$\sum_m w_m \hat{\boldsymbol{\Omega}}_m \cdot \hat{\mathbf{n}}_3 \frac{|\lambda_3|}{2} \psi_{m,p,q,4}^{\lambda_3,(0)} + \sum_m w_m \hat{\boldsymbol{\Omega}}_m \cdot \hat{\mathbf{n}}_4 \frac{|\lambda_4|}{2} \psi_{m,p,q,4}^{\lambda_4,(0)} = 0. \quad (115d)$$

Now, consider the node shown in Figure 14. The node is bordered by zones  $(p, q)$ ,

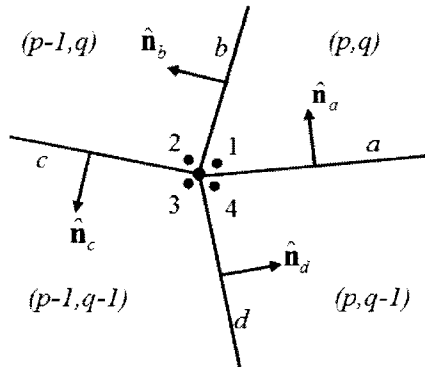


Figure 14: Node with Logically Rectangular Connectivity

$(p-1, q)$ ,  $(p-1, q-1)$ , and  $(p, q-1)$ , and by edges  $a$ ,  $b$ ,  $c$ , and  $d$ . The corners

are numbered 1 through 4, and the normals for the edges are also shown. Writing Eqs. (115) around this node and substituting in Eqs. (113) gives us

$$\begin{aligned} & \frac{|\lambda_a|}{2} \sum_{m: \hat{\Omega}_m \cdot \hat{n}_a < 0} w_m \hat{\Omega}_m \cdot \hat{n}_a \psi_{m,p,q,1}^{(0)} + \frac{|\lambda_a|}{2} \sum_{m: \hat{\Omega}_m \cdot \hat{n}_a > 0} w_m \hat{\Omega}_m \cdot \hat{n}_a \psi_{m,p,q-1,4}^{(0)} \\ & + \frac{|\lambda_b|}{2} \sum_{m: \hat{\Omega}_m \cdot \hat{n}_b < 0} w_m \hat{\Omega}_m \cdot \hat{n}_b \psi_{m,p-1,q,2}^{(0)} + \frac{|\lambda_b|}{2} \sum_{m: \hat{\Omega}_m \cdot \hat{n}_b > 0} w_m \hat{\Omega}_m \cdot \hat{n}_b \psi_{m,p,q,1}^{(0)} = 0, \end{aligned} \quad (116a)$$

$$\begin{aligned} & \frac{|\lambda_c|}{2} \sum_{m: \hat{\Omega}_m \cdot \hat{n}_c < 0} w_m \hat{\Omega}_m \cdot \hat{n}_c \psi_{m,p-1,q-1,3}^{(0)} + \frac{|\lambda_c|}{2} \sum_{m: \hat{\Omega}_m \cdot \hat{n}_c > 0} w_m \hat{\Omega}_m \cdot \hat{n}_c \psi_{m,p-1,q,2}^{(0)} \\ & + \frac{|\lambda_b|}{2} \sum_{m: \hat{\Omega}_m \cdot \hat{n}_b < 0} w_m \hat{\Omega}_m \cdot \hat{n}_b \psi_{m,p-1,q,2}^{(0)} + \frac{|\lambda_b|}{2} \sum_{m: \hat{\Omega}_m \cdot \hat{n}_b > 0} w_m \hat{\Omega}_m \cdot \hat{n}_b \psi_{m,p,q,1}^{(0)} = 0, \end{aligned} \quad (116b)$$

$$\begin{aligned} & \frac{|\lambda_c|}{2} \sum_{m: \hat{\Omega}_m \cdot \hat{n}_c < 0} w_m \hat{\Omega}_m \cdot \hat{n}_c \psi_{m,p-1,q-1,3}^{(0)} + \frac{|\lambda_c|}{2} \sum_{m: \hat{\Omega}_m \cdot \hat{n}_c > 0} w_m \hat{\Omega}_m \cdot \hat{n}_c \psi_{m,p-1,q,2}^{(0)} \\ & + \frac{|\lambda_d|}{2} \sum_{m: \hat{\Omega}_m \cdot \hat{n}_d < 0} w_m \hat{\Omega}_m \cdot \hat{n}_d \psi_{m,p,q-1,4}^{(0)} + \frac{|\lambda_d|}{2} \sum_{m: \hat{\Omega}_m \cdot \hat{n}_d > 0} w_m \hat{\Omega}_m \cdot \hat{n}_d \psi_{m,p-1,q-1,3}^{(0)} = 0, \end{aligned} \quad (116c)$$

$$\begin{aligned} & \frac{|\lambda_a|}{2} \sum_{m: \hat{\Omega}_m \cdot \hat{n}_a < 0} w_m \hat{\Omega}_m \cdot \hat{n}_a \psi_{m,p,q,1}^{(0)} + \frac{|\lambda_a|}{2} \sum_{m: \hat{\Omega}_m \cdot \hat{n}_a > 0} w_m \hat{\Omega}_m \cdot \hat{n}_a \psi_{m,p,q-1,4}^{(0)} \\ & + \frac{|\lambda_d|}{2} \sum_{m: \hat{\Omega}_m \cdot \hat{n}_d < 0} w_m \hat{\Omega}_m \cdot \hat{n}_d \psi_{m,p,q-1,4}^{(0)} + \frac{|\lambda_d|}{2} \sum_{m: \hat{\Omega}_m \cdot \hat{n}_d > 0} w_m \hat{\Omega}_m \cdot \hat{n}_d \psi_{m,p-1,q-1,3}^{(0)} = 0. \end{aligned} \quad (116d)$$

We make the following definitions:

$$\zeta_{m,a} = \hat{\Omega}_m \cdot \hat{n}_a, \quad (117a)$$

$$\zeta_{m,b} = \hat{\Omega}_m \cdot \hat{n}_b, \quad (117b)$$

$$\zeta_{m,c} = \hat{\Omega}_m \cdot \hat{n}_c, \quad (117c)$$

$$\zeta_{m,d} = \hat{\Omega}_m \cdot \hat{n}_d. \quad (117d)$$

Substituting Eqs. (117) and (111) into Eq. (116) yields

$$\begin{aligned} \frac{|\lambda_a|}{4W} \phi_{p,q,1}^{(0)} \sum_{m:\zeta_{m,a}<0} w_m \zeta_{m,a} + \frac{|\lambda_a|}{4W} \phi_{p,q-1,4}^{(0)} \sum_{m:\zeta_{m,a}>0} w_m \zeta_{m,a} \\ + \frac{|\lambda_b|}{4W} \phi_{p-1,q,2}^{(0)} \sum_{m:\zeta_{m,b}<0} w_m \zeta_{m,b} + \frac{|\lambda_b|}{4W} \phi_{p,q,1}^{(0)} \sum_{m:\zeta_{m,b}>0} w_m \zeta_{m,b} = 0, \end{aligned} \quad (118a)$$

$$\begin{aligned} \frac{|\lambda_c|}{4W} \phi_{p-1,q-1,3}^{(0)} \sum_{m:\zeta_{m,c}<0} w_m \zeta_{m,c} + \frac{|\lambda_c|}{4W} \phi_{p-1,q,2}^{(0)} \sum_{m:\zeta_{m,c}>0} w_m \zeta_{m,c} \\ + \frac{|\lambda_b|}{4W} \phi_{p-1,q,2}^{(0)} \sum_{m:\zeta_{m,b}<0} w_m \zeta_{m,b} + \frac{|\lambda_b|}{4W} \phi_{p,q,1}^{(0)} \sum_{m:\zeta_{m,b}>0} w_m \zeta_{m,b} = 0, \end{aligned} \quad (118b)$$

$$\begin{aligned} \frac{|\lambda_c|}{4W} \phi_{p-1,q-1,3}^{(0)} \sum_{m:\zeta_{m,c}<0} w_m \zeta_{m,c} + \frac{|\lambda_c|}{4W} \phi_{p-1,q,2}^{(0)} \sum_{m:\zeta_{m,c}>0} w_m \zeta_{m,c} \\ + \frac{|\lambda_d|}{4W} \phi_{p,q-1,4}^{(0)} \sum_{m:\zeta_{m,d}<0} w_m \zeta_{m,d} + \frac{|\lambda_d|}{4W} \phi_{p-1,q-1,3}^{(0)} \sum_{m:\zeta_{m,d}>0} w_m \zeta_{m,d} = 0, \end{aligned} \quad (118c)$$

$$\begin{aligned} \frac{|\lambda_a|}{4W} \phi_{p,q,1}^{(0)} \sum_{m:\zeta_{m,a}<0} w_m \zeta_{m,a} + \frac{|\lambda_a|}{4W} \phi_{p,q-1,4}^{(0)} \sum_{m:\zeta_{m,a}>0} w_m \zeta_{m,a} \\ + \frac{|\lambda_d|}{4W} \phi_{p,q-1,4}^{(0)} \sum_{m:\zeta_{m,d}<0} w_m \zeta_{m,d} + \frac{|\lambda_d|}{4W} \phi_{p-1,q-1,3}^{(0)} \sum_{m:\zeta_{m,d}>0} w_m \zeta_{m,d} = 0. \end{aligned} \quad (118d)$$

We know that

$$\rho_a = \sum_{m:\zeta_a>0} w_m \zeta_{m,a} = - \sum_{m:\zeta_a<0} w_m \zeta_{m,a} \approx 1, \quad (119a)$$

$$\rho_b = \sum_{m:\zeta_b>0} w_m \zeta_{m,b} = - \sum_{m:\zeta_b<0} w_m \zeta_{m,b} \approx 1, \quad (119b)$$

$$\rho_c = \sum_{m:\zeta_c>0} w_m \zeta_{m,c} = - \sum_{m:\zeta_c<0} w_m \zeta_{m,c} \approx 1, \quad (119c)$$

$$\rho_d = \sum_{m:\zeta_d>0} w_m \zeta_{m,d} = - \sum_{m:\zeta_d<0} w_m \zeta_{m,d} \approx 1, \quad (119d)$$

and

$$\rho_a = \rho_b = \rho_c = \rho_d \equiv \rho. \quad (120)$$

Substituting into Eq. (118) gives

$$\frac{|\lambda_a|}{4W}\rho\left(\phi_{p,q-1,4}^{(0)} - \phi_{p,q,1}^{(0)}\right) + \frac{|\lambda_b|}{4W}\rho\left(\phi_{p,q,1}^{(0)} - \phi_{p-1,q,2}^{(0)}\right) = 0, \quad (121a)$$

$$\frac{|\lambda_c|}{4W}\rho\left(\phi_{p-1,q,2}^{(0)} - \phi_{p-1,q-1,3}^{(0)}\right) + \frac{|\lambda_b|}{4W}\rho\left(\phi_{p,q,1}^{(0)} - \phi_{p-1,q,2}^{(0)}\right) = 0, \quad (121b)$$

$$\frac{|\lambda_c|}{4W}\rho\left(\phi_{p-1,q,2}^{(0)} - \phi_{p-1,q-1,3}^{(0)}\right) + \frac{|\lambda_d|}{4W}\rho\left(\phi_{p-1,q-1,3}^{(0)} - \phi_{p,q-1,4}^{(0)}\right) = 0, \quad (121c)$$

$$\frac{|\lambda_a|}{4W}\rho\left(\phi_{p,q-1,4}^{(0)} - \phi_{p,q,1}^{(0)}\right) + \frac{|\lambda_d|}{4W}\rho\left(\phi_{p-1,q-1,3}^{(0)} - \phi_{p,q-1,4}^{(0)}\right) = 0. \quad (121d)$$

From this, we can conclude

$$\phi_{p,q,1}^{(0)} = \phi_{p-1,q,2}^{(0)} = \phi_{p-1,q-1,3}^{(0)} = \phi_{p,q-1,4}^{(0)}; \quad (122)$$

therefore, the leading order scalar flux is continuous around a node.

We now multiply Eq. (112) by  $\hat{\Omega}_m$  and sum over the quadrature set.

$$\begin{aligned} & \sum_m w_m \hat{\Omega}_m \left[ \hat{\Omega}_m \cdot \underline{\underline{S}}_{p,q}^h \underline{\underline{N}}_{p,q} \underline{\psi}_{m,p,q}^{h,(0)} + \hat{\Omega}_m \cdot \underline{\underline{S}}_{p,q}^v \underline{\underline{U}}_{p,q} \underline{\psi}_{m,p,q}^{v,(0)} \right] \\ & + \sum_m w_m \hat{\Omega}_m \left[ \sigma_{t,p,q} \underline{\underline{M}}_{p,q} \underline{\psi}_{m,p,q}^{(1)} - (\mu_m \underline{\underline{L}}_{p,q} + \eta_m \underline{\underline{K}}_{p,q}) \underline{\psi}_{m,p,q}^{(0)} - \frac{\sigma_{t,p,q}}{W} \underline{\underline{M}}_{p,q} \underline{\phi}_{p,q}^{(1)} \right] = 0. \end{aligned} \quad (123)$$

We define the  $O(1)$  current as

$$\underline{\mathbf{J}}_{p,q}^{(1)} = \sum_m w_m \hat{\Omega}_m \underline{\psi}_{m,p,q}^{(1)}, \quad (124)$$

and we simplify Eq. (123) by noting that

$$\sum_m w_m \mu_m^2 \underline{\psi}_{m,p,q}^{(0)} = \sum_m w_m \eta_m^2 \underline{\psi}_{m,p,q}^{(0)} = \frac{1}{3} \underline{\phi}_{p,q}^{(0)}, \quad (125a)$$

$$\sum_m w_m \mu_m \eta_m \underline{\psi}_{m,p,q}^{(0)} = 0, \quad (125b)$$

and

$$\underline{\psi}_{m,p,q}^{h,(0)} = \underline{\psi}_{m,p,q}^{v,(0)} = \underline{\psi}_{m,p,q}^{(0)}. \quad (125c)$$

Therefore, we now have

$$\frac{1}{3} (\underline{\mathbf{S}}_{p,q}^h \underline{N}_{p,q} + \underline{\mathbf{S}}_{p,q}^v \underline{U}_{p,q}) \underline{\phi}_{p,q}^{(0)} + \sigma_{t,p,q} \underline{M}_{p,q} \underline{\mathbf{J}}_{p,q}^{(1)} - \frac{1}{3} (\underline{L}_{p,q} \hat{\mathbf{e}}_x + \underline{K}_{p,q} \hat{\mathbf{e}}_y) \underline{\phi}_{p,q}^{(0)} = 0. \quad (126)$$

Solving for the current, we get the discretized form of Fick's Law:

$$\underline{\mathbf{J}}_{p,q}^{(1)} = -D_{p,q} \underline{M}_{p,q}^{-1} [\underline{\mathbf{S}}_{p,q}^h \underline{N}_{p,q} + \underline{\mathbf{S}}_{p,q}^v \underline{U}_{p,q} - \underline{L}_{p,q} \hat{\mathbf{e}}_x - \underline{K}_{p,q} \hat{\mathbf{e}}_y] \underline{\phi}_{p,q}^{(0)}, \quad (127)$$

where

$$D_{p,q} = \frac{1}{3\sigma_{t,p,q}}. \quad (128)$$

The order  $\epsilon^{(1)}$  equation is

$$\begin{aligned} & \hat{\Omega}_m \cdot \underline{\mathbf{S}}_{p,q}^h \underline{N}_{p,q} \underline{\psi}_{m,p,q}^{h,(1)} + \hat{\Omega}_m \cdot \underline{\mathbf{S}}_{p,q}^v \underline{U}_{p,q} \underline{\psi}_{m,p,q}^{v,(1)} + \sigma_{t,p,q} \underline{M}_{p,q} \underline{\psi}_{m,p,q}^{(2)} \\ & - (\mu_m \underline{L}_{p,q} + \eta_m \underline{K}_{p,q}) \underline{\psi}_{m,p,q}^{(1)} - \frac{1}{W} \underline{M}_{p,q} (\sigma_{t,p,q} \underline{\phi}_{p,q}^{(2)} - \sigma_{a,p,q} \underline{\phi}_{p,q}^{(0)}) - \underline{M}_{p,q} \underline{q}_{m,p,q} = 0. \end{aligned} \quad (129)$$

Summing this equation over the quadrature set yields:

$$\begin{aligned} & \sum_m w_m \left[ \hat{\Omega}_m \cdot \underline{\mathbf{S}}_{p,q}^h \underline{N}_{p,q} \underline{\psi}_{m,p,q}^{h,(1)} + \hat{\Omega}_m \cdot \underline{\mathbf{S}}_{p,q}^v \underline{U}_{p,q} \underline{\psi}_{m,p,q}^{v,(1)} \right] \\ & - (\underline{L}_{p,q} \underline{\mathbf{J}}_{p,q}^{(1)} \cdot \hat{\mathbf{e}}_x + \underline{K}_{p,q} \underline{\mathbf{J}}_{p,q}^{(1)} \cdot \hat{\mathbf{e}}_y) + \underline{M}_{p,q} (\sigma_{a,p,q} \underline{\phi}_{p,q}^{(0)} - \underline{Q}_{p,q}) = 0, \end{aligned} \quad (130)$$

where

$$\underline{Q}_{p,q} = \sum_{m=1}^M w_m \underline{q}_{m,p,q}. \quad (131)$$

We shall now write Eq. (130) around a node. The equation for corner 1 in zone  $(p, q)$  is

$$\begin{aligned} & \left[ \sum_m w_m \hat{\Omega}_m \cdot \underline{\mathbf{S}}_{p,q}^h \underline{N}_{p,q} \underline{\psi}_{m,p,q}^{h,(1)} \right]_1 + \left[ \sum_m w_m \hat{\Omega}_m \cdot \underline{\mathbf{S}}_{p,q}^v \underline{U}_{p,q} \underline{\psi}_{m,p,q}^{v,(1)} \right]_1 \\ & - \left[ \underline{L}_{p,q} \underline{\mathbf{J}}_{p,q}^{(1)} \cdot \hat{\mathbf{e}}_x + \underline{K}_{p,q} \underline{\mathbf{J}}_{p,q}^{(1)} \cdot \hat{\mathbf{e}}_y \right]_1 + \left[ \underline{M}_{p,q} (\sigma_{a,p,q} \underline{\phi}_{p,q}^{(0)} - \underline{Q}_{p,q}) \right]_1 = 0. \end{aligned} \quad (132)$$

The equation for corner 2 in zone  $(p-1, q)$  is:

$$\begin{aligned}
& \left[ \sum_m w_m \hat{\Omega}_m \cdot \underline{\underline{S}}_{p-1,q}^h \underline{\underline{N}}_{p-1,q} \underline{\underline{\psi}}_{m,p-1,q}^{h,(1)} \right]_2 + \left[ \sum_m w_m \hat{\Omega}_m \cdot \underline{\underline{S}}_{p-1,q}^v \underline{\underline{U}}_{p-1,q} \underline{\underline{\psi}}_{m,p-1,q}^{v,(1)} \right]_2 \\
& - \left[ \underline{\underline{L}}_{p-1,q} \underline{\underline{J}}_{p-1,q}^{(1)} \cdot \hat{\mathbf{e}}_x + \underline{\underline{K}}_{p-1,q} \underline{\underline{J}}_{p-1,q}^{(1)} \cdot \hat{\mathbf{e}}_y \right]_2 \\
& + \left[ \underline{\underline{M}}_{p-1,q} \left( \sigma_{a,p-1,q} \phi_{p-1,q}^{(0)} - \underline{\underline{Q}}_{p-1,q} \right) \right]_2 = 0. \quad (133)
\end{aligned}$$

The equation for corner 3 in zone  $(p-1, q-1)$  is:

$$\begin{aligned}
& \left[ \sum_m w_m \hat{\Omega}_m \cdot \underline{\underline{S}}_{p-1,q-1}^h \underline{\underline{N}}_{p-1,q-1} \underline{\underline{\psi}}_{m,p-1,q-1}^{h,(1)} \right]_3 \\
& + \left[ \sum_m w_m \hat{\Omega}_m \cdot \underline{\underline{S}}_{p-1,q-1}^v \underline{\underline{U}}_{p-1,q-1} \underline{\underline{\psi}}_{m,p-1,q-1}^{v,(1)} \right]_3 \\
& - \left[ \underline{\underline{L}}_{p-1,q-1} \underline{\underline{J}}_{p-1,q-1}^{(1)} \cdot \hat{\mathbf{e}}_x + \underline{\underline{K}}_{p-1,q-1} \underline{\underline{J}}_{p-1,q-1}^{(1)} \cdot \hat{\mathbf{e}}_y \right]_3 \\
& + \left[ \underline{\underline{M}}_{p-1,q-1} \left( \sigma_{a,p-1,q-1} \phi_{p-1,q-1}^{(0)} - \underline{\underline{Q}}_{p-1,q-1} \right) \right]_3 = 0. \quad (134)
\end{aligned}$$

The equation for corner 4 in zone  $(p, q-1)$  is:

$$\begin{aligned}
& \left[ \sum_m w_m \hat{\Omega}_m \cdot \underline{\underline{S}}_{p,q-1}^h \underline{\underline{N}}_{p,q-1} \underline{\underline{\psi}}_{m,p,q-1}^{h,(1)} \right]_4 + \left[ \sum_m w_m \hat{\Omega}_m \cdot \underline{\underline{S}}_{p,q-1}^v \underline{\underline{U}}_{p,q-1} \underline{\underline{\psi}}_{m,p,q-1}^{v,(1)} \right]_4 \\
& - \left[ \underline{\underline{L}}_{p,q-1} \underline{\underline{J}}_{p,q-1}^{(1)} \cdot \hat{\mathbf{e}}_x + \underline{\underline{K}}_{p,q-1} \underline{\underline{J}}_{p,q-1}^{(1)} \cdot \hat{\mathbf{e}}_y \right]_4 \\
& + \left[ \underline{\underline{M}}_{p,q-1} \left( \sigma_{a,p,q-1} \phi_{p,q-1}^{(0)} - \underline{\underline{Q}}_{p,q-1} \right) \right]_4 = 0. \quad (135)
\end{aligned}$$

By adding these equations the shared boundary terms cancel, and we get

$$\begin{aligned}
& - \left[ \underline{L}_{p,q} \underline{\mathbf{J}}_{p,q}^{(1)} \cdot \hat{\mathbf{e}}_x + \underline{K}_{p,q} \underline{\mathbf{J}}_{p,q}^{(1)} \cdot \hat{\mathbf{e}}_y \right]_1 - \left[ \underline{L}_{p-1,q} \underline{\mathbf{J}}_{p-1,q}^{(1)} \cdot \hat{\mathbf{e}}_x + \underline{K}_{p-1,q} \underline{\mathbf{J}}_{p-1,q}^{(1)} \cdot \hat{\mathbf{e}}_y \right]_2 \\
& - \left[ \underline{L}_{p-1,q-1} \underline{\mathbf{J}}_{p-1,q-1}^{(1)} \cdot \hat{\mathbf{e}}_x + \underline{K}_{p-1,q-1} \underline{\mathbf{J}}_{p-1,q-1}^{(1)} \cdot \hat{\mathbf{e}}_y \right]_3 \\
& - \left[ \underline{L}_{p,q-1} \underline{\mathbf{J}}_{p,q-1}^{(1)} \cdot \hat{\mathbf{e}}_x + \underline{K}_{p,q-1} \underline{\mathbf{J}}_{p,q-1}^{(1)} \cdot \hat{\mathbf{e}}_y \right]_4 + \left[ \underline{M}_{p,q} (\sigma_{a,p,q} \phi_{p,q}^{(0)} - \underline{Q}_{p,q}) \right]_1 \\
& + \left[ \underline{M}_{p-1,q} (\sigma_{a,p-1,q} \phi_{p-1,q}^{(0)} - \underline{Q}_{p-1,q}) \right]_2 + \left[ \underline{M}_{p-1,q-1} (\sigma_{a,p-1,q-1} \phi_{p-1,q-1}^{(0)} - \underline{Q}_{p-1,q-1}) \right]_3 \\
& + \left[ \underline{M}_{p,q-1} (\sigma_{a,p,q-1} \phi_{p,q-1}^{(0)} - \underline{Q}_{p,q-1}) \right]_4 = 0. \quad (136)
\end{aligned}$$

Substituting in Eq. (127), we find a node-based diffusion equation:

$$\begin{aligned}
& \left[ (D_{p,q} \underline{T}_{p,q} + \sigma_{a,p,q} \underline{M}_{p,q}) \phi_{p,q}^{(0)} \right]_1 + \left[ (D_{p-1,q} \underline{T}_{p-1,q} + \sigma_{a,p-1,q} \underline{M}_{p-1,q}) \phi_{p-1,q}^{(0)} \right]_2 \\
& + \left[ (D_{p-1,q-1} \underline{T}_{p-1,q-1} + \sigma_{a,p-1,q-1} \underline{M}_{p-1,q-1}) \phi_{p-1,q-1}^{(0)} \right]_3 \\
& + \left[ (D_{p,q-1} \underline{T}_{p,q-1} + \sigma_{a,p,q-1} \underline{M}_{p,q-1}) \phi_{p,q-1}^{(0)} \right]_4 = \left[ \underline{M}_{p,q} \underline{Q}_{p,q} \right]_1 + \left[ \underline{M}_{p-1,q} \underline{Q}_{p-1,q} \right]_2 \\
& + \left[ \underline{M}_{p-1,q-1} \underline{Q}_{p-1,q-1} \right]_3 + \left[ \underline{M}_{p,q-1} \underline{Q}_{p,q-1} \right]_4, \quad (137)
\end{aligned}$$

where

$$\begin{aligned}
\underline{T}_{p,q} &= \underline{L}_{p,q} \underline{M}_{p,q}^{-1} (\hat{\mathbf{e}}_x \cdot \underline{\mathbf{S}}_{p,q}^h \underline{N}_{p,q} + \hat{\mathbf{e}}_x \cdot \underline{\mathbf{S}}_{p,q}^v \underline{U}_{p,q} - \underline{L}_{p,q}) \\
&+ \underline{K}_{p,q} \underline{M}_{p,q}^{-1} (\hat{\mathbf{e}}_y \cdot \underline{\mathbf{S}}_{p,q}^h \underline{N}_{p,q} + \hat{\mathbf{e}}_y \cdot \underline{\mathbf{S}}_{p,q}^v \underline{U}_{p,q} - \underline{K}_{p,q}). \quad (138)
\end{aligned}$$

Without lumping, Eq. (137) will have a nine-point leakage term (the terms involving  $\underline{T}$ ) and a nine-point removal term (the terms involving  $\underline{M}$ ). A removal term that is tightly coupled spatially is known to cause unphysical oscillations. Mass-lumping (Section 2.3.1) creates a one-point removal term. In addition, it is also known that a nine-point leakage term can cause unphysical oscillations or cause the solution to go negative [Pal 93]. Lumping the leakage matrices and surface matrices will create a leakage term with a five-point coupling. Surface-matrix lumping is also required to enforce continuity of the leading order angular

flux. For these reasons, full-lumping provides a more robust discretization of the transport equation.



## 6 DIFFUSION SYNTHETIC ACCELERATION

Typically, the transport equation is solved through an iterative process. After discretization, one is left with a coupled set of equations with two unknowns, angular flux and scalar flux, (see Eqs. (20) and (22)). The most common solution method is called source iteration (also known as Richardson iteration), in which a guess is made for the scalar flux, which specifies the scattering source in an isotropic problem. With this guess the entire right-hand side of the transport equation is known and the angular flux can be calculated. Solving for the angular flux typically involves sweeping through the mesh zone-by-zone in each angle. Then the values for angular flux are used to calculate a new value for the scalar flux. The process repeats until the scalar flux has converged. For our discretization, we first solve

$$\begin{aligned} \hat{\Omega}_m \cdot \underline{\underline{S}}_{p,q}^h \underline{\underline{N}}_{p,q} \underline{\underline{\psi}}_{m,p,q}^h + \hat{\Omega}_m \cdot \underline{\underline{S}}_{p,q}^v \underline{\underline{U}}_{p,q} \underline{\underline{\psi}}_{m,p,q}^v \\ + (\sigma_{t,p,q} \underline{\underline{M}}_{p,q} - \mu_m \underline{\underline{L}}_{p,q} - \eta_m \underline{\underline{K}}_{p,q}) \underline{\underline{\psi}}_{m,p,q} = \frac{\sigma_{s,p,q}}{W} \underline{\underline{M}}_{p,q} \underline{\underline{\phi}}_{p,q} + \underline{\underline{M}}_{p,q} \underline{\underline{q}}_{m,p,q}, \end{aligned} \quad (139)$$

using an initial guess for the scalar flux. We then solve for the scalar flux using

$$\underline{\underline{\phi}}_{p,q} = \sum_{m=1}^M w_m \underline{\underline{\psi}}_{m,p,q}. \quad (140)$$

Source iteration works well for problems that are optically thin or have a low scattering ratio. As the scattering ratio increases, however, the number of iterations required for convergence increases. The spectral radius  $\rho_{SI}$  for source iteration is equal to the scattering ratio,

$$\rho_{SI} = c \equiv \frac{\sigma_s}{\sigma_t}. \quad (141)$$

A large scattering ratio can also cause false-convergence. False-convergence occurs when the relative error from one iteration to the next is small (due to slow convergence), but the error relative to the true solution is much larger. Typically, one

would expect the iterations to cease when

$$\|\psi^{(k)} - \psi^{(k-1)}\| \leq e, \quad (142)$$

where  $\psi^{(k)}$  and  $\psi^{(k-1)}$  are the angular flux solutions at iteration  $k$  and  $k-1$ , respectively, and  $e$  is some predetermined convergence criterion. However, to guard against false convergence the iterations should not cease until [Ada 02]:

$$\frac{\rho}{1-\rho} \|\psi^{(k)} - \psi^{(k-1)}\| \leq e. \quad (143)$$

Guarding against false convergence does not solve the problem of source iteration requiring a large number of iterations when problems are thick and diffusive, which are the types of problems we wish to study. In order to solve optically thick and diffusive problems, we must use an acceleration scheme (also called a preconditioner). The most common way to accelerate source iteration is through a technique called diffusion synthetic acceleration (DSA). DSA uses a diffusion equation to calculate a correction to the scalar flux between source iterations. DSA is designed to dampen out the largest error mode of source iteration. This error mode is dominant in optically-thick highly-scattering problems, and using DSA can cause dramatic reductions in the number of iterations necessary to achieve convergence.

It has been found that the discretization of the DSA equations cannot be done independently of the transport discretization. For stability, the two discretizations must be “consistent,” meaning they must be related in some way. We shall derive and employ “asymptotic DSA” [War 92], which is DSA based upon the asymptotic diffusion equation that is the limit of the transport equation in thick diffusive regions (see Section 5).

## 6.1 Asymptotic Diffusion Synthetic Acceleration

In Section 2.2 we derived the discretized  $S_N$  equation for a quadrilateral, which we restate here for convenience:

$$\begin{aligned} \hat{\Omega}_m \cdot \underline{\underline{S}}_{p,q}^h \underline{N}_{p,q} \underline{\psi}_{m,p,q}^h + \hat{\Omega}_m \cdot \underline{\underline{S}}_{p,q}^v \underline{U}_{p,q} \underline{\psi}_{m,p,q}^v \\ + (\sigma_{t,p,q} \underline{M}_{p,q} - \mu_m \underline{L}_{p,q} - \eta_m \underline{K}_{p,q}) \underline{\psi}_{m,p,q} = \frac{\sigma_{s,p,q}}{W} \underline{M}_{p,q} \underline{\phi}_{p,q} + \underline{M}_{p,q} \underline{q}_{m,p,q}. \end{aligned} \quad (144)$$

This can be written in operator form at iteration  $k$  as:

$$\underline{\underline{H}} \underline{\psi}_{m,p,q}^{(k+1/2)} = \underline{\underline{R}} \underline{\phi}_{p,q}^{(k)} + \underline{M}_{p,q} \underline{q}_{m,p,q}, \quad (145)$$

where  $\underline{\underline{H}}$  is the left-hand side of the transport operator and  $\underline{\underline{R}}$  is the right-hand side portion of the transport operator that acts on the scalar flux. Subtracting this from the converged solution we obtain

$$\underline{\underline{H}} \underline{f}_{m,p,q} = \underline{\underline{R}} (\underline{\phi}_{p,q}^{(conv)} - \underline{\phi}_{p,q}^{(k)}). \quad (146)$$

where  $\underline{f}_{m,p,q}$  is the error between the exact solution and  $\underline{\phi}_{m,p,q}$ . If we could calculate this error, we could calculate the converged angular flux solution immediately. Unfortunately, this equation is as difficult to solve as the original transport equation. To circumvent this, we will replace the transport operators in Eq. (146) with the asymptotic diffusion operator we found in Section 5. If we define the integrated correction as

$$\underline{F}_{p,q}^{(k+1/2)} = \sum_m w_m \underline{f}_{m,p,q}^{(k+1/2)}, \quad (147)$$

then our DSA equation, based around a node is

$$\begin{aligned}
& \left[ (D_{p,q} \underline{T}_{p,q} + \sigma_{a,p,q} \underline{M}_{p,q}) \underline{F}_{p,q}^{(k+1/2)} \right]_1 + \left[ (D_{p-1,q} \underline{T}_{p-1,q} + \sigma_{a,p-1,q} \underline{M}_{p-1,q}) \underline{F}_{p-1,q}^{(k+1/2)} \right]_2 \\
& + \left[ (D_{p-1,q-1} \underline{T}_{p-1,q-1} + \sigma_{a,p-1,q-1} \underline{M}_{p-1,q-1}) \underline{F}_{p-1,q-1}^{(k+1/2)} \right]_3 \\
& + \left[ (D_{p,q-1} \underline{T}_{p,q-1} + \sigma_{a,p,q-1} \underline{M}_{p,q-1}) \underline{F}_{p,q-1}^{(k+1/2)} \right]_4 = \left[ \sigma_{s,p,q} \underline{M}_{p,q} (\underline{\phi}_{p,q}^{(k+1/2)} - \underline{\phi}_{p,q}^{(k)}) \right]_1 \\
& + \left[ \sigma_{s,p-1,q} \underline{M}_{p-1,q} (\underline{\phi}_{p-1,q}^{(k+1/2)} - \underline{\phi}_{p-1,q}^{(k)}) \right]_2 \\
& + \left[ \sigma_{s,p-1,q-1} \underline{M}_{p-1,q-1} (\underline{\phi}_{p-1,q-1}^{(k+1/2)} - \underline{\phi}_{p-1,q-1}^{(k)}) \right]_3 \\
& + \left[ \sigma_{s,p,q-1} \underline{M}_{p,q-1} (\underline{\phi}_{p,q-1}^{(k+1/2)} - \underline{\phi}_{p,q-1}^{(k)}) \right]_4. \quad (148)
\end{aligned}$$

Our asymptotic derivation of the diffusion operator concentrated on the interior of the problem only. It is, therefore, implicitly correct on the boundary in the case of reflecting boundaries. However, for vacuum and incident boundaries, a slight change is necessary. Consider a diffusion correction equation

$$-\nabla \cdot D_{p,q} \nabla \underline{F}_{p,q}(x, y) + \sigma_{a,p,q} \underline{F}_{p,q}(x, y) = \underline{Q}_{p,q}(x, y). \quad (149)$$

If we take the first term of Eq. (149) and expand the scalar flux in terms of basis functions, and then apply the method of weighted residuals with Galerkin weighting, we find

$$\iint_{\Lambda} b_i(x, y) (-\nabla \cdot D_{p,q} \nabla \underline{F}_{p,q} b_j(x, y)) \, d\Lambda. \quad (150)$$

Applying the divergence theorem to this term yields

$$\begin{aligned}
& \iint_{\Lambda} b_i(x, y) (-\nabla \cdot D_{p,q} \nabla \underline{F}_{p,q} b_j(x, y)) \, d\Lambda = \\
& \iint_{\Lambda} \nabla b_i(x, y) \cdot D_{p,q} \nabla \underline{F}_{p,q} b_j(x, y) \, d\Lambda - \int_{\lambda} b_i(x, y) \hat{\mathbf{n}} \cdot D_{p,q} \nabla \underline{F}_{p,q} b_j(x, y) \, d\lambda. \quad (151)
\end{aligned}$$

Now consider the surface term

$$- \int_{\lambda} b_i(x, y) \hat{\mathbf{n}} \cdot D_{p,q} \nabla \underline{F}_{p,q} b_j(x, y) \, d\lambda. \quad (152)$$

If we define a current correction

$$\underline{\mathbf{G}}_{p,q}(x, y) = -D_{p,q} \nabla \underline{F}_{p,q} b_j(x, y), \quad (153)$$

then the surface term becomes

$$\int_{\lambda} b_i(x, y) \hat{\mathbf{n}} \cdot \underline{\mathbf{G}}_{p,q}(x, y) d\lambda. \quad (154)$$

Because the flux corrections  $\underline{F}_{p,q} b_j(x, y)$ , and thus the current corrections  $\underline{\mathbf{G}}_{p,q}(x, y)$  are continuous, this term is cancelled out on all interior surfaces. For the reflecting boundary,

$$\hat{\mathbf{n}} \cdot \underline{\mathbf{G}}_{p,q}(x, y) = 0, \quad (155)$$

and so this term is also zero on all reflecting boundaries.

For incident and vacuum boundaries,

$$\hat{\mathbf{n}} \cdot \underline{\mathbf{G}}_{p,q}(x, y) = \frac{\underline{F}_{p,q} b_j(x, y)}{2} - 2\underline{G}_{p,q}^-(x, y), \quad (156)$$

where  $\underline{G}_{p,q}^-(x, y)$  is the incident partial current correction. However, our incident angular flux boundary condition is exact. Therefore,  $\underline{G}_{p,q}^-(x, y) = 0$  and

$$\int_{\lambda} b_i(x, y) \hat{\mathbf{n}} \cdot \underline{\mathbf{G}}_{p,q}(x, y) d\lambda = \frac{1}{2} \underline{F}_{p,q} \int_{\lambda} b_i(x, y) b_j(x, y) d\lambda. \quad (157)$$

See Section 4.2 on how to perform this integral. This term should only be added to node positions in the matrix that are on an incident or vacuum boundary. Opposing reflecting boundaries require a special acceleration procedure which we will not examine here. A reference to this procedure may be found in [Ada 02].

The scalar flux correction should be added to the scalar flux at the end of the iteration. To summarize, the iteration equations for the asymptotic DSA are

$$\begin{aligned} & \hat{\Omega}_m \cdot \underline{\mathbf{S}}_{p,q}^h \underline{N}_{p,q} \psi_{m,p,q}^{h,(k+1/2)} + \hat{\Omega}_m \cdot \underline{\mathbf{S}}_{p,q}^v \underline{U}_{p,q} \psi_{m,p,q}^{v,(k+1/2)} \\ & + (\sigma_{t,p,q} \underline{M}_{p,q} - \mu_m \underline{L}_{p,q} - \eta_m \underline{K}_{p,q}) \psi_{m,p,q}^{(k+1/2)} = \frac{\sigma_{s,p,q}}{W} \underline{M}_{p,q} \phi_{p,q}^{(k)} + \underline{M}_{p,q} \underline{q}_{m,p,q}, \end{aligned} \quad (158a)$$

$$\underline{\phi}_{p,q}^{(k+1/2)} = \sum_{m=1}^M w_m \underline{\psi}_{m,p,q}^{(k+1/2)}, \quad (158b)$$

$$\begin{aligned} & \left[ (D_{p,q} \underline{T}_{p,q} + \sigma_{a,p,q} \underline{M}_{p,q}) \underline{F}_{p,q}^{(k+1/2)} \right]_1 + \left[ (D_{p-1,q} \underline{T}_{p-1,q} + \sigma_{a,p-1,q} \underline{M}_{p-1,q}) \underline{F}_{p-1,q}^{(k+1/2)} \right]_2 \\ & + \left[ (D_{p-1,q-1} \underline{T}_{p-1,q-1} + \sigma_{a,p-1,q-1} \underline{M}_{p-1,q-1}) \underline{F}_{p-1,q-1}^{(k+1/2)} \right]_3 \\ & + \left[ (D_{p,q-1} \underline{T}_{p,q-1} + \sigma_{a,p,q-1} \underline{M}_{p,q-1}) \underline{F}_{p,q-1}^{(k+1/2)} \right]_4 = \left[ \sigma_{s,p,q} \underline{M}_{p,q} (\underline{\phi}_{p,q}^{(k+1/2)} - \underline{\phi}_{p,q}^{(k)}) \right]_1 \\ & + \left[ \sigma_{s,p-1,q} \underline{M}_{p-1,q} (\underline{\phi}_{p-1,q}^{(k+1/2)} - \underline{\phi}_{p-1,q}^{(k)}) \right]_2 \\ & + \left[ \sigma_{s,p-1,q-1} \underline{M}_{p-1,q-1} (\underline{\phi}_{p-1,q-1}^{(k+1/2)} - \underline{\phi}_{p-1,q-1}^{(k)}) \right]_3 \\ & + \left[ \sigma_{s,p,q-1} \underline{M}_{p,q-1} (\underline{\phi}_{p,q-1}^{(k+1/2)} - \underline{\phi}_{p,q-1}^{(k)}) \right]_4, \quad (158c) \end{aligned}$$

$$\underline{\phi}_{p,q}^{(k+1)} = \underline{\phi}_{p,q}^{(k+1/2)} + \underline{F}_{p,q}^{(k+1/2)}. \quad (158d)$$

## 6.2 Asymptotic-P1 Diffusion Synthetic Acceleration

Asymptotic DSA does not always perform well for all problems in the thick diffusive limit. Warcing [War 92] found that continuous asymptotic DSA could be improved dramatically by calculating discontinuous flux corrections from the continuous asymptotic DSA flux corrections. Our derivation starts with the discretized  $S_N$  equation, Eq. (144), but we will replace the flux with the flux correction:

$$\begin{aligned} & \hat{\Omega}_m \cdot \underline{\mathbf{S}}_{p,q}^h N_{p,q} f_{m,p,q}^{h,(k+1/2)} + \hat{\Omega}_m \cdot \underline{\mathbf{S}}_{p,q}^v U_{p,q} f_{m,p,q}^{v,(k+1/2)} \\ & + \left[ \left( \sigma_{t,p,q} - \frac{\sigma_{s,p,q}}{W} \sum_{m=1}^N w_m \right) \underline{M}_{p,q} - \mu_m \underline{L}_{p,q} - \eta_m \underline{K}_{p,q} \right] \underline{f}_{m,p,q}^{(k+1/2)} = \\ & \frac{\sigma_{s,p,q}}{W} \underline{M}_{p,q} (\underline{\phi}_{p,q}^{(k+1/2)} - \underline{\phi}_{p,q}^{(k)}). \quad (159) \end{aligned}$$

Taking the zeroth angular moment of Eq. (159) gives us

$$\begin{aligned}
& (\underline{\mathbf{S}}_{p,q}^h \underline{N}_{p,q}) \cdot \underline{\mathbf{G}}_{p,q}^{h,(k+1/2)} + (\underline{\mathbf{S}}_{p,q}^v \underline{U}_{p,q}) \cdot \underline{\mathbf{G}}_{p,q}^{v,(k+1/2)} + \sigma_{a,p,q} \underline{M}_{p,q} \underline{F}_{p,q}^{(k+1/2)} \\
& - \underline{L}_{p,q} \underline{\mathbf{G}}_{p,q}^{(k+1/2)} \cdot \hat{\mathbf{e}}_x - \underline{K}_{p,q} \underline{\mathbf{G}}_{p,q}^{(k+1/2)} \cdot \hat{\mathbf{e}}_y = \sigma_{s,p,q} \underline{M}_{p,q} (\underline{\phi}_{p,q}^{(k+1/2)} - \underline{\phi}_{p,q}^{(k)}) . \quad (160)
\end{aligned}$$

We now take the first angular moment of Eq. (159), but we make the following change:

$$\underline{F}_{p,q}^h = \underline{F}_{p,q}^v = \underline{F}_{p,q} . \quad (161)$$

This yields

$$\begin{aligned}
& \frac{1}{3} (\underline{\mathbf{S}}_{p,q}^h \underline{N}_{p,q} + \underline{\mathbf{S}}_{p,q}^v \underline{U}_{p,q}) \underline{F}_{p,q}^{(k+1/2)} \\
& + \frac{2}{3} [(\underline{\mathbf{S}}_{p,q}^h \underline{N}_{p,q}) \cdot \underline{\mathbf{H}}_{p,q}^{h,(k+1/2)} + (\underline{\mathbf{S}}_{p,q}^v \underline{U}_{p,q}) \cdot \underline{\mathbf{H}}_{p,q}^{v,(k+1/2)}] \\
& + \sigma_{a,p,q} \underline{M}_{p,q} \underline{\mathbf{G}}_{p,q}^{(k+1/2)} - \frac{1}{3} (\underline{L}_{p,q} \hat{\mathbf{e}}_x + \underline{K}_{p,q} \hat{\mathbf{e}}_y) \underline{F}_{p,q}^{(k+1/2)} \\
& - \frac{2}{3} (\underline{L}_{p,q} \hat{\mathbf{e}}_x + \underline{K}_{p,q} \hat{\mathbf{e}}_y) \cdot \underline{\mathbf{H}}_{p,q}^{(k+1/2)} = 0 , \quad (162)
\end{aligned}$$

where

$$\underline{\mathbf{H}}_{p,q}^h = \sum_{m=1}^N (P_2(\mu_m) \hat{\mathbf{e}}_x + P_2(\eta_m) \hat{\mathbf{e}}_y) w_m \underline{f}_{m,p,q}^h , \quad (163a)$$

$$\underline{\mathbf{H}}_{p,q}^v = \sum_{m=1}^N (P_2(\mu_m) \hat{\mathbf{e}}_x + P_2(\eta_m) \hat{\mathbf{e}}_y) w_m \underline{f}_{m,p,q}^v , \quad (163b)$$

and

$$\underline{\mathbf{H}}_{p,q} = \sum_{m=1}^N (P_2(\mu_m) \hat{\mathbf{e}}_x + P_2(\eta_m) \hat{\mathbf{e}}_y) w_m \underline{f}_{m,p,q} . \quad (163c)$$

We now rewrite Eqs. (160) and (162), but we advance all indices to  $(k+1)$  (except the residual), and we discard the higher flux moments. Solving Eq. (162) for the current correction gives us Fick's Law:

$$\underline{\mathbf{G}}_{p,q}^{(k+1)} = -\frac{1}{3\sigma_{t,p,q}} \underline{M}_{p,q}^{-1} [\underline{\mathbf{S}}_{p,q}^h \underline{N}_{p,q} + \underline{\mathbf{S}}_{p,q}^v \underline{U}_{p,q} - \underline{L}_{p,q} \hat{\mathbf{e}}_x - \underline{K}_{p,q} \hat{\mathbf{e}}_y] \underline{F}_{p,q}^{(k+1)} , \quad (164)$$

while Eq. (160) rewritten is

$$\begin{aligned}
& (\underline{\mathbf{S}}_{p,q}^h \underline{N}_{p,q}) \cdot \underline{\mathbf{G}}_{p,q}^{h,(k+1)} + (\underline{\mathbf{S}}_{p,q}^v \underline{U}_{p,q}) \cdot \underline{\mathbf{G}}_{p,q}^{v,(k+1)} + \sigma_{a,p,q} \underline{M}_{p,q} F_{p,q}^{(k+1)} \\
& - \underline{L}_{p,q} \underline{\mathbf{G}}_{p,q}^{(k+1)} \cdot \hat{\mathbf{e}}_x - \underline{K}_{p,q} \underline{\mathbf{G}}_{p,q}^{(k+1)} \cdot \hat{\mathbf{e}}_y = \sigma_{s,p,q} \underline{M}_{p,q} (\phi_{p,q}^{(k+1/2)} - \phi_{p,q}^{(k)}) . \quad (165)
\end{aligned}$$

We wish to eliminate the current correction on the zone edges in order to compute discontinuous corrections that are local to a zone. We know that

$$\hat{\mathbf{n}}_f \cdot \underline{\mathbf{G}}_{p,q}^{\lambda_f} = G_{p,q}^{\lambda_f,+} - G_{p,q}^{\lambda_f,-} , \quad (166)$$

where  $G_{p,q}^{\lambda_f,+}$  is the exiting partial current on edge  $\lambda_f$  in zone  $(p,q)$ , and  $G_{p,q}^{\lambda_f,-}$  is the incident partial current. Diffusion theory states:

$$G_{p,q}^{\lambda_f,-} = \frac{F_{p,q}^{\lambda_f}}{4} - \frac{\hat{\mathbf{n}}_f \cdot \underline{\mathbf{G}}_{p,q}^{\lambda_f}}{2} , \quad (167)$$

$$G_{p,q}^{\lambda_f,+} = \frac{F_{p,q}^{\lambda_f}}{4} + \frac{\hat{\mathbf{n}}_f \cdot \underline{\mathbf{G}}_{p,q}^{\lambda_f}}{2} . \quad (168)$$

Adding the partial currents together and solving for the incident partial current reveals

$$G_{p,q}^{\lambda_f,-} = \frac{F_{p,q}^{\lambda_f}}{2} - G_{p,q}^{\lambda_f,+} . \quad (169)$$

By substituting this result into Eq. (166) we find

$$\hat{\mathbf{n}}_f \cdot \underline{\mathbf{G}}_{p,q}^{\lambda_f} = 2G_{p,q}^{\lambda_f,+} - \frac{F_{p,q}^{\lambda_f}}{2} . \quad (170)$$

The exiting partial current can be calculated from the in-cell flux and current correction vectors. We calculate the edge flux corrections using the asymptotic flux correction given in the last section. Substituting in the definitions for the exiting partial currents given above yields

$$\hat{\mathbf{n}}_f \cdot \underline{\mathbf{G}}_{p,q}^{\lambda_f} = \frac{F_{p,q} - F_{p,q}^{cc}}{2} + \hat{\mathbf{n}}_f \cdot \underline{\mathbf{G}}_{p,q} . \quad (171)$$

where  $F_{p,q}^{cc}$  is the continuous flux correction acquired from the asymptotic DSA, Section 6.1.



Substituting back into Eq. (165) gives

$$\begin{aligned}
& (\underline{N}_{p,q} + \underline{U}_{p,q}) \left( \frac{\underline{F}_{p,q}^{(k+1)} - \underline{F}_{p,q}^{cc,(k+1/2)}}{2} \right) + \sigma_{a,p,q} \underline{M}_{p,q} \underline{F}_{p,q}^{(k+1)} \\
& + (\underline{S}_{p,q}^h \underline{N}_{p,q} + \underline{S}_{p,q}^v \underline{U}_{p,q}) \cdot \underline{G}_{p,q}^{(k+1)} \\
& - \underline{L}_{p,q} \underline{G}_{p,q}^{(k+1)} \cdot \hat{\mathbf{e}}_x - \underline{K}_{p,q} \underline{G}_{p,q}^{(k+1)} \cdot \hat{\mathbf{e}}_y = \sigma_{s,p,q} \underline{M}_{p,q} (\phi_{p,q}^{(k+1/2)} - \phi_{p,q}^{(k)}) . \quad (172)
\end{aligned}$$

Inserting Eq. (164) into the equation above and rearranging yields:

$$\begin{aligned}
& \left[ \frac{1}{2} (\underline{N}_{p,q} + \underline{U}_{p,q}) + \sigma_{a,p,q} \underline{M}_{p,q} - \frac{1}{3\sigma_{t,p,q}} \underline{\mathbf{V}}_{p,q} \cdot \underline{M}_{p,q}^{-1} \underline{\mathbf{V}}_{p,q} \right] \underline{F}_{p,q}^{(k+1)} = \\
& \sigma_{s,p,q} \underline{M}_{p,q} (\phi_{p,q}^{(k+1/2)} - \phi_{p,q}^{(k)}) + \frac{1}{2} (\underline{N}_{p,q} + \underline{U}_{p,q}) \underline{F}_{p,q}^{cc,(k+1/2)} , \quad (173)
\end{aligned}$$

where

$$\underline{\mathbf{V}}_{p,q} = \underline{S}_{p,q}^h \underline{N}_{p,q} + \underline{S}_{p,q}^v \underline{U}_{p,q} - \underline{L}_{p,q} \hat{\mathbf{e}}_x - \underline{K}_{p,q} \hat{\mathbf{e}}_y . \quad (174)$$

To summarize, the iteration equations for the asymptotic-P1 DSA are

$$\begin{aligned}
& \hat{\Omega}_m \cdot \underline{S}_{p,q}^h \underline{N}_{p,q} \psi_{m,p,q}^{h,(k+1/2)} + \hat{\Omega}_m \cdot \underline{S}_{p,q}^v \underline{U}_{p,q} \psi_{m,p,q}^{v,(k+1/2)} \\
& + (\sigma_{t,p,q} \underline{M}_{p,q} - \mu_m \underline{L}_{p,q} - \eta_m \underline{K}_{p,q}) \psi_{m,p,q}^{(k+1/2)} = \frac{\sigma_{s,p,q}}{W} \underline{M}_{p,q} \phi_{p,q}^{(k)} + \underline{M}_{p,q} q_{m,p,q} , \quad (175a)
\end{aligned}$$

$$\phi_{p,q}^{(k+1/2)} = \sum_{m=1}^M w_m \psi_{m,p,q}^{(k+1/2)} , \quad (175b)$$

$$\begin{aligned}
& \left[ (D_{p,q} \underline{T}_{p,q} + \sigma_{a,p,q} \underline{M}_{p,q}) \underline{F}_{p,q}^{cc,(k+1/2)} \right]_1 \\
& + \left[ (D_{p-1,q} \underline{T}_{p-1,q} + \sigma_{a,p-1,q} \underline{M}_{p-1,q}) \underline{F}_{p-1,q}^{cc,(k+1/2)} \right]_2 \\
& + \left[ (D_{p-1,q-1} \underline{T}_{p-1,q-1} + \sigma_{a,p-1,q-1} \underline{M}_{p-1,q-1}) \underline{F}_{p-1,q-1}^{cc,(k+1/2)} \right]_3 \\
& + \left[ (D_{p,q-1} \underline{T}_{p,q-1} + \sigma_{a,p,q-1} \underline{M}_{p,q-1}) \underline{F}_{p,q-1}^{cc,(k+1/2)} \right]_4 = [\sigma_{s,p,q} \underline{M}_{p,q} (\underline{\phi}_{p,q}^{(k+1/2)} - \underline{\phi}_{p,q}^{(k)})]_1 \\
& + \left[ \sigma_{s,p-1,q} \underline{M}_{p-1,q} (\underline{\phi}_{p-1,q}^{(k+1/2)} - \underline{\phi}_{p-1,q}^{(k)}) \right]_2 \\
& + \left[ \sigma_{s,p-1,q-1} \underline{M}_{p-1,q-1} (\underline{\phi}_{p-1,q-1}^{(k+1/2)} - \underline{\phi}_{p-1,q-1}^{(k)}) \right]_3 \\
& + \left[ \sigma_{s,p,q-1} \underline{M}_{p,q-1} (\underline{\phi}_{p,q-1}^{(k+1/2)} - \underline{\phi}_{p,q-1}^{(k)}) \right]_4, \quad (175c)
\end{aligned}$$

$$\begin{aligned}
& \left[ \frac{1}{2} (\underline{N}_{p,q} + \underline{U}_{p,q}) + \sigma_{a,p,q} \underline{M}_{p,q} - \frac{1}{3\sigma_{t,p,q}} \underline{\mathbf{V}}_{p,q} \cdot \underline{M}_{p,q}^{-1} \underline{\mathbf{V}}_{p,q} \right] \underline{F}_{p,q}^{(k+1)} = \\
& \sigma_{s,p,q} \underline{M}_{p,q} (\underline{\phi}_{p,q}^{(k+1/2)} - \underline{\phi}_{p,q}^{(k)}) + \frac{1}{2} (\underline{N}_{p,q} + \underline{U}_{p,q}) \underline{F}_{p,q}^{cc,(k+1)}, \quad (175d)
\end{aligned}$$

$$\underline{\phi}_{p,q}^{(k+1)} = \underline{\phi}_{p,q}^{(k+1/2)} + \underline{F}_{p,q}^{(k+1)}. \quad (175e)$$

## 7 NUMERICAL RESULTS

We now present three test problems that analyze different aspects of the Wachspres rational function discretization. Test problem 1 will look at the robustness of the method, test problem 2 will examine the convergence of the method in the thick diffusive limit, and test problem 3 will compare the accuracy of Wachspres rational functions versus isoparametric bilinear discontinuous functions on skewed zones.

### 7.1 Test Problem 1

This problem is adapted from [Pal 93]. In this test problem, we consider a square region one centimeter on a side, containing five material regions. The orthogonal and skewed meshes used are shown in Figures 15 and 16. The materials

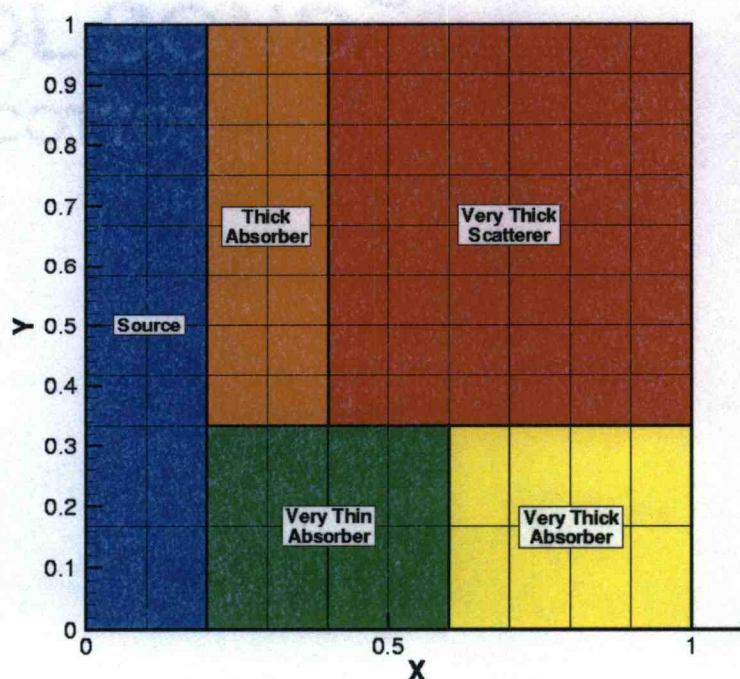


Figure 15: Problem 1 — Orthogonal Mesh Configuration

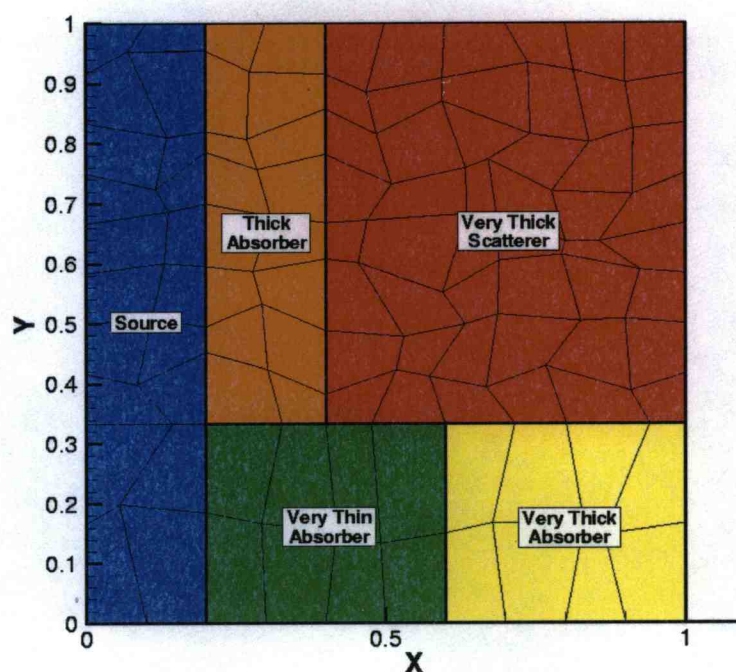


Figure 16: Problem 1 — Skewed Mesh Configuration

Material Region	$\sigma_t$ [ $\text{cm}^{-1}$ ]	$\sigma_s$ [ $\text{cm}^{-1}$ ]
Source	1.0	1.0
Very Thin Absorber	0.0001	0.0
Thick Absorber	10.0	0.0
Very Thick Absorber	100.0	0.0
Very Thick Scatterer	1000.0	1000.0

Table 3: Problem 1 — Material Cross Sections



used in this test problem are shown in Table 3. This problem has a reflecting boundary on the left and vacuum boundaries on the top, bottom, and right. The source region has an isotropic particle source of strength 1.0. We ran the problem with an  $S_4$  quadrature set, and used Wachspress rational basis functions on both the orthogonal and skewed meshes.

This problem illustrates the ability of the Wachspress rational function discretization to model a difficult problem on both orthogonal and skewed meshes. The solution varies across the problem by about ten orders of magnitude. Physically, particles are born in the source region on the left of the problem. Most particles are either absorbed in the thick absorber, or stream through the very thin absorber and impinge upon the very thick scatterer.

We first analyze the results for the orthogonal case. Figures 17 and 18 show results for both the unlumped and fully lumped cases. The white patches in the unlumped solution depict where the solution is negative. This illustrates the usefulness of lumping the matrices, because the discretization is more robust and negative solutions are avoided. Figure 19 shows the base-ten logarithm of the flux for the fully lumped case, which more clearly shows the flux contours in the regions where the flux is small.

Figures 20 and 21 show the results for both the unlumped and fully lumped cases on the skewed mesh. Figure 22 shows the base-ten logarithm of the flux for the fully lumped case.

Our results clearly indicate that the Wachspress rational function discretization is able to capture the solution correctly on skewed zones. Some mesh effects are evident, but the discretization performs robustly in the thick diffusive limit provided full matrix lumping is used.

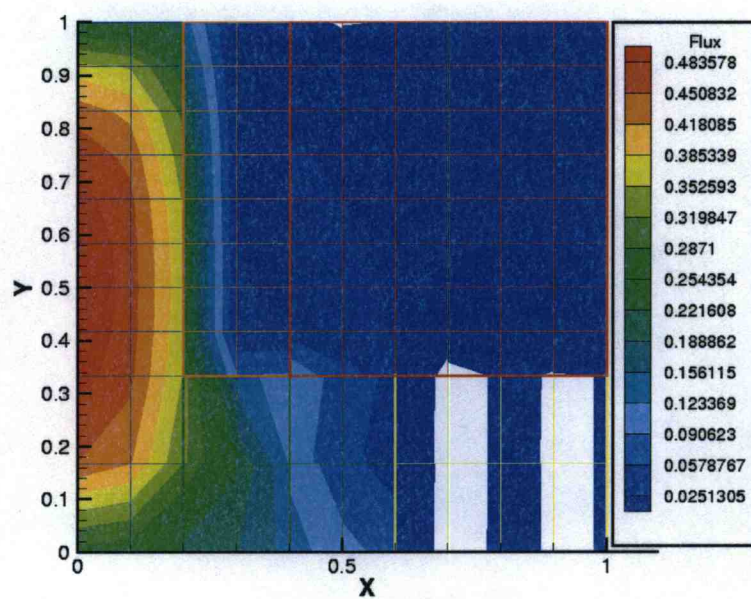


Figure 17: Problem 1 — Orthogonal Unlumped Solution

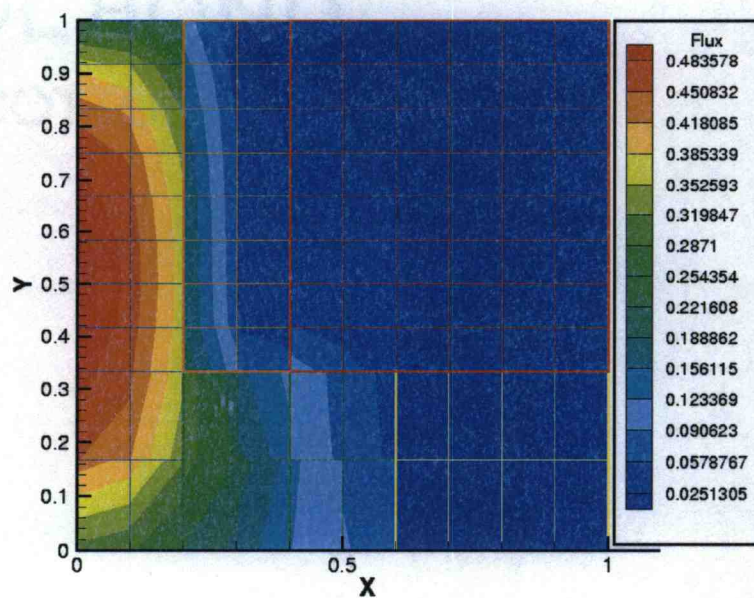


Figure 18: Problem 1 — Orthogonal Fully Lumped Solution



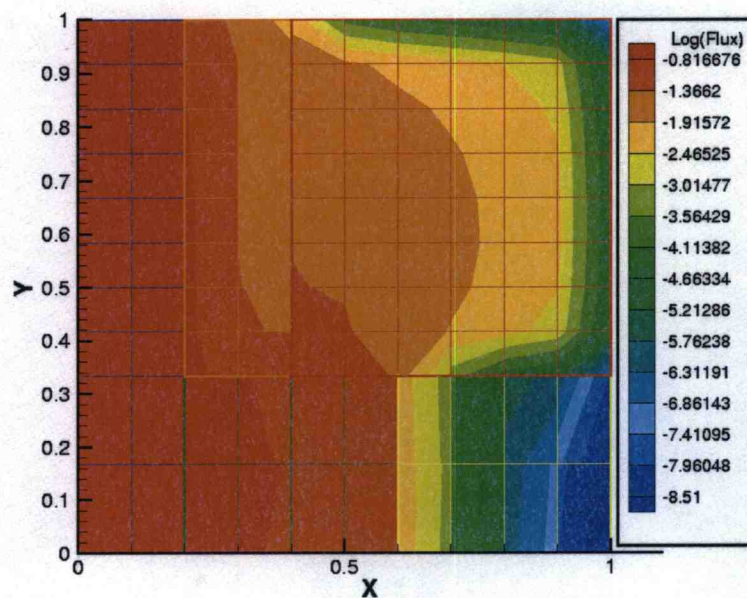


Figure 19: Problem 1 — Orthogonal Log(Flux) Solution

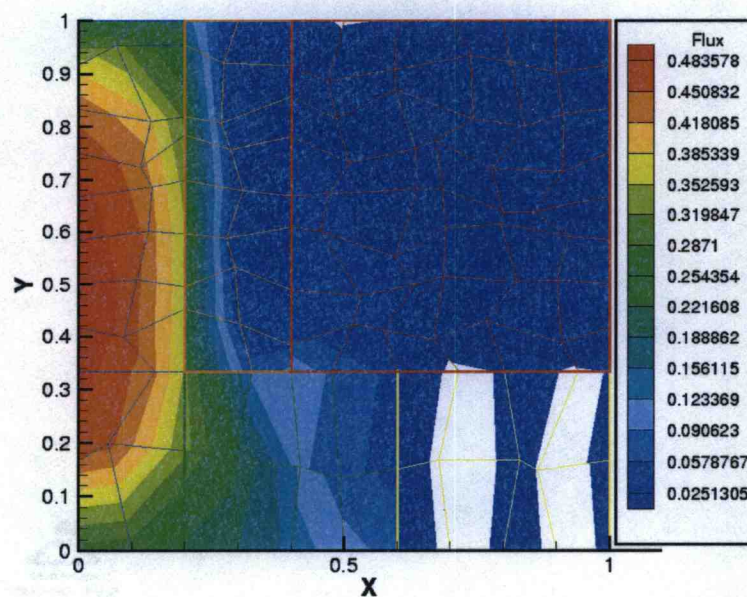


Figure 20: Problem 1 — Skewed Unlumped Solution



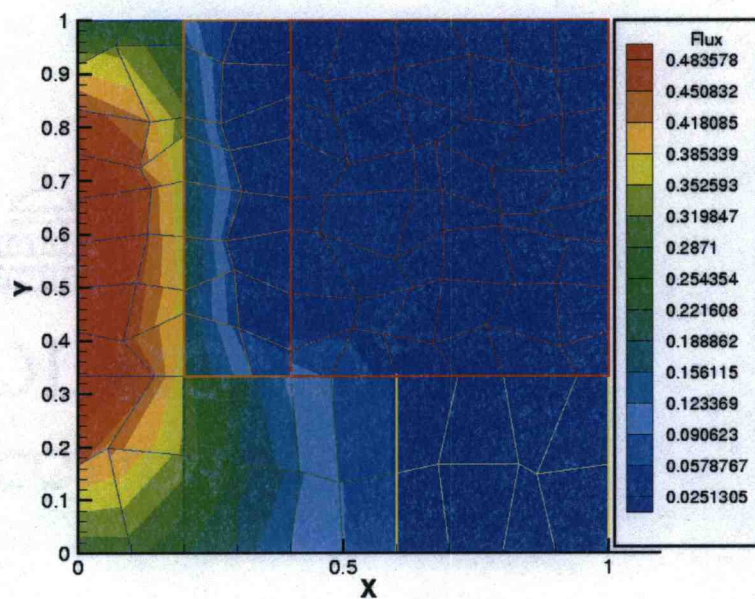


Figure 21: Problem 1 — Skewed Fully Lumped Solution

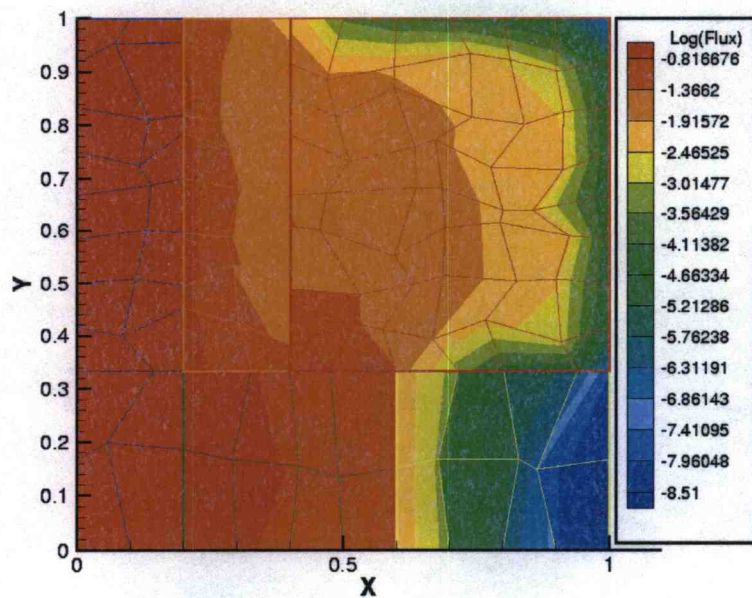


Figure 22: Problem 1 — Skewed Log(Flux) Solution



## 7.2 Test Problem 2

For this test problem, we wish to test our asymptotic analysis on both orthogonal and skewed meshes for the fully lumped scheme. This problem is taken from [War 92]. The spatial domain is discretized into a 10x10 grid ( $0 \leq x \leq 0.5$ ,  $0 \leq y \leq 0.5$ ) filled with a homogenous material with the following properties:

$$q_m = \epsilon, \quad (176a)$$

$$\sigma_t = \frac{1}{\epsilon}, \quad (176b)$$

and

$$\sigma_s = \frac{1}{\epsilon} - \epsilon. \quad (176c)$$

We vary  $\epsilon$  from  $10^{-1}$  to  $10^{-5}$ . There are reflecting boundaries on the right and top, and vacuum boundaries on the bottom and left, and we used a  $S_2$  quadrature set.

On the same spatial grid, we solved the asymptotically derived diffusion discretization of the following diffusion problem:

$$-\frac{1}{3} \frac{\partial^2}{\partial x^2} \phi(x, y) - \frac{1}{3} \frac{\partial^2}{\partial y^2} \phi(x, y) + \phi(x, y) = 1, \quad (177)$$

with reflecting boundaries on the right and top, and  $\phi(x, y) = 0$  boundaries on the left and bottom.

If the asymptotic analysis is correct, the transport solution should converge to the diffusion solution as the transport problem becomes increasingly thick and diffusive, that is as  $\epsilon \rightarrow 0$ . Figure 23 shows the diffusion solution on an orthogonal grid, and Figure 24 shows the diffusion solution on a skewed grid.

The error difference between the transport solution and the orthogonal solution should decrease as epsilon decreases. Figures 25-30 show the decreasing error function.

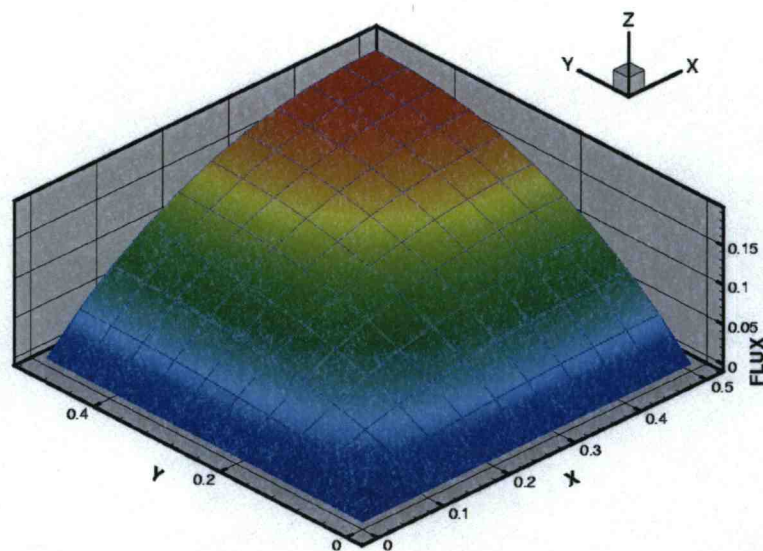


Figure 23: Problem 2 — Diffusion Solution on an Orthogonal Grid

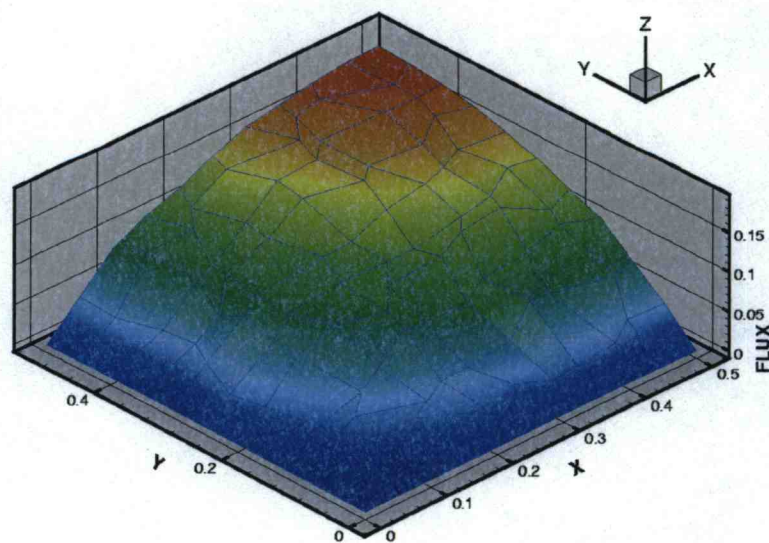


Figure 24: Problem 2 — Diffusion Solution on a Skewed Grid



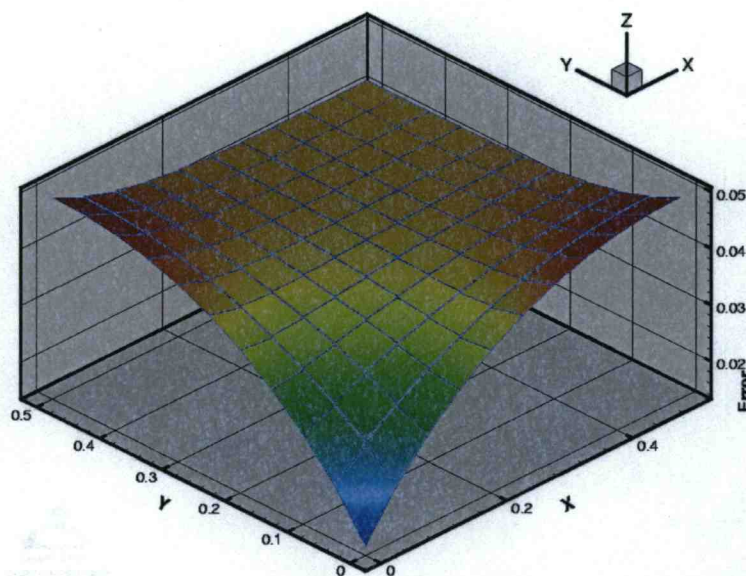


Figure 25: Problem 2 — Error Function for Orthogonal Grid,  $\epsilon = 10^{-1}$

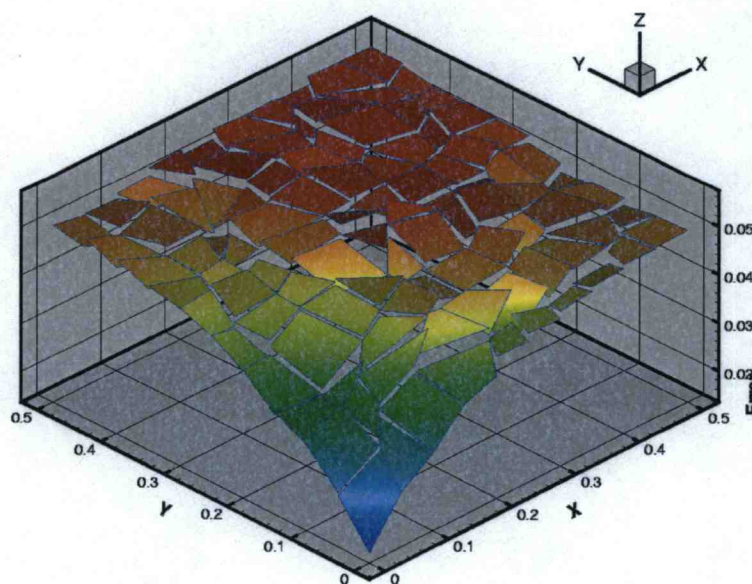


Figure 26: Problem 2 — Error Function for Skewed Grid,  $\epsilon = 10^{-1}$



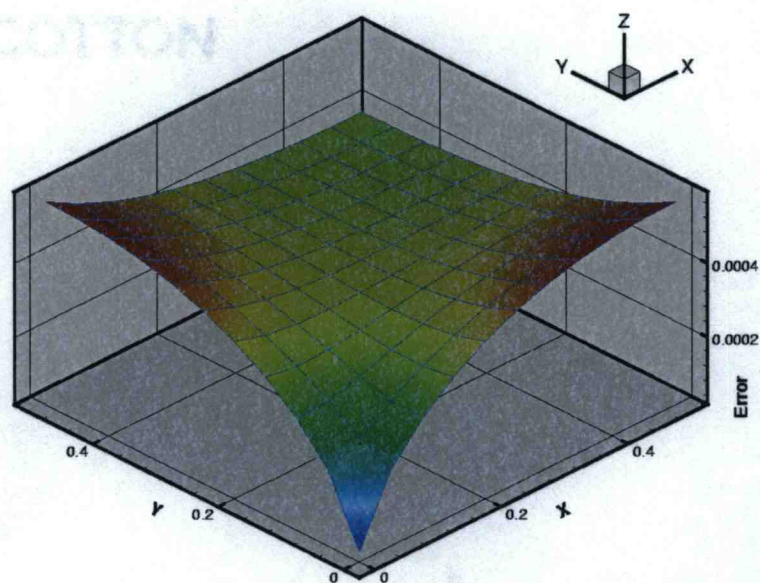


Figure 27: Problem 2 — Error Function for Orthogonal Grid,  $\epsilon = 10^{-3}$

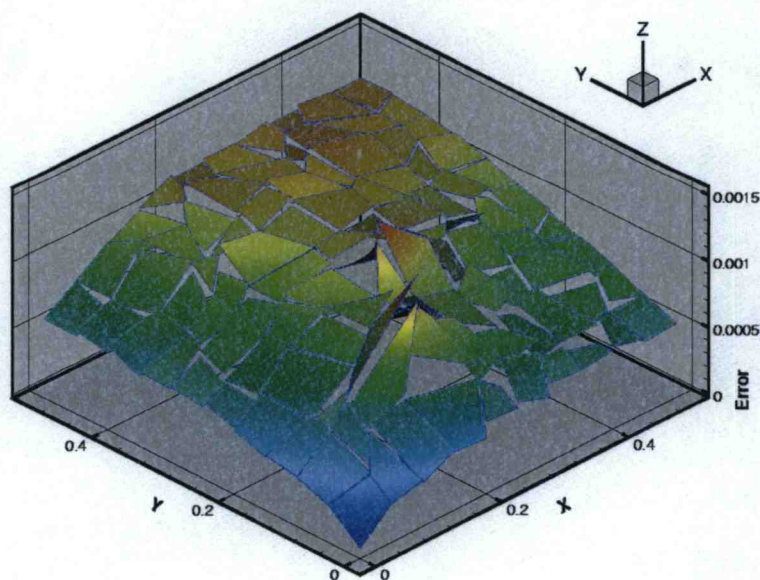


Figure 28: Problem 2 — Error Function for Skewed Grid,  $\epsilon = 10^{-3}$



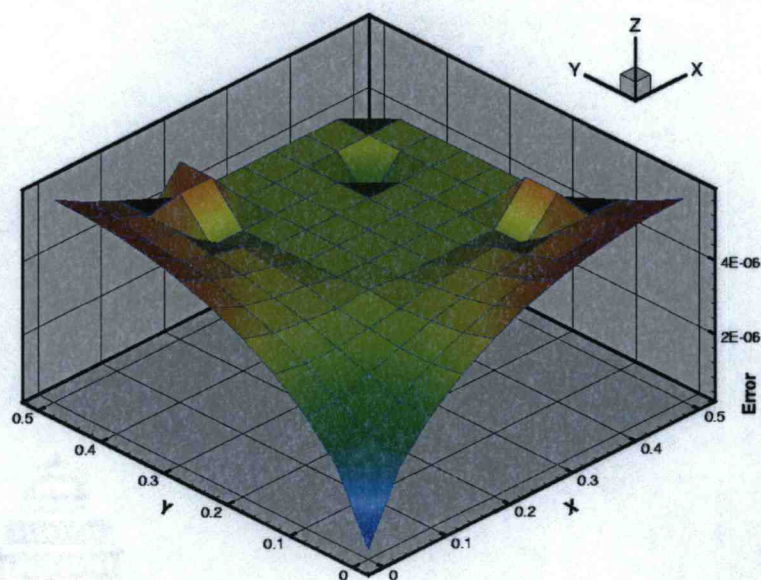


Figure 29: Problem 2 — Error Function for Orthogonal Grid,  $\epsilon = 10^{-5}$

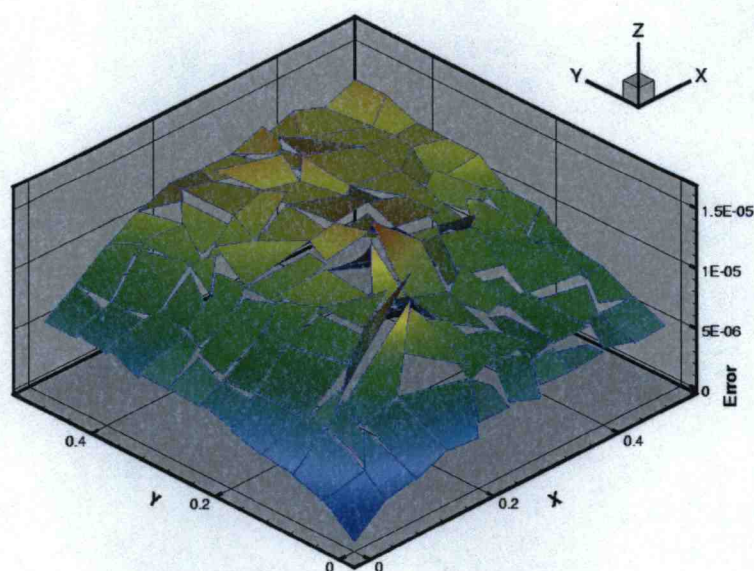


Figure 30: Problem 2 — Error Function for Skewed Grid,  $\epsilon = 10^{-5}$



Note that in Figures 25-30, the magnitude of the error decreases as  $\epsilon$  is decreased. The error function shape stays roughly constant for the orthogonal case, with some slight bumps appearing in the solution when  $\epsilon = 10^{-5}$ . This is likely due to roundoff error. For the skewed solution, we find the error is greater than in the case of the orthogonal zones. This is likely due to mesh effects in both the diffusion and transport solutions. In addition, spikes can be seen in the error function in two locations; these are most pronounced in the  $\epsilon = 10^{-5}$  case. These locations are where a zone is nearly triangular, and likely represents a roundoff or truncation error in the construction or integration routines.

In Figure 31 we can see how the transport solution converges to the diffusion solution as epsilon decreases for both orthogonal and skewed meshes. This indicates that our asymptotic analysis is correct.

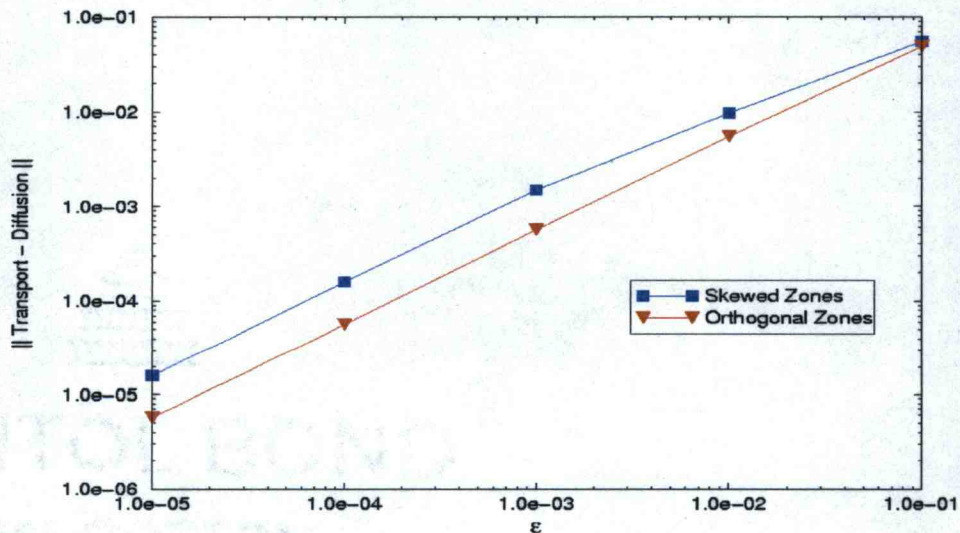


Figure 31: Problem 2 — Convergence of Transport to Diffusion

### 7.3 Test Problem 3

For our third test problem we wish to compare the accuracy of solutions using isoparametric bilinear basis functions to solutions using Wachspress rational basis



functions on a skewed mesh. To do this we will reexamine test problem 1 (Section 7.1). First, this test problem was solved on a fine mesh. Figure 32 shows the solution on a 1200x1000 orthogonal grid for the lumped mass-matrix case. Ray effects can be seen in the very thin absorber region. This is a result of the coarse angular discretization ( $S_4$ ).

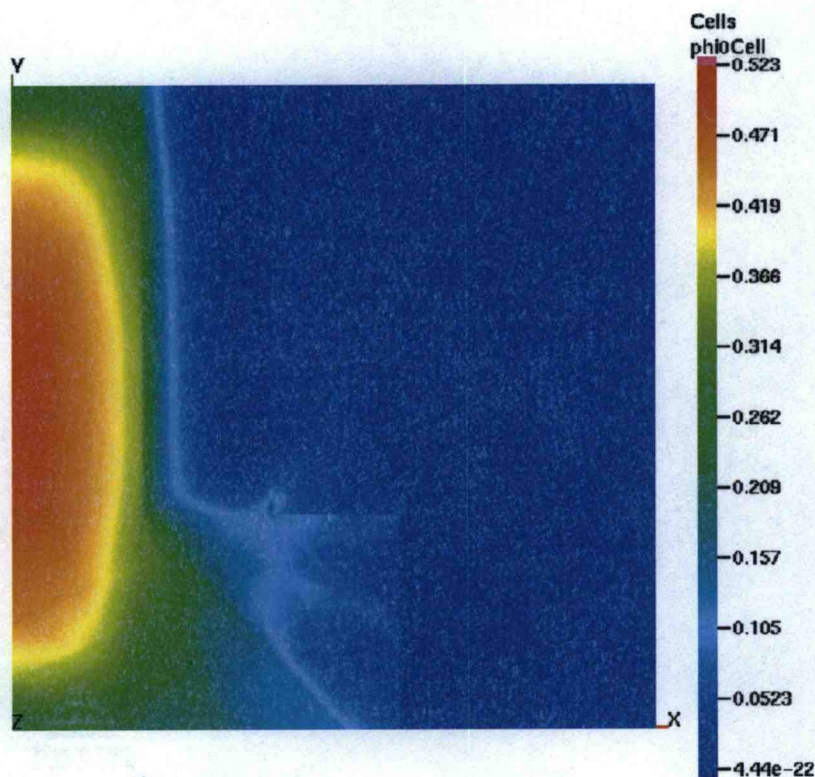


Figure 32: Problem 3 — Fine Mesh Solution

The test problem was then solved on a coarse grid, first using isoparametric bilinear basis functions, and then again using Wachspress rational basis functions. In each case the coarse mesh solution was calculated with the fully-lumped version of the discretization. Figures 33 and 34 show the error and the logarithm of the error, respectively, of the coarse mesh isoparametric bilinear basis function solution versus the fine mesh solution. Figures 35 and 36 show the error and the logarithm of the error, respectively, of the coarse mesh Wachspress rational basis function



solution versus the fine mesh solution. In each case the error is calculated as the absolute value of the difference between the solutions.

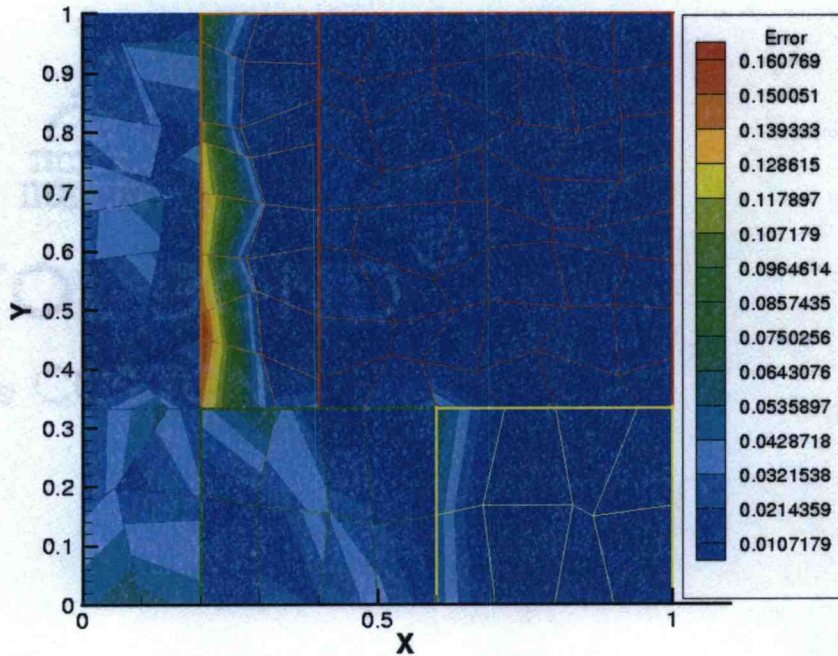


Figure 33: Problem 3 — Error of BLD Coarse Solution

Table 4 shows the maximum error for the isoparametric bilinear basis function solution and the Wachspress rational basis function solution. From the figures and

Coarse and Fine Solution Comparison	Maximum Absolute Error
Bilinear vs. Fine Mass-Matrix Lumped	0.171399
Bilinear vs. Fine Unlumped	0.171487
Wachspress vs. Fine Mass-Matrix Lumped	0.172121
Wachspress vs. Fine Unlumped	0.172033

Table 4: Problem 3 — Maximum Error for Each Discretization

from the table we can see that the maximum error in the solutions for both the isoparametric bilinear basis function and the Wachspress rational basis function discretizations are similar, whether being compared to the fine mesh solution for the unlumped discretization or the fine mesh solution for the lumped mass-matrix discretization. For both basis functions, the absolute error is highest near material



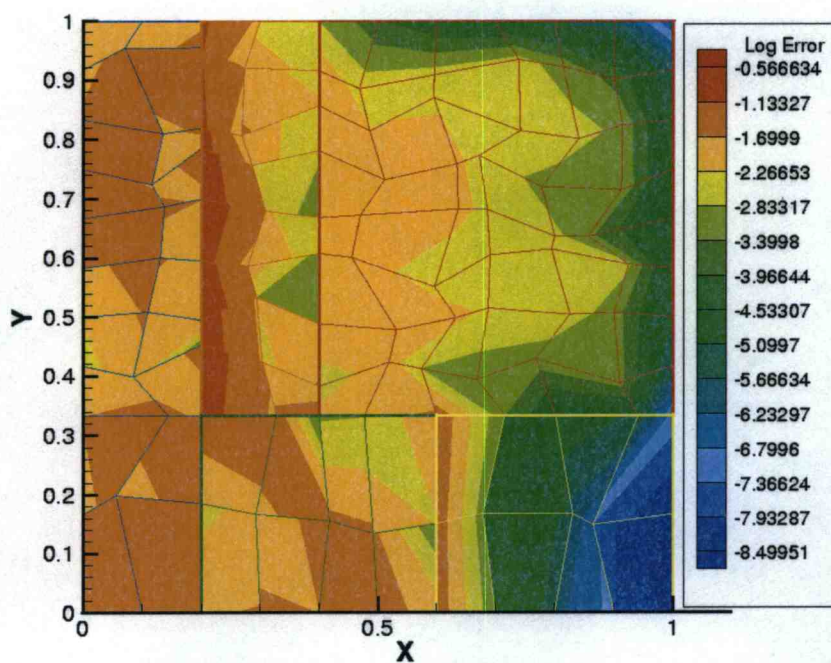


Figure 34: Problem 3 — Logarithm of Error of BLD Coarse Solution

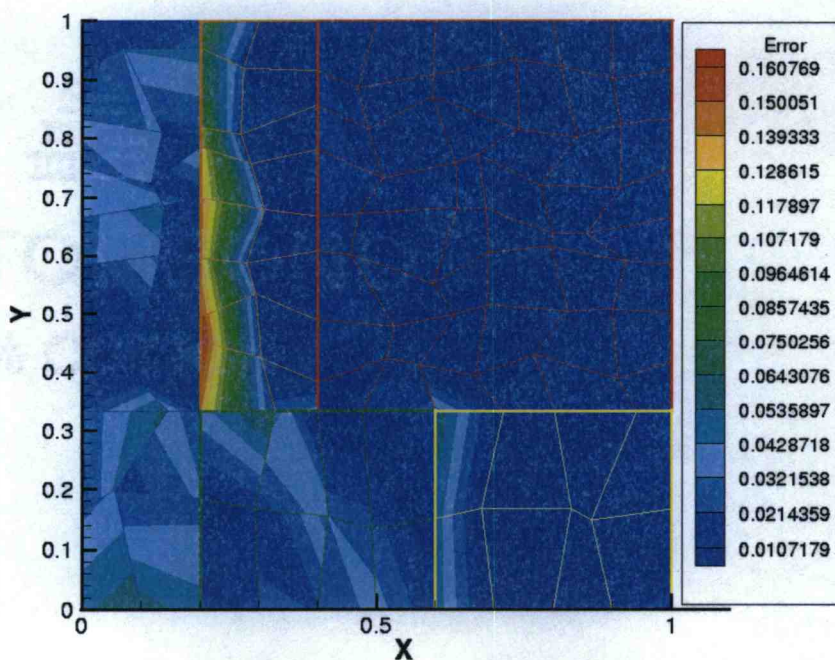


Figure 35: Problem 3 — Error of Wachspress Coarse Solution



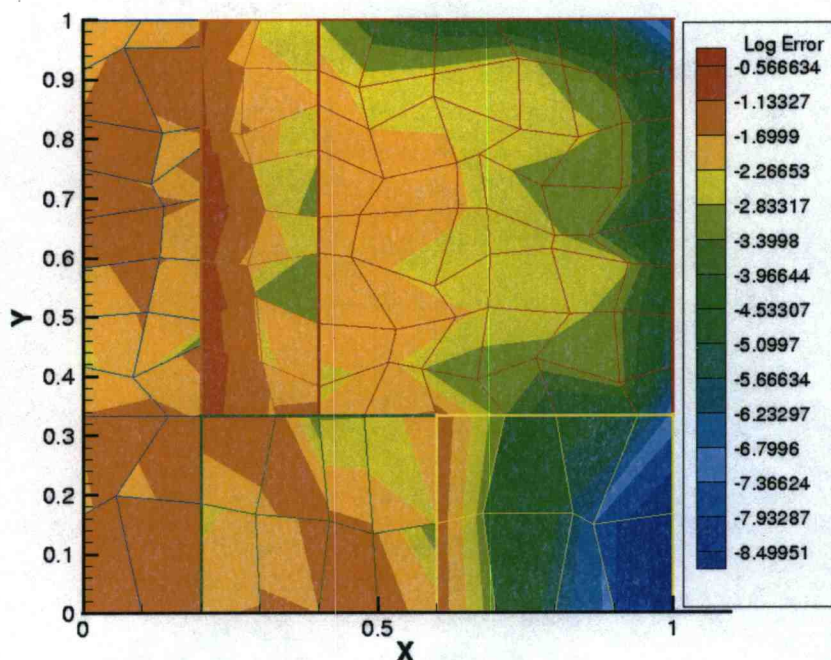


Figure 36: Problem 3 — Logarithm of Error of Wachspress Coarse Solution

boundaries, as we would expect, since the coarse mesh solutions cannot capture the boundary layers as accurately as the fine mesh solutions can. We also see that the error in comparison to the fine mesh solution for the lumped mass-matrix discretization is somewhat less than the error in comparison to the fine mesh solution for the unlumped discretization. This is not surprising since both of the coarse mesh solutions employed a (fully) lumped discretization.

We also see that the solution using isoparametric bilinear basis functions is somewhat more accurate than the solution using Wachspress rational basis functions. The difference may be due to slight inaccuracies in the integration or construction algorithms for the Wachspress rational functions. More numerical testing of the method may be necessary to completely understand its behavior in the wide variety of transport problems encountered in nature.

## 8 CONCLUSION

In this study we have presented an analysis of discontinuous finite element transport using Wachspress rational basis functions in the thick diffusive limit. These basis functions are continuous in the zone, interpolate a constant field exactly, and are linear on the boundary. One of the principle advantages of Wachspress rational basis functions is that they can be constructed on arbitrary polygons and polyhedra. Adams [Ada 01] provided new reasons to investigate Wachspress rational functions. Adams predicted theoretically that discontinuous finite element transport discretizations using certain classes of weight functions, including Wachspress rational functions, would perform well in the thick, diffusive limit. While Adams provided numerical evidence for certain weight functions (including bilinear discontinuous), he did not provide numerical evidence for Wachspress rational functions. In this study, we have attempted to provide a thorough investigation of Wachspress rational functions on convex quadrilaterals, including their construction, integration, and performance in thick, diffusive regions.

We began our study by deriving a general finite element discretization in Section 2.1. This derivation is performed in two spatial dimensions for general basis functions and weight functions on a general zone. In Section 2.2, we simplify this derivation for quadrilateral zones and Galerkin weighting. This is the derivation that was implemented to produce the numerical results in Section 7. In Section 2.3, we discuss three types of matrix lumping: mass-matrix lumping, surface-matrix lumping, and full lumping. Lumping helps to “localize” the transport discretization. This adds robustness to the method in thick problems, causing the solution to be nonnegative and less susceptible to non-physical oscillations.

In Section 3 we discuss how to construct the two bases we used in our study.

The first basis, which we discuss in Section 3.1, is the isoparametric bilinear (BLD) basis. This is the “standard” method for solving transport problems on general quadrilaterals. The second basis is the Wachspress rational basis. We presented two methodologies for constructing these basis functions. The first, presented in Section 3.2, we have called the direct method. This method operates by calculating the external diameter (which is needed for the denominator of the rational basis function) directly. In Section 3.3, we have presented Dasgupta’s method [Das 03a], an alternative method for constructing Wachspress rational basis functions. This method uses the linearity of Wachspress rational basis functions on the boundary of the zone to construct the denominator. This method has the advantage of avoiding the construction of the external diameter. However, in Section 3.4 we find that Dasgupta’s method is slower than the direct method for quadrilaterals. On the other hand, the complexity of the direct method increases significantly as one moves beyond linear external diameters. For this reason, we recommend using the direct method when constructing Wachspress rational functions on meshes composed purely of quadrilaterals, and using Dasgupta’s method otherwise.

In order to construct the matrices in our discontinuous finite element discretization, we must calculate integrals of basis functions. These integrals come in two forms: integrals over the area of the zone, and integrals over the boundary of the zone. We present several methods for integrating over the area of the zone. For the isoparametric bilinear basis functions, these functions are integrated in the isoparametric space in which they were constructed, and that integral is then mapped into the Cartesian space of the zone (Section 4.1.1). The integrals are performed using a Gauss-Legendre quadrature set. For the Wachspress rational basis functions, our implementation maps the basis functions into the isoparametric space, and integrates them using a Gauss-Legendre quadrature set. The

integrals are then mapped back into Cartesian space. This is described in Section 4.1.2. Dasgupta has also suggested a method for integrating over the area of a zone [Das 03b]. This involves repeatedly applying the divergence theorem to the integral until it is simplified to a line integral, and is described in Section 4.1.3. Unfortunately, our integrand (involving products of Wachspress rational functions and their derivatives) is algebraically complex, making Dasgupta's method prohibitively difficult to implement in a compiled language like C++. On the other hand, the isoparametric method can only be applied to quadrilaterals. There may be other integration methods, such as Gauss-Legendre quadrature on triangular sub-cells, that may offer a solution. More research is needed in this area. We leave this problem unsolved at this time. Due to the linearity of Wachspress rational basis functions and isoparametric bilinear basis functions, integration over the edges of a zone is trivial, and is described in Section 4.2.

In order to accelerate our transport iterations, and in order to understand how our discretization will behave in the thick, diffusive limit, an asymptotic analysis was performed in Section 5. This analysis resulted in a diffusion discretization that is consistent with our transport discretization. The need for acceleration was addressed in Section 6. We used our asymptotically derived diffusion discretization, and our derived boundary conditions, to create an asymptotic DSA preconditioner to accelerate our iterations. The asymptotic DSA preconditioner is known to degrade on problems with highly scattering regions however, so we derived the asymptotic-P1 DSA preconditioner in Section 6.2. This preconditioner was first developed in [War 92], and is known to perform well on highly scattering problems with orthogonal or skewed meshes. This acceleration scheme was used to generate all of our numerical results.

Finally, we presented three test problems and their numerical results. Test

problem 1 (Section 7.1) demonstrates the performance of Wachspress rational functions on both orthogonal and skewed grids. This problem is strongly heterogeneous, with highly scattering regions adjacent to highly absorbing regions. We solved this problem with both unlumped and fully lumped schemes, demonstrating the need for lumping to ensure a robust solution. The implementation performs well on both the orthogonal and the skewed grids.

Test problem 2 (Section 7.2) shows the convergence of the transport discretization to the asymptotically derived diffusion discretization as the problem becomes increasingly optically thick and diffusive. This problem was solved on both orthogonal and skewed meshes. As expected, the discretization correctly converges to the diffusion limit. The error is greater in the skewed case, and this is likely due to mesh effects, as well as some error inherent in the construction and integration algorithms on highly skewed zones, and is to be expected.

Test problem 3 (Section 7.3) compared the accuracy of a solution using a Wachspress rational basis function discretization and a solution using an isoparametric bilinear basis function discretization on a coarse, skewed mesh by comparing them to solutions using a bilinear basis function discretization on a fine orthogonal mesh. We found that the error is always largest near material boundaries because the coarse solutions cannot capture boundary layers as accurately as the fine solution. In addition, we found that the error of the isoparametric bilinear basis function solution is somewhat less, possibly due to small inaccuracies in the construction and integration algorithms for the Wachspress rational functions.

There are several areas involving Wachspress rational functions that warrant further investigation. Of utmost importance is the discovery of an efficient method for integration of Wachspress rational functions over the area (or volume) of an arbitrary polygonal or polyhedral zone. We believe this may be one of the last

hurdles to overcome before Wachspress rational functions can be made available for widespread use. Other topics that warrant future investigation are the behavior of Wachspress rational functions on polyhedra, as well as zones with curved (non-linear) sides and faces. We are also interested in the use of Wachspress rational basis functions in characteristic-based transport discretizations.

## BIBLIOGRAPHY

- [Ada 01] Adams, M.L., "Discontinuous Finite Element Transport Solutions in Thick Diffusive Problems", *Nuclear Science and Engineering*, **137**, 298 (2001).
- [Ada 02] Adams, M.L. and Larsen, E.W., "Fast Iterative Methods for Discrete-Ordinates Particle Transport Calculations", *Progress in Nuclear Energy*, **40**, No. 1, 3 (2002).
- [Das 01] Dasgupta, G., "Boundary Element Color Interpolation for Instrumentation, Imaging and Internet Graphics Industries", Available online: [www.columbia.edu/~gd18/BECOLOR.pdf](http://www.columbia.edu/~gd18/BECOLOR.pdf) (2001).
- [Das 03a] Dasgupta, G., "Interpolants within Convex Polygons: Wachspress' Shape Functions", *Journal of Aerospace Engineering*, **16**, No. 1, 1 (2003).
- [Das 03b] Dasgupta, G., "Integration within Polygonal Finite Elements", *Journal of Aerospace Engineering*, **16**, No. 1, 9 (2003).
- [Lew 93] Lewis, E.E. and Miller, W.F., **Computational Methods of Neutron Transport**, American Nuclear Society, Inc., La Grange Park, IL (1993).
- [Lar 02] Larsen, E.W., et. al., "Simplified  $P_N$  Approximations to the Equations of Radiative Heat Transfer and Applications", *Journal of Computational Physics*, **183**, 652 (2002).
- [Pal 93] Palmert, T.S., "Curvilinear Geometry Transport Discretizations in Thick Diffusive Regions", Doctoral Dissertation, Lawrence Livermore National Laboratory, Livermore, CA (1993).
- [Rat 00] Rathkopf, J.A., et. al., "Kull: LLNL's ASCI Inertial Confinement Fusion Simulation Code", *Proceedings of the International Topical Meeting on Advances in Reactor Physics and Mathematics and Computation into the Next Millennium*, Session VIII.A1, Paper No. 5, pg. 1-24, Pittsburgh, PA, May 7-11 (2000).
- [Seg 84] Segerlind, L.J., **Applied Finite Element Analysis**, John Wiley and Sons, New York (1984).
- [Wac 75] Wachspress, E.L., **A Rational Finite Element Basis**, Academic Press, Inc., New York (1975).
- [War 92] Wareing, T.A. (1992), "Asymptotic Diffusion Accelerated Discontinuous Finite Element Methods for Transport Problems", Doctoral Dissertation, LA-12425-T, Los Alamos National Laboratory, Los Alamos, NM.
- [Zie 00] Zienkiewicz, O.C. and Taylor, R.L. (2000), **The Finite Element Method: Volume 1 The Basis**, Butterworth-Heinemann, Oxford.